2009

RAPID FABRICATION OF MICROMOLD MASTERS FOR THE REPLICATION OF POLYMER MICROFLUIDIC DEVICES

Pun-Pang (Matthew) Shiu
Western University

RAPID FABRICATION OF MICROMOLD MASTERS FOR THE REPLICATION OF POLYMER MICROFLUIDIC DEVICES

(Spine title: Fabrication of Micromolds for Polymer Microfluidic Devices)

(Thesis format: Monograph)

by

Pun-Pang (Matthew) Shiu

Graduate Program in Engineering Science
Department of Mechanical & Materials Engineering

A thesis submitted in partial fulfillment
of the requirements for the degree of
Doctor of Philosophy

The School of Graduate and Postdoctoral Studies
The University of Western Ontario
London, Ontario, Canada

ABSTRACT

Lab-on-a-chip devices play an important role in a variety of applications such as analyzing DNA and RNA, medical screening, monitoring the environment, and chemical analysis. Often these devices must be disposable because they can only be used once to avoid sample contaminations. The cost of unit microfluidic devices then becomes a critical factor of the commercial success of the devices. These devices are typically produced using conventional microfabrication techniques such as photolithography and electroplating, which involve harmful chemicals extensively. Electroplating process typically requires long plating hours to reach the required thickness. To address these practical needs of fabricating inexpensive disposable devices, the ability to fabricate micromold masters for replication of polymeric microfluidic devices rapidly and with greener fabrication technologies is necessary.

This dissertation illustrates new approaches to fabricate micromold masters based on non-lithographic processes and the minimal usage of chemicals. This thesis is organized into two major parts. The first part described the microfabrication technologies developed to manufacture micromold masters for replicating low cost disposable polymer microfluidic devices. Three methods were developed and laser was employed to fabricate the mask having microfluidic network patterns on a thin metallic sheet. The pattern on this mask was transferred onto a substrate to create the master. Three techniques to transfer the mask pattern onto the mold master substrates have been explored including the laser microwelding, micro-spark erosion, and partial hot embossing (hot intrusion) process. The method that required the use of the laser welding is termed as Laser Cutting, laser Welding, and Molding (LCWM). The method that required the use of the micro-spark erosion to remove materials in order to produce the master is termed as Laser cutting, Electro-Discharging, and Molding ($LEDM^2$). The method that employed the partial hot embossing process to create the polymeric mold masters is termed as Laser cutting, Hot embossing, and Molding (LHEM). Proof-of-concept demonstrations of these three methods were experimentally validated. Each method has its unique advantages and

disadvantages and the selection of the developed methods used in fabrication of micromold masters depends on the requirements of the intended application.

The second part of this dissertation described the further investigations of the LHEM method because of its fabrication simplicity, rapid process, and produced high quality surface finishes. An extensive series of experimentations and analysis were conducted. Subsequently, an empirical model was derived to characterize the experimental observations. A finite element method (FEM) model was also developed to gain further understanding of the hot intrusion process. The FEM predictions were in good agreements with the experimental data. Both experimental data and FEM analysis reveal a strong positive correlation between the extruded height and width of cross-sectional extruded microreliefs created by the hot intrusion. This correlation, if employed innovatively, enables us to fabricate 3D microfeatures. Several examples including a 3D micronozzle were demonstrated.

KEYWORDS: Micromold, polymer microfluidic devices, laser micromachining, laser microwelding, micro-EDM, hot intrusion, non-lithography microfabrication, LCWM, $LEDM^2$, LHEM.

ACKNOWLEDGEMENTS

The journey towards a Ph.D. degree can be physically and mentally exhausting but also excitingly delightful. I truly thank those who helped me through in the hard times and shared the happiness in the good times throughout my graduate work. I would first like to thank my parents, Y.L. Leung and K.C. Shiu, my brothers, S. Shiu, T. Shiu, J. Shiu for their constant encouragement and supports. They are a constant source of strength to me in completing this program.

I must also express my gratitude towards my supervisor, Prof. George K. Knopf, and my co-supervisors, Dr. M. Ostojic, and Dr. S. Nikumb, for giving me the chance to work on such a challenging research project. Without their encouragement, and support, this work could not be possible. My special appreciation goes to S.K. Lee, B. Wong, N. Santo, J. Nagata, D. Arnold, B. Butt, S. Salo, and M. Merit for their continuing supports on various parts of this project, as well as for the great company. During the past four years, they were always ready to lend a helping hand. There are not enough words to express my gratitude to them. Many people have enriched my research experience during the past five years. Finally, I would like to thank my friends who have kept me sane and provided me with fond memories of my time at Western: K. Sareen, S. Cheong, W.J. Cheong, B. Wong, and N. Sato.

TABLE OF CONTENTS

LIST OF FIGURES

LIST OF TABLES

LIST OF ABBREVIATIONS

2D	Two-dimensional
3D	Three-dimensional
AVIA	UV laser, Coherent Inc., USA
CE	Micro Capillary Electrophoresis
CNC	Computer Numerical Control
COC	Cycloolefine Copolymer
DEEMO	Deep Etching, Electroplated, Molding
DNA	Deoxyribonucleic Acid
DRIE	Deep Reactive Ion Etching
μEDM	Micro-Electro-Discharging Machining
FDA	Food and Drug Administration
FEM	Finite Element Method
HE	Hot Embossing
HI	Hot Intrusion
IC	Integrated Circuit
LCWM	Laser Cutting, Laser Welding, and Molding
$LEDM^2$	Laser Cutting, Micro-Electro-Discharging Machining, and Molding
LHEM	Laser cutting, Hot Embossing, and Molding
LIGA	Lithography, Galvanoforming – electroplating - and plastic molding
LOC	Lab-On-a-Chip or Lab-On-Chips
MEMS	Micro-Electro-Mechanical Systems
NiCo	Nickel Cooper
NiFe	Nickel Iron
PA	Polyamide
PC	Polycarbonate
PDMS	Polydimethylsiloxane
PEEK	polyyetheretherketone

PET	Polyethylene Terephtalate
PFA	Perfluoralkoxy Copolymer
PMMA	Polymethylmethacrylate
POM	Polyoxymethylene
PP	Polypropylene
PS	Polystyrene
PVC	Polyvinylchloride
PVDF	Polyvinylidenefluoride
RNA	Ribonucleic Acid
SEM	Scanning Electron Micrograph
SU-8	Photoresist for UV photolithography application
Tg	Glass Transition Temperature
Tm	Melting Temperature
UV	Ultra-Violet
UV-LIGA	Ultra-Violet-LIGA
μTAS	Micro-Total Analysis Systems

CHAPTER 1

INTRODUCTION

1.1 The Problem

Commercialization of *micro-electromechanical systems* (MEMS) has exploded in recent years because these low-cost versatile devices have provided compact solutions for a variety of applications in automotive, consumer product, telecommunications, and medicine. Some of the early commercial successes include MEMS accelerometers, pressure sensors, air-bag sensors, and printer heads (Atkinson and Ounaies, 2006).

Another important area where MEMS devices have revolutionized modern technology is the development of efficient *micro-Total Analysis Systems* (μTAS) and *Lab-on-a-Chip* (LOC) (Wang and Soper, 2007). LOC is based on the notion that conventional laboratory analysis of biological or chemical samples can be performed more effectively on a miniaturized platform (Whitesides, 2006; Manz and Widmer, 1990) that supports passive and active microfluidic components including fluidic microchannels, micro-valves (Hong and Quake, 2003; Weibel et al., 2005), micro-pumps (Laser and Santiago, 2004), and micro-mixers (Nguyen and Wu, 2005; Gunther et al., 2005). In addition, these devices contain signal detection elements such as electrical, chemical, and optical sensors (Garcia and Henry, 2007; Janz et al., 2008).

Microsystems have become an important tool in modern diagnostics because these microfluidic devices enable control and precise delivery of small quantities of liquid. These fluidic networks are commonly used for analyzing DNA and RNA, medical screening, monitoring airborne toxins and contaminants in the environment, or performing chemical analysis in the field to identify dangerous substances (Geschke et al., 2004). The potential benefits of using miniaturized microfluidic systems in life and environmental sciences are a significant reduction in the time to perform the experiment, the ability to perform multiple tests simultaneously, and the requirement for only low quantities of bio-samples and reagents. The small size of the microfluidic system reduces

the need for expensive reagents and enables the entire analysis laboratory to be portable for in-field use. The system portability and short analysis time significantly reduce the setup overhead costs for testing a single sample and costs with the technician's time.

To avoid sample contamination and maintain diagnostic accuracy, it is often necessary to make these microsystems disposable. From a practical and commercialization perspective, it is essential that engineers develop manufacturing methods that enable large production volumes of high quality, low-cost microfluidic and LOC devices. Several manufacturing methods for the mass production of disposable fluidic devices have been explored including hot embossing and microinjection molding. Unfortunately, these fabrication methods usually require an expensive metallic micromold master to be constructed prior to unit production. The capability of a manufacturer to rapidly and inexpensively fabricate multiple micromold masters is desirable for large parallel production runs and, equally important in the design phase, for reducing the concept-to-market product development cycle.

1.2 Fabrication of Microfluidic Devices

Early microfluidic systems were created using the same silicon based *Integrated Circuit* (IC) microfabrication techniques used to manufacture electronic computer chips and microprocessors. However, a number of problems emerged with these silicon-based devices. For example, optical detection methods commonly used in life science would not be possible because the silicon substrates is opaque to the visible and ultraviolet spectrum and, further, silicon substrates may not be suitable in handling certain biological samples (Whitesides, 2006; Becker and Heim, 2000). Clear glass substrates and chemical etching processes were then used to address this problem but these LOC devices are relatively expensive. LOC devices also require a larger surface area than conventional microelectronic chips to house a number of passive features (reservoirs, mixers) and these large area complex fluidic network patterns resulting in a significant increase in silicon fabrication costs. Furthermore, as applications require thinner and thinner substrates to increase the portability, silicon and glass becomes more difficult to manipulate without breakage.

To reduce the fabrication and assembly costs associated with silicon-based microfluidic devices, a number of researchers have begun to explore other materials and microfabrication technologies. Becker et al. (Becker and Heim, 2000) was one of the first to suggest polymer-processing technologies because there is a large selection of bio-compatible polymers and manufacturing techniques that are low cost for large volume production. Nguyen and Wereley (Nguyen and Wereley, 2006) estimated the cost of using silicon or glass (boron-float glass and boron-silicate glass) for creating a microfluidic device to be 10 to 100 times more expensive than an equally compatible polymer material. Polymers enable the manufacturer to exploit a number of well-established processes such as hot embossing (Becker, 2000; Heckele et al., 1998) and microinjection molding (Piotter et al., 1997; Larsson, et al., 1997).

Many polymer based replication methods use micromold masters to produce large volumes of identical devices. LIGA (lithography, galvanoforming - elctroplating and plastic molding) is one of the more commonly known methods for fabricating high-resolution and high aspect ratio micromold masters (Becker et al., 1986; Abgrall and Gue, 2007). The method uses X-ray lithography to transfer patterns onto polymethyl-methacrylate (PMMA) resists. The PMMA microstructures are then electroplated using nickel or nickel based alloys (NiCo, NiFe). The metal master is finally released by dissolving the PMMA resists in chemicals such as a mixture of tetrahydro-1, 4-oxazine and 2-aminoethanol-1. The resultant mold masters can be used for either injection molding, soft-molding or hot embossing plastic replicates. The primary advantage of this method is that high aspect ratio masters can be produced. However, the disadvantages of the LIGA method include the relatively high cost of the lithographic and electroplating processes, difficulty in accessing the technology because an expensive X-ray source is required (Becker et al., 1986; Abgrall and Gue, 2007), and the harmful impact on the environment of the various chemicals used throughout the manufacturing process. The electroplating step of the LIGA process usually requires lengthy process times, lasting hours or days, for depositing the plating material to the desired thickness. Furthermore, post processing is often needed to flatten the back of the plated metal because of varied deposited thicknesses of metal layer created by the deposition process. Shortening the mold fabrication time and reducing the number of process steps involved are, therefore,

essential to lowering overall fabrication costs for producing medium-to-high volume devices.

Alternative fabrication methods that are simpler and require lower cost equipment have also been investigated. Researchers at Harvard University (Whitesides et al., 2001) developed a soft-lithography technique to rapidly fabricate polymer microfluidic devices (Duffy et al., 1998; McDonald et al., 2000; Becker and Locascio, 2002; Nguyen and Wereley, 2002; McDonald and Whitesides, 2002). In general, soft-lithography is based on the UV-LIGA process, without the electroplating stage (McDonald et al., 2000). The mold masters are made from SU-8 photoresist by first using a high-resolution printer to create a low cost mask, or template, with the desired microchannel pattern (Banks, 2006). SU-8 photoresist is then spun coated on a silicon wafer, or glass substrate, and soft-baked. After this step the printed mask is aligned with the SU-8 coated wafer and exposed to UV light, hard baked and chemically developed by dissolving the non-cross-linked SU-8. An elastomer such as polydimethylsiloxane (PDMS) is finally cast over these SU-8 molds to replicate a microfluidic device with the desired channel pattern and cured. Once it is cured, the PDMS layer is peeled off and bonded with another PDMS, glass, or silicon substrate layer. Without the electroplating process, the fabrication cost of these micromold masters is significantly lower than those created using the LIGA approach. Furthermore, the simplicity of the process makes it the most popular method for fabricating microfluidic prototypes in academic research laboratories.

1.3 Motivation of this Work

Polymer replication technologies are currently the most promising methods to economically mass produce disposable microfluidic devices. Unfortunately, it requires mold masters produced by methods such as LIGA and soft-lithography which use harsh chemicals that are often inadvertently released into the environment by the manufacturing process. Therefore, several research groups have begun to explore non-lithographic fabrication technologies that support the concept of less production chemicals and "green manufacturing". In this regard, Hupert et al. (Hupert et al., 2007) proposed the use of high-speed micromilling to machine metallic micromold masters for the replication of

disposable polymer microfluidic chips. However, the disadvantage of micromilling is that it can only machine microfeatures of limited size. In addition, micromilling operations commonly take days or weeks to produce one mold master. Developing innovative mold master fabrication techniques is necessary and desirable in order to rapidly, economically, and with minimal negative impact on the environment to manufacture low cost disposable microfluidic devices.

1.4 Objectives of the Research

The primary goal of this thesis is to develop nonlithographic microfabrication techniques that enable the "green" production of low-cost disposable polymer microfluidic devices. The production costs are associated with materials, fabrication methodology, and the impact of the manufacturing processes (equipment, chemical waste) on the environment. The focus of the research project is, therefore, to introduce novel microfabrication methods to create micromold masters based on the laser micro-machining technology that does not require the chemical etching or electroplating and the proposed microfabrication techniques will meet the following design and process requirements:

1. minimal use of environmentally harmful chemicals
2. minimal number of operational steps or material processing stages
3. rapid fabrication of micromolds with accurate relief features
4. enable the production of polymer replicate devices with microchannel widths between 1μm and 1000μm (ie. range of typical microchannel dimensions).

The design and fabrication of complex bio-chips with embedded sensors and actuators is beyond the scope of this dissertation. Rather the thesis will be limited to the introduction and validation of new methods that rapidly manufacture precision micromolds for hot embossing and soft-molding multiple polymer microfluidic chips with simple passive features (fluid reservoirs, channels, mixers).

1.5 Overview of the Thesis

The remainder of this thesis is organized into nine chapters. Chapter 2 provides a detailed overview of several microfabrication techniques that have been proposed in the literature for manufacturing microfluidic chips. The primary focus of this discussion will be on methods that support the replication of polymer microfluidic devices.

Chapter 3 describes the first microfabrication method that exploits Laser Cutting, microWelding, and soft Molding (LCWM) in detail. The technique exploits the precision material removal capabilities of industrial lasers to cut the inverted profiles of microfeatures (e.g. liquid flow channels, reservoirs, passive micro-mixers) on thin metallic sheets. The precisely machined micropatterns are then assembled onto a substrate material by laser microwelding to form the functional mold master.

An alternative technique that involves Laser cutting, micro-ElectroDischarge Machining, and Molding ($LEDM^2$) is introduced in Chapter 4. This proposed manufacturing process utilizes laser micromachining to cut the negative two-dimensional profiles of the desired microfeatures and fluidic network patterns on a 100μm thick brass sheet. The positive relief of the cut pattern is then created by using electro-discharge micromachining (micro-EDM) to die sink the metallic mask onto a brass substrate. The final substrate with the desired relief pattern becomes the mold master used for either elastomer casting or thermoplastic hot embossing.

Finally, the third proposed microfabrication method is presented in Chapter 5. The manufacturing method involves Laser micromachining, partial Hot Embossing, and Molding (LHEM) to create polymethylmethacrylate (PMMA) mold masters for device replication. A metallic hot embossing mask with the desired microfeatures is first laser micromachined and the mask is then pressed onto a PMMA substrate under applied heat and pressure to create the master. The resultant microreliefs have near optical quality surface finishes.

Comparisons of the three developed micromold fabrication techniques are provided in Chapter 6. Experimental characterization and modeling of the hot embossing process for the LHEM method is given in Chapter 7. This study includes the design of

experiments, an extensive series of experimentations, data analysis, and the development of an empirical model. A finite element method (FEM) model that describes the formation of the extruded microreliefs by the hot embossing process in the LHEM method and the validation of the FEM results are presented in Chapter 8. Finally, a summary of the research contributions and the limitations of the proposed microfabrication methods are given in Chapter 9. Recommendations for future work are also provided.

CHAPTER 2

REVIEW OF POLYMERIC MICROFLUIDIC DEVICES

2.1 Introduction

The earliest example of a microfluidic system was developed at Stanford University in the late 1970's (Terry et al., 1979). The simple gas chromatography system was constructed on a 2-inch diameter silicon wafer and incorporated a 1.5m long microchannel, valve, and signal detector. The microchannel was created on the silicon substrate using chemical wet etching. This gas chromatography system illustrated the potential of microfluidics and demonstrated that a large substrate surface area is necessary to house very long microfluidic channels. Consequently, as discussed in the previous chapter, the cost of fabricating silicon microfluidic and LOC devices can be high. In this regard, Abgrall et al. (Abgrall and Gue, 2007) and Heckele et al. (Heckele and Schomburg, 2004) suggest using polymers instead of glass/silicon as substrate materials for microfluidic devices because the material costs are typically 10 to 100 times less.

This chapter presents a literature review of several methods for fabricating polymeric LOC devices and is organized in the following manner. The key properties of polymer materials used to manufacture LOC devices are first described followed by an overview of several microfabrication methods for replicating polymer microfluidic devices. Details about each stage of the micromolding process are described. A summary of the current state-of-the-art in research and development trends in microfluidic device fabrication is also provided.

2.2 Key Properties of Polymers

In addition to material cost and bio-compatible, polymers have several clear advantages over silicon substrates for producing LOC devices. In general, polymers have a number of useful properties such as high stability over a wide range of temperatures, optical transparency for light detection, and chemical resistance. For example, polyyetheretherketone (PEEK) remains stable at temperatures up to 250°C and it can resist chemicals such as alkaline solutions, acids, and solvents. If an optical grade polymer is required then polymethylmethacrylate (PMMA), polycarbonate (PC), and cyclo-olefine copolymer (COC) are suitable because they all exhibit high optical transparency over the visible wavelengths. Furthermore, a polymer is a natural electrical insulator but with proper additives, it can be turned into an electrical conductor, heat sink, or a magnet. Polymers such as polyvinylidene fluoride (PVDF) have a piezo-electric effect. Elastomers such as polydimethylsiloxane, (PDMS) have an elastic property that is suitable for creating micro-membrane structures such as micropumps.

In general, polymers are organic materials having long chains formed during the polymerization and are classified either an *amorphous* or *semi-crystalline*. The polymer is often characterized by its glass transition temperature (T_g) and melting temperature (T_m). At ambient temperature, amorphous polymers such as polymmethacrylate (PMMA) behave as a hard, rigid and optical clear material. However, as temperature increases the mechanical properties of PMMA can undergo significant changes. Some amorphous polymers such as PMMA become "rubber like" or "solid-rubber" state when the temperature is increased above its glass transition temperature (T_g). At this transition state, the molecules of the heated polymer tend to align themselves in the direction of stress. If the material is then cooled below its T_g, while maintaining the applied pressure, the polymer hardens at that state.

Polymers are also separated into two categories: *thermoplastic* and *thermosetting* polymers. Thermoplastic polymers are weakly bonded together; therefore, it softens upon heating and hardens when cooling below its T_g. The shape of these polymers can be modified by applying heat and pressure. Typical thermoplastics are soluble in organic

solvents. Examples of such polymers are polymethylmethacrylate (PMMA), cyclo-olefin copolymer (COC), and polycarbonate (PC).

The thermosetting polymers are usually not soluble in organic solvents and the final shape must be defined before cross-linking occurred. The thermosetting materials can be cross-linked by heat, photo initiation, or chemical reaction via mixing with the base and curing agent. The examples are epoxy resists, and elastomers such as PDMS. Typical polymers used in polymer microfabrication are listed in Table 2.1. Detailed information about the properties of polymers can be found in various manuals and text-books (Ward and Sweeney, 2004; Young and Lovell, 1991).

2.3 Fabrication of Polymer Microfluidic Devices

An overview of the manufacturing process used to create polymer microfluidic devices is shown in Figure 2.1. The overall sequence of operations starts with the design of a microfluidic device followed by the fabrication of micromold master - the negative relief pattern of the desired fluidic network and microstructures. An appropriate replication (molding) process such as hot embossing, or injection molding is then used to create the replicated parts. Finally, post-processing operations, such as assembling, sealing, and surface treatment, are performed.

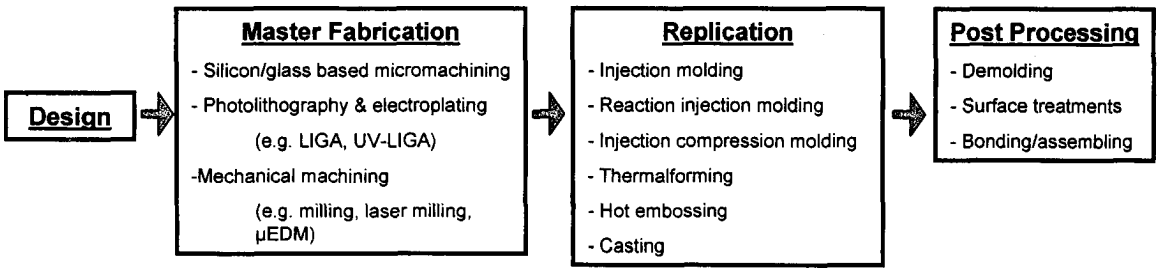

Figure 2.1. Typical sequence of manufacturing operations employed to replicate polymer microfluidic devices.

Table 2.1 Typical polymers used in the fabrication of polymer microfluidic devices (Heckele and Schomburg, 2004; Abgrall and Gue, 2007).

Acronym	Full name	Tg (°C)	Tm (°C)	Thermal expansion coefficient (ppm/K)	Properties	Structure
COC	Cyclo-olefine copolymer	140	/	/	High transparency	Amorphous
PMMA	Polymethyl-methacrylate	105	130-140	70-77	High transparency	Amorphous
PC	Polycarbonate	150	/	66-70	High transparency	Amorphous
PS	Polystyrene	100	/	30-210	Transparent	Amorphous
POM	Polyoxy-Methylene	/	160	80-120	Low friction	Semi-crystalline
PFA	Perfluoralkoxy copolymer	/	310	/	High chemical resistance	Semi-crystalline
PVC	Polyvinyl-chloride	90	/	50-180	Low cost	Amorphous
PP	Polypropylene	/	170	100-180	Mechanical properties	Semi-crystalline
PET	Polyethylene terephtalate	80	265	20-80	Transparent & low friction	Semi-crystalline
PEEK	Polyether-etherketone	150	340	50-110	High temperature resistance	Semi-crystalline
PA	Polyamide	50	260	80-95	Good mechanical properties	Semi-crystalline
PVDF	Polyvinylidene fluoride	40	210	80-140	Chemically inert, piezo-electric	Semi-crystalline
PDMS Sylgard 184	Polydimethy-lsiloxane	/	/	310	Transparent & elastic properties	Amorphous
SU-8	-	200	/	50	Good mechanical properties	Amorphous

2.4 Design of Microfluidic Devices

The design of a microfluidic device depends upon the specific requirements of the application. For example, the rapid mixing of two liquids on a microfluidic device can be accomplished by either using an active mixer or a passive mixer. If a passive mixer is selected then the design goal is to find the shortest microchannel possible. The passive mixing of fluids in the microscale is most often accomplished by molecular diffusion. However, the diffusion requires relatively long microchannels to ensure the thorough mixing (Whitesides, 2006). The high aspect ratios, large depth per width ratios, of microchannels make these structures particularly useful in passive mixing because of the large interfacial areas between the fluidic streams. Large interfacial areas ensure a more rapid rate of molecular diffusion. Jacobson et al. (Jacobson et al., 1999) introduced an improved mixer design that splits the fluids into multiple channels and then recombines the resultant mixture. Other researchers have introduced novel designs such as a three dimensional L-shaped serpentine channel (Vijiayendran et al., 2003) that rotates the microflows at a specific Reynolds number, thereby improving the mixing process. The passive microfluidic mixers described above do not represent a comprehensive review of mixers rather they illustrate how a variety of diverse microstructures can be used to achieve the desired functionality and performance.

2.5 Micromold Masters for Replicating Microfluidic Devices

The micromold masters for creating polymeric microfluidic devices are a negative imprint of the desired microstructures and fluidic network patterns. Once a micromold master is fabricated, the replication of numerous functional parts is possible using this master. Silicon micromachining, photolithography, and CNC machining (Becker and Locascio, 2002) have all been proposed as viable fabrication methods for micromold masters. Each fabrication method has its own unique advantages and drawbacks. However, a number of critical micromold design and manufacturing requirements must be addressed and these are briefly discussed in the next section.

2.5.1 Micromold master design requirements

It is necessary to have good surface finishes on the micromold master because the replicated microchannels should be smooth enough to allow bio-fluids to freely pass through without adhering onto the surfaces of microchannels. In addition, a high-quality surface finish enables the improved optical sensing. From a maintenance perspective, a mold master with a rough or poor surface finish will reduce the tool life because of higher frictional forces during the separation of the molded parts from the mold master, demolding. These friction forces can lead to the tearing of microfeatures during demolding resulting the failure of replicated parts. If the intended application permits, trapezoidal cross-sections of microchannels are preferred to facilitate the demolding. The design of fluidic network microstructure, the selection of molding material, and the required volume of replicated parts all strongly influence how the micromold master should be constructed. Furthermore, microstructures are inherently fragile – this further precipitates the problem when high aspect ratio microstructures are involved; therefore, the selection of a stronger material for the mold master is desirable to allow maximum number of molding cycles before a replacement is needed.

Frequently chemical mold release agents are applied onto the mold masters to promote the separation of the molded parts from the masters. However, when molding polymer microfluidic/LOC devices, the mold release agents may become inter-mixed with the microfeature surfaces and, thereby alter the surface composition or chemically contaminate the surface from which an inaccurate analysis may be resulted. In this regard, mold release agents are usually avoided to prevent contaminations in microchannels. As a result, the demolding process at the micro-scale is more challenging than at the macro-scale.

2.5.2 Micromold master fabrication methods

This section presents several fabrication techniques generally used to create micromold masters for replication of polymeric microfluidic devices. As mentioned, one of the most commonly known micromold fabrication method is LIGA method (German words of

Lithographie, **G**alvanoformung, and **A**bformung - lithography, electroplating, and plastic molding) (Banks, 2006; Heckele and Schomburg, 2004; Abgrall and Gue, 2007). This method is capable of producing high resolution and high aspect ratio micromold masters with fine microfeatures up to 1000μm in height and a theoretical aspect ratio of up to 1000:1 (Banks, 2006; Becker et al., 1986). High aspect ratio microstructures are usually defined as features with a large ratio of height or depth to width. The sequence of LIGA method is illustrated in Figure 2.2. PMMA resist is spun coated on a wafer. A suitable X-ray mask is then fabricated and placed on top of the photoresist, usually PMMA. The X-ray is used to transfer mask patterns onto PMMA resists. Once completed the PMMA microstructures are electroplated using nickel or nickel based alloys (NiCo, NiFe). Finally, these masters can be used either for casting elastomer, hot embossing, or injection molding to produce plastic replicates.

The mask used in the process is, however, subjected to high level of X-ray radiation, which the mask is easily heated up and thermal distortion of the mask is resulted, final dimensional accuracy of microstructures is affected. Mask making for LIGA is expensive; ensuring a design is correct before proceeding onto the X-ray photolithographic process (Banks, 2006) is necessary. If a thick backing plate of the LIGA mold master is designed, it may take long hours of electroplating time, up to weeks (Becker et al., 2002).

Another consideration is that the electroplating is sensitive to the distribution of microstructure. Therefore, the thickness of the plating is not even and grinding a flat surface of the backing is necessary before dissolving the PMMA. The good control of the chemical concentration during electroplating process is also important to reduce the mechanical stress of the final mold master. Because LIGA process uses the expensive synchrotron radiation sources and this requirement makes X-lithography and LIGA limited to specialized applications (Becker et al., 1986; Abgrall et al., 2007; Banks, 2006).

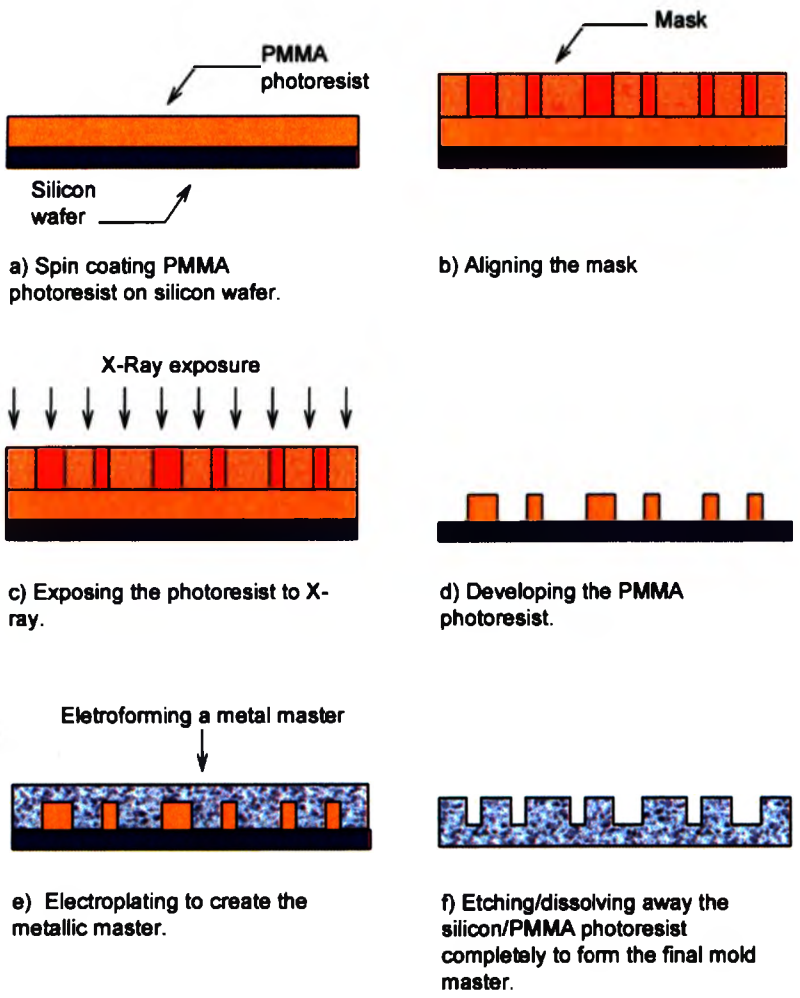

Figure 2.2. Typical sequence of LIGA method (X-ray lithography, electroforming, and molding) method to fabricate nickel based metallic mold masters.

Silicon and glass have been used as the substrates for mold masters. Wet bulk micromachining etching is typically used to create the microstructures (Martynova et al., 1997; McCormick et al., 1997; Lee et al., 2001). The problem associated with isotropic wet etching is that silicon is etched uniformly in all direction, therefore, rounded microchannel cross-sections and undercuts are produced. Isotropic wet etching requires consistent agitation to make microchannel geometries reproducible. In anisotropic wet etching, the etched geometry of microchannels is limited because of the chemicals attacks the crystal orientation of the single crystalline materials (Martynova et al., 1997).

The key drawback of these silicon mold masters is the limited number of replication cycles, typically less than 10, because of the brittle nature of silicon; therefore, silicon molds are only suitable for manufacturing a small number of prototypes (Heckele et al., 2002; Cameron et al., 2006). To avoid these brittle silicon molds, Cameron et al. (Cameron et al., 2006) suggests silicon molds use only as the negative reliefs and to be electroplated to create metal masters. The silicon is simply etched away once electroplated.

To create higher aspect ratio structures, Elders et al. (Elders et al., 1995) suggest using Deep Reactive Ion Etching (DRIE) to etch microreliefs in silicon and is termed as DEEMO (Deep Etching, Electroplated, MOlding). DRIE allows the silicon to be etched with high directionality and selectivity, implying a better geometry control over the anisotropic wet etching. The surface roughness is, however, high when using a high DRIE etching rate.

To avoid both the expensive sources of X-ray and the rough surface finishes produced by DEEMO process, conventional UV-photoresist has been used directly to pattern the microstructures on silicon wafer and to be electroplated to create the metal master. Silicon and photoresist are then etched/dissolved away completely (Banks, 2006). The key drawback of using conventional photoresists is the limited spin-coated thickness, typically only about 0.5 to 3μm, therefore, it is only suitable for low aspect ratio microstructures. The popular brand of general-purpose photoresists is Shipley S1800 series (Rohm & Haas), Marlborough, MA (electronicmaterials.rohmhaas.com) or some thicker photoresist by Clariant Corp., Somerville, NJ (www.azresist.com).

When SU-8 photoresist became available in 1990s, it is then possible to create higher aspect ratio microstructures using conventional UV-lithography. This SU-8 allows spin coating up to a resist layer thickness of 200μm and can be purchased from MicroChem Corp., Newton, MA (www.microchem.com). Once SU-8 is cross-linked, it is difficult to strip off and can be dissolved only in aggressive chemicals (Nguyen, 2002). The SU-8 resist is, however, very desirable when used as mechanical microstructures. Piotter et al. (Piotter et al., 1997) suggest using SU-8 spun coated on silicon wafer to directly create mold masters. This eliminates the electroplating process and the need of

dissolving the silicon and resists. However, these mold masters break easily after a number of molding cycles due to the delamination of SU-8 from silicon caused by the thermal stress building up at the interfacial layer, as a result of the difference in the thermal expansion coefficients.

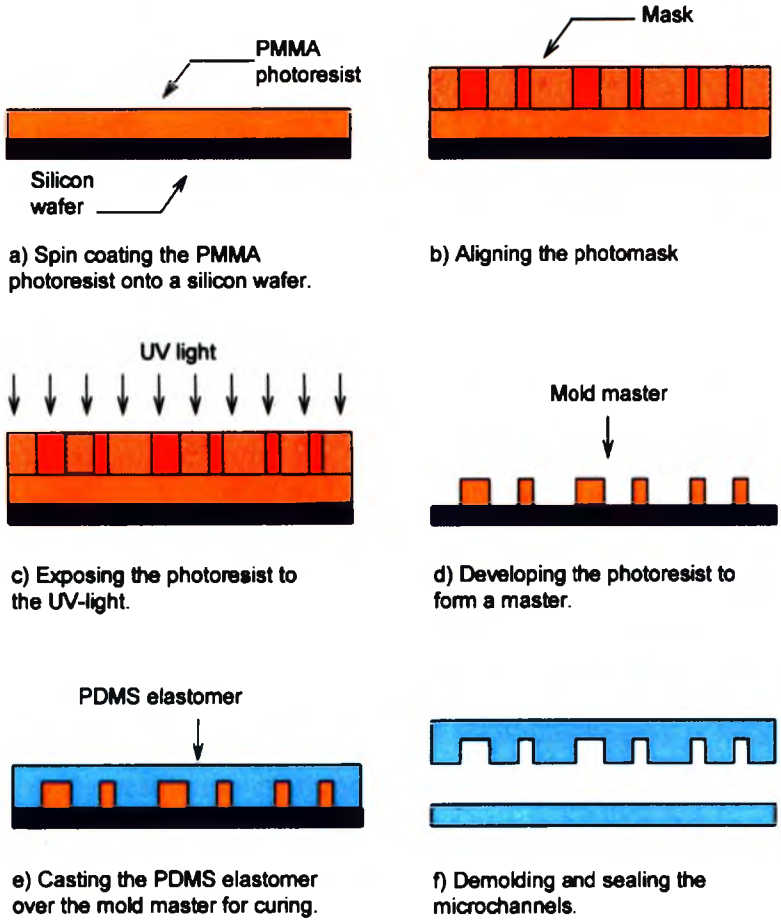

Figure 2.3. Typical sequence of soft-photolithography to create SU-8 micromold masters for replicating PDMS microfluidic devices.

Soft lithography was developed to produce microfluidic devices in the late 1990s (Duffy et al., 1998; McDonald et al., 2000; Whitesides et al., 2001; McDonald et al., 2002). The inexpensive process combined with simplicity makes it the most popular fabrication method of microfluidic devices in the research field of microfluidics (Banks, 2006). Figure 2.3 illustrates the sequence of the process where begins by first printing the mask using a high resolution laser printer. Photoresist SU-8 is spun coated on a silicon wafer and soft-baked. UV light is exposed to the pattern for cross-linking and for

subsequent hard baking, and finally developing. Elastomer such as polydimethylsiloxane (PDMS) is then poured over these molds to replicate microchannels (McDonald, 2002).

Researchers also suggest exploring the miniaturization of traditional mechanical machining to create micromold masters. Hupert et al. (Hupert et al., 2007) described using CNC micromilling operation to machine metal masters for replication of polymer microfluidic devices. Micromilling is, in fact, a traditional CNC milling operation that the milling tool bits are replaced with "micromilling" bits, Figure 2.4. Some commercial tool making services are available such as Kern Micro-und Feinwerktechnik GmbH & Co. KG, Murnau, Germany, and Automationstechnik GmbH, Karlsruhe, Germany. Micromilling is, however, limited to machine mostly soft metals such as brass and aluminum and not suitable to machine tool steels. The key drawback of micromilling is the tool diameter limitation, about 200μm as the smallest reported by Heckele et al. (Heckele et al., 2004). As a result, the resolution of machined microfeatures is in the order of 50 to 100μm (Abgrall et al, 2007). Post polishing of micromilled molds is often required to improve surface finishes. Furthermore, a small tool diameter implies a slow material removal rate. It is not uncommon to complete a micromilling operation taking a few days or a week. However, the key advantage of micromilling is the ability to machine three-dimensional (3D) features which photolithography is very limited in this aspect. However, the resolution of these micromilled 3D features is, again, relatively large, which limits its applications. Further, large machined rounded corners are difficult to avoid because of the tool diameter.

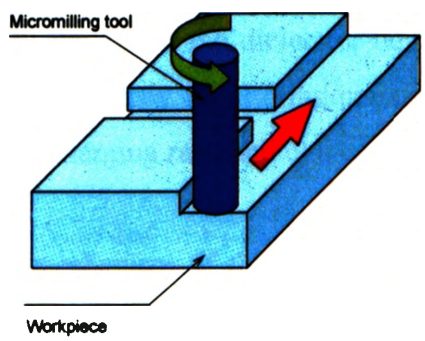

Figure 2.4. Typical operation of micromilling to create mold masters for the replication of microfluidic devices.

The manufacture of macro-scale mold masters using micro-electrodischarge machining (MicroEDM) has been used for decades. Heckele et al. (Heckele et al., 2002) suggest the use of wire EDM process to machine mold inserts. However, limited studies in the published literature demonstrate that the microEDM process can be used in machining micromold masters for the replication of microfluidic devices. The key advantage of microEDM process is the ability to fabricate any conductive materials regardless of its hardness and often harden steel or tool steel is conductive. High strength metallic mold masters are desirable for applications that require the masters to undergo high pressure and high temperature. This also makes the microEDM a very useful process for the high volume production of parts.

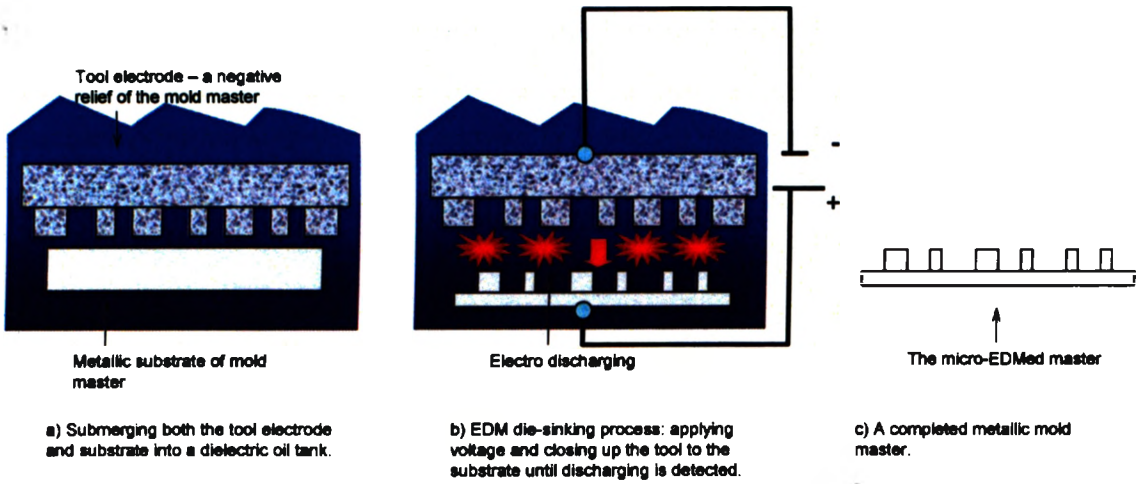

Figure 2.5. Typical sequence of the microEDM die-sinking process, a) submerging the tool electrode and metallic substrate into the dielectric liquid, b) applying a voltage to create the discharging and continuously monitoring/maintaining a small gap between parts to delivery a consistent discharging rate, and c) a completed mold master.

The material removal mechanism of the microEDM is based on spark-erosion. The spark erosion effect is created by separating positive and negative electrodes with a small gap and then applying high voltage. The spark generated by electro-discharging can produce a temperature of nearly 8000 to 12,000°C, which causes the targeted material to be removed through melting and sublimation. Unfortunately, both electrodes are spark

eroded simultaneously as discharging, but at a significant different rate. As a result, the machining of hardened steels is possible. The key drawback of the EDM process is the continual dimensional change of tool electrodes, which this tool wear results in the imprecision of machined parts. To maintain machining precision, continuous wire feeding system is used to provide a fresh electrode surface to maintain the tool dimension.

Laser micromachining used in fabricating micromold masters has received attention recently because it is a non-contact process that does not induce tool bending as in micromilling. The laser machining involves minimal chemicals and is able to machine a wide range of materials such as glass, polymers, metals, composite, and ceramics. However, the typical laser machined surface is relatively rough. Youn et al. (2007) reported the work of comparing the micromold masters machined using ultra short pulse femto-second laser, excimer laser, and focus ion beam (FIB). The result found that FIB produces a better surface finish than the other two. The sequential nature of the laser machining process is the key drawback, however, this sequential nature makes this process flexible.

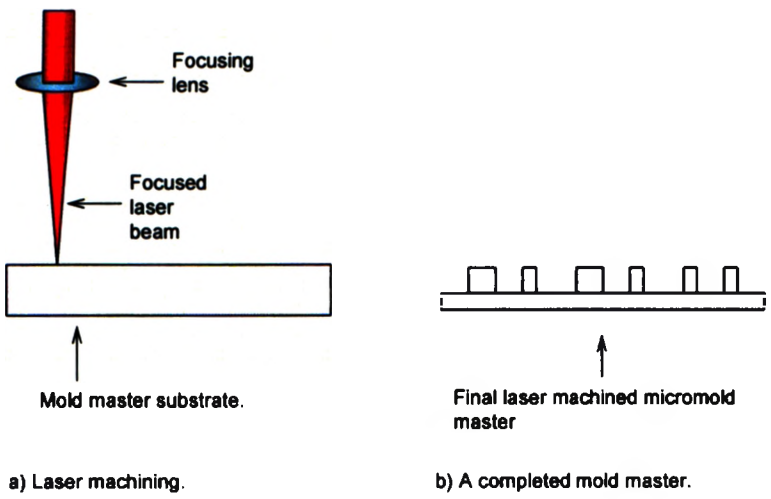

Figure 2.6. Typical sequence of the laser micromachining to sequentially scan the entire surface to create micromold masters.

2.6 Micromolding Processes

2.6.1 Requirements for micromolding

The replication processes used to reproduce the final microchannel networks can be injection molding, hot embossing, or casting of polymers. The selection of the molding process depends strongly on the microstructure of microfluidic networks, the required surface properties, and the selected polymer as well as the number of the produced parts. For small-to-medium volume production, hot embossing and casting processes are suitable because the setup is simple and inexpensive. For high volume fabrication, injection molding is suitable due to the short molding cycle time, in the order of seconds to minutes.

The difficulties of demolding high aspect ratio microstructures needs to be addressed by any proposed micromolding process such as the mechanical strength of high aspect ratio microstructures is essentially weak and it is difficult to withstand the shear forces of demolding. The improper design of mold masters would result in easily tearing the molded parts when demolding or even the valuable mold master would be damaged, a replacement is needed.

2.6.2 Common types of micromolding processes

Although this thesis supports the development of new fabrication methods of micromold masters, the following discussion of micromolding processes provides the reader with a better understanding of how mold masters should be designed and fabricated. Once a micromold master is fabricated, the replication of the functional parts can be started using a suitable molding process. Micromolding processes can be classified into six basic types: injection molding, reaction injection molding, injection compression molding, thermoforming, hot embossing, and casting.

Injection molding is a well-established macro-process and has been adapted into molding microcomponents recently (Hanemann et al., 2000). Wallrabe et al. (Wallrabe et

al., 2002) reported the injection molding used in manufacturing high volume fiber optical connectors. The short cycle time of injection molding is the biggest advantage.

Figure 2.7 illustrates the sequence of injection molding. The process is first closing the mold master (cavity) and the molten thermoplastic polymers are then injected with a high pressure into the cavities. The typical level of injection pressures is from 500 to 2000 bars (Niggemann, 1999; Gerlach, 2001). The filled polymer is then cooled below the polymer's T_g by the mold, for subsequent demolding. Companies like Battenfeld Kunststoffmaschinen GmbH, Germany, markets an injection molding machine Microsystem 50 for high volume productions.

A mold designed with long polymer flow networks is undesirable because the higher residue stresses in the molded parts are induced from a high injection pressure used to fill the cavities. In addition, a higher injection pressure typically shortens the tool life.

At the cooling phase, maintaining a high pressure is needed for "packing" polymers in order to reduce the shrinkage effect of the molded parts. The ratio of this thermal shrinkage is related to its thermal expansion coefficient, for typical thermoplastics it range from 30 to 310ppm/K. For example, PMMA has a thermal expansion coefficient of 70-77ppm/K but silicon has only 2.5ppm/K.

Circulating cooling water in the mold is often used to shorten the time of cooling in order to increase the production speed. However, one must be careful in the selection of the cooling rate, where a higher cooling rate often results a higher residue stress in the molded part. A balance between the acceptable quality of products and the production speed must be weighted in order to select the optimal process parameters.

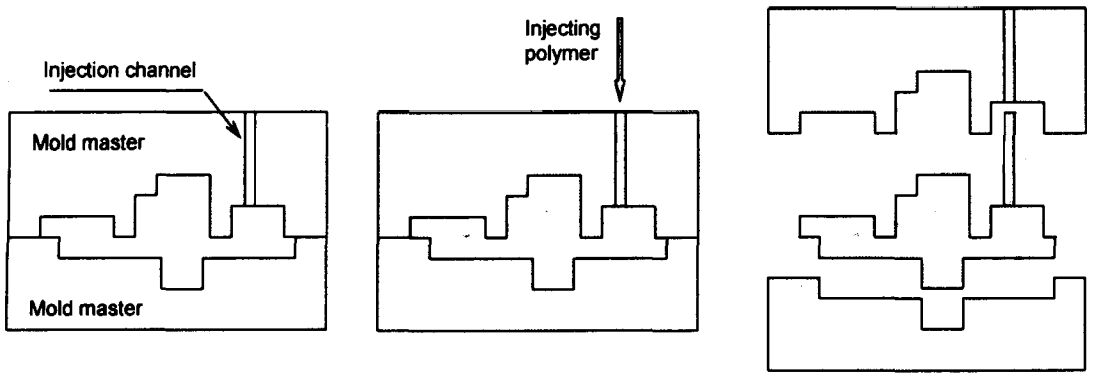

Figure 2.7. Typical sequence of the injection molding: a) closing mold master cavity and evacuating the air, b) injecting the molten thermoplastic polymer into the cavity with high pressure, and cooling the polymer below T_g, and c) demolding the parts.

The reaction injection molding process is similar to the injection molding but the molded shape is cured by a chemically induced polymerization. Figure 2.8 shows the process sequence is firstly closing the mold cavities and evacuating the air. Secondly, the pre-mixed polymer is injected into the cavities and the polymer is heated up to initialize the polymerization. Finally, the molded parts are separated from the masters.

Thermosetting polymers such as silicone are typically used in the reaction injection. The early development of the process found it difficult to maintain high quality molded parts, because of the mixing chemical compounds completely is difficult and it is even more challenging in micro-scale. Further, the heat-initiated curing cycle was much longer than the injection molding cycle which makes the process less popular. However, the advancement of UV-curable polymers replaces the heat-initiated ones, significantly shortening the cycle.

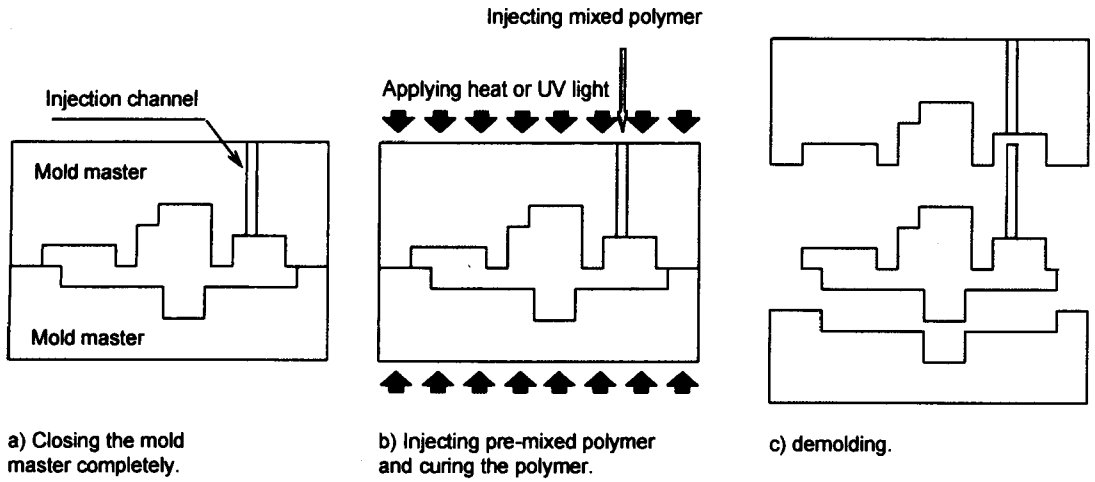

Figure 2.8. Typical sequence of the reaction injection molding: a) closing mold master cavity and evacuating the air, b) injecting the pre-mixed polymer into mold cavities and applying heat to initiate the polymerization to consolidate the shape, and c) demolding the parts.

Hot embossing is popular in research laboratories because of the setup is simple and low cost. A number of commercial hot embossing systems is available such as hot embossing machine HEX03 from Jenoptik Mikrotechnik GmbH, hot embossing Stamp Press MS 1 from Wickert Maschinenbau GmbH, and hot embossing system EVG® 520HE from EVG Group. Typical steps in hot embossing are shown in Figure 2.9. A thermoplastic thin sheet is placed in the hot press under the mold master and air is then evacuated. The mold master is heated to above the softening temperature, T_g, of the polymer sheet and pressure is applied onto this sheet to force the soften polymer into microcavities. The master along with the plastic sheet is then cooled to a de-embossing temperature. The part is then separated from the master for the subsequent post processing step. Note that the mold master was not entirely closed in the process and the residue polymer layer, later diced away, is a characteristic of the hot embossing process.

The flow distance of the soften polymer as it fills the cavities is relatively shorter than the distance travelled in injection molding. As a result, less residue stress is generated in the parts. Heckele and Schomburg (2004) suggest the hot embossing process

is suitable for replicating microlenses and optical waveguides. In addition, the thermal shrinkage in hot embossed parts is typically small because of a narrower thermal loading of the process - the thermoplastics were only needed to heat up to slightly higher than the glass transition temperature. This smaller thermal shrinkage rate is particularly suitable for replicating high aspect ratio microstructures.

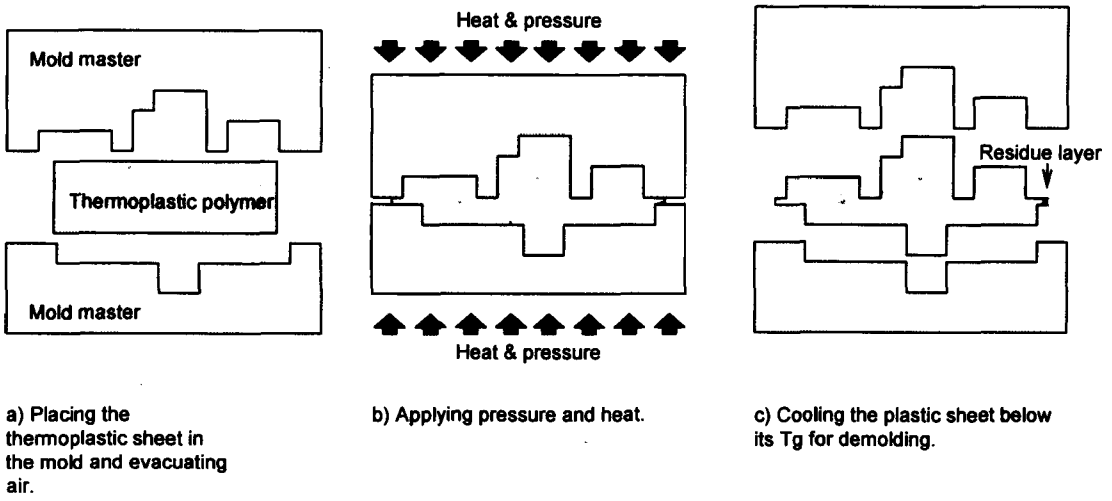

Figure 2.9. Typical sequence of the hot embossing process: a) placing a thermoplastic sheet under the mold master and evacuating the air, b) applying the heat and pressure to force the soften polymer into the microcavities, and cooling the plastic sheet below the softening temperature, and c) demolding the parts.

The tool changing in hot embossing is easy, performed in minutes, and, therefore, it is particularly suitable for the small-to-medium production of microfluidic devices. It is even more desirable for a production environment that requires frequent tool changing. With some modifications, such as using a continuous polymer sheets feeding system, the production volume can be easily scale up. Because of the smaller residue stress found in hot embossed parts, the shear forces at demolding are less than injection-molding ones. Thus, the tool life is typically prolonged. Reducing mold damages is especially important for those expensively fabricated mold masters, such as LIGA mold masters. The biggest drawback of the hot embossing is the longer molding cycle than the injection molding. A

30-minute hot embossing cycle is typical because the plastic sheet is heating up and cooling down by the mold; the cooling phase is especially long.

Injection compression molding is a process combining both the injection molding and hot embossing. The process sequence is shown in Figure 2.10. First, the molten polymer is injected into a semi-opened micromold cavity. While the temperature is maintained, the micromold is closed, similar to the hot embossing, to replicate the microfeatures. The key advantage of this process is that the replication cycle is much shorter because of the mold master is not used for heating up and cooling down the polymer sheet as in the hot embossing. In fact, the cycle is almost as fast as in the injection molding. In addition, the molded parts have a lower residue stress due to the shortening of flow paths of molten polymers. Thus, injection compression molding is often used in the production of DVD and CD to replicate sub micrometer and low aspect ratio features. Because of the low aspect ratio of these nano-features of DVD, demolding is not problematic (Heckele et al., 2004; Abgrall et al., 2007; Nguyen and Wereley, 2006). Ferromatik Milacron Maschinenau GmbH markets some of the commercial injection molding machines for CD replications.

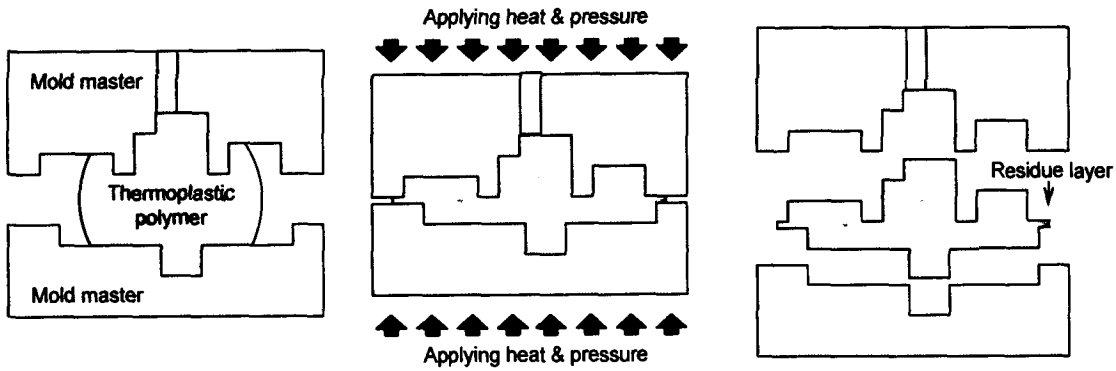

Figure 2.10. Typical sequence of the injection compression molding: a) semi-closing the mold master, injecting the molten polymer into cavity, b) closing the mold master completely like hot embossing and cooling the polymer below the T_g, and c) demolding the parts.

The thermoforming sequence is illustrated in Figure 2.11. A very thin thermoplastic polymer sheet is clamped in the mold master closed tightly. The mold is then heated up to the polymer's softening temperature T_g. A noble gas is injected into one side of the master where applying a high pressure to deform the plastic sheet into the shape of the mold. The polymer is then cooled for demolding. The key drawback of this process is that the process replicates only low aspect ratio microfeatures due to the limited sterchability of the polymer. The rounded microchannel is typically replicated and is the characteristic feature of this process.

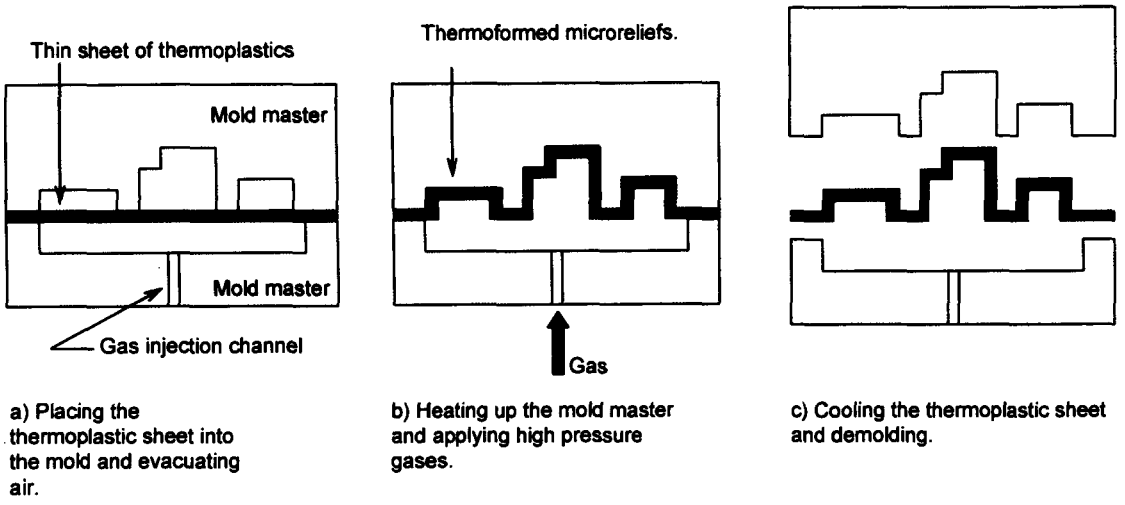

Figure 2.11. Typical sequence of the thermoforming: a) placing a thermoplastic sheet under the mold master and evacuating the air, b) applying the heat and high gas pressure to force the soften polymer sheet to conform the mold shape, and cooling the plastic sheet, and c) demolding the parts.

The replication of various metals using casting techniques has been around since Bronze Age. Interestingly, the basic casting technique is widely used in micromolding microfluidic devices via casting PDMS elastomer over SU-8 molds. This technique was first developed at Harvard University (Duffy et al., 1998) and was referred to as soft-lithography. Further discussion is omitted here as this process has mentioned in the previous section.

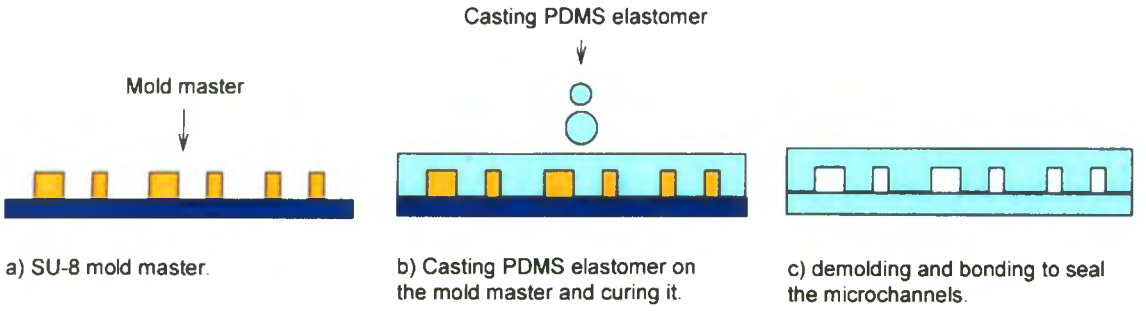

Figure 2.12. Casting PDMS elastomer on a SU-8 mold master to replicate microchannels.

2.7 Post Processing

Post processing is often referred to as the packaging and assembling of LOC devices. The post processing would be bonding and sealing of the devices, calibrating the electrical signals of the production batch, or functionalizing the devices by embedding subsystems such as electrical sensors or optical detectors. Bonding and sealing of the microchannels are critical to ensure the LOC devices delivering a consistent and correct analysis. Often fluidic connections such as holes for syringe needles are needed. The bonding method depends heavily on the type of polymer materials in use, for example, the PDMS microchannels can be bonded and sealed permanently by treating the surface with oxygen plasma and pressing two PDMS layers together (Jo et al, 2000). The first example of the MEMS gas chromatography system (Terry et al., 1997) had the microchannels sealed using adhesive tapes which is, sometimes, desirable because the low bonding temperature.

2.8 Concluding Remarks

This chapter presented a review of several fabrication methods for creating micromold masters that can be used to manufacture multiple copies of the desired polymer microfluidic devices. The current micro-replication technologies for microfluidic devices still heavily use photolithography methods, which is the main stream micromachining techniques in MEMS industries. The photolithography typically used to create microfluidic patterns on a mold involves hazardous chemicals heavily in etching and in

electroplating and these chemical wastes are often inevitably released into the environment. Therefore, it is desirable to eliminate or reduce the chemical usage in the fabrication processes.

In the early development, the LIGA method was perceived as a next generation mainstream lithography technique because of the excellent advantages it provided in producing high aspect ratio microstructures. However, the high cost of X-ray sources prevents it from widely used. Subsequently, the simpler, lower cost fabrication methods dominate the research laboratories especially when applications allow the use of low aspect ratio microstructures. To summarize the trend of the current fabrication techniques of mold masters for polymer microfluidic device, it is moving toward developing a fabrication method that is simple and required fewer processing steps. In addition, it is also necessary for the process to be free of chemicals and to use a molding material that is recyclable and low cost.

CHAPTER 3

LCWM FABRICATION METHOD (Laser Cutting, Micro-Welding, and Molding)

3.1 Introduction

Several techniques that have been described in the literature for fabricating micromold masters were presented in the previous chapter. As discussed, photolithography and electroplating are the most common techniques for creating metallic mold masters for the mass production of polymeric LOC devices. The electroplating stage of the manufacturing process often requires several hours or days to deposit the metal at the desired thickness. Furthermore, post-processing operations such as grinding is required to flatten the back of the plated metal because the thickness of the electroplated metallic layer is non-uniform. From a manufacturing perspective, the cost of these expensive micromold masters can be further reduced by minimizing the number of fabrication steps and shortening the overall production time.

In this chapter, the first nonlithographic method for fabricating metallic micromold masters is presented. The proposed manufacturing technique involves using industrial lasers to cut the desired fluidic network pattern from thin metallic sheets and then assemble the relief patterns onto a suitable substrate by microwelding to form the final mold master. The subsequent replication process of creating the polymer microfluidic device involves either casting the elastomer polydimethyl-siloxane (PDMS) or hot embossing the thermoplastic poly-methyl methacrylate (PMMA). For simplicity, the methodology is abbreviated as LCWM (Laser microCutting, Welding, and Molding). To verify the method, several metallic mold masters and replicates with simple microstructures are created and tested for dimensional accuracy and surface roughness. The advantages and disadvantages of using the proposed masters for casting PDMS and hot-embossing PMMA parts are discussed.

3.2 Laser Cutting, Welding, and Molding (LCWM) Method

The LCWM (Laser Cutting, Welding and Molding) method is based on the observation that most microfluidic components (eg. channels, mixers, reservoirs) are planar and the micromolds used to create more complicated three-dimensional network designs can be manufactured by stacking and assembling multiple 2D micro-patterns. The key benefit of the proposed LCWM method of fabricating metallic mold masters is that the production engineer can produce multiple 2D imprint microfeatures as separated mold reliefs and then fuse them together on a common substrate by a suitable joining procedure (ie. microwelding).

Laser micromachining was selected for this task because it is a flexible machining tool that enables the precise cutting of 2D imprint microfeatures. Furthermore, it is a non-contact machining process, which is not affected by the tool distortion problems that regularly occur with traditional mechanical material removal processes such as milling operations. Laser micromachining also has the advantage of being able to accurately cut a large variety of materials such as soft polymers, hardened metals, composites, and brittle ceramics (Ready, 2001; Charschan, 1993).

Unfortunately, laser micromachining is a sequential process which limits its cost-effectiveness to small volume production. This limitation is, however, not a disadvantage if the machining process is being used to fabricate a rigid high-precision tool for large volume production such as a 2D stencil mask or 3D mold master. In this research laser micromachining is used to cut the desired relief patterns and then microwelded by laser onto the metallic substrate to complete the functional mold master. Microwelding has the added advantage of being able to join dissimilar materials. Under optimal process parameters, the weld pool can be made as small as 50 to 100μm in diameter with a relatively smooth surface finish. The non-contact nature of laser welding also makes it a viable joining technique for creating metallic parts with fine features.

As illustrated in Figure 3.1, the two basic steps involved in creating a mold master using the LCWM method involves laser machining the desired relief patterns and then laser microwelding the cut patterns onto the metallic mold substrate to form the completed mold master. The sequence can be repeated if the design goal is to create a

more complicated multi-level microchannel master. Furthermore, the same proposed method can be used to fabricate metallic masters for either casting soft elastomers or hot embossing thermoplastic sheets. The simple two-step process makes the LCWM method easy to implement and very cost-effective. If the mold master becomes damaged during production then it can be easily repaired or rapidly replaced, minimizing the expensive downtime.

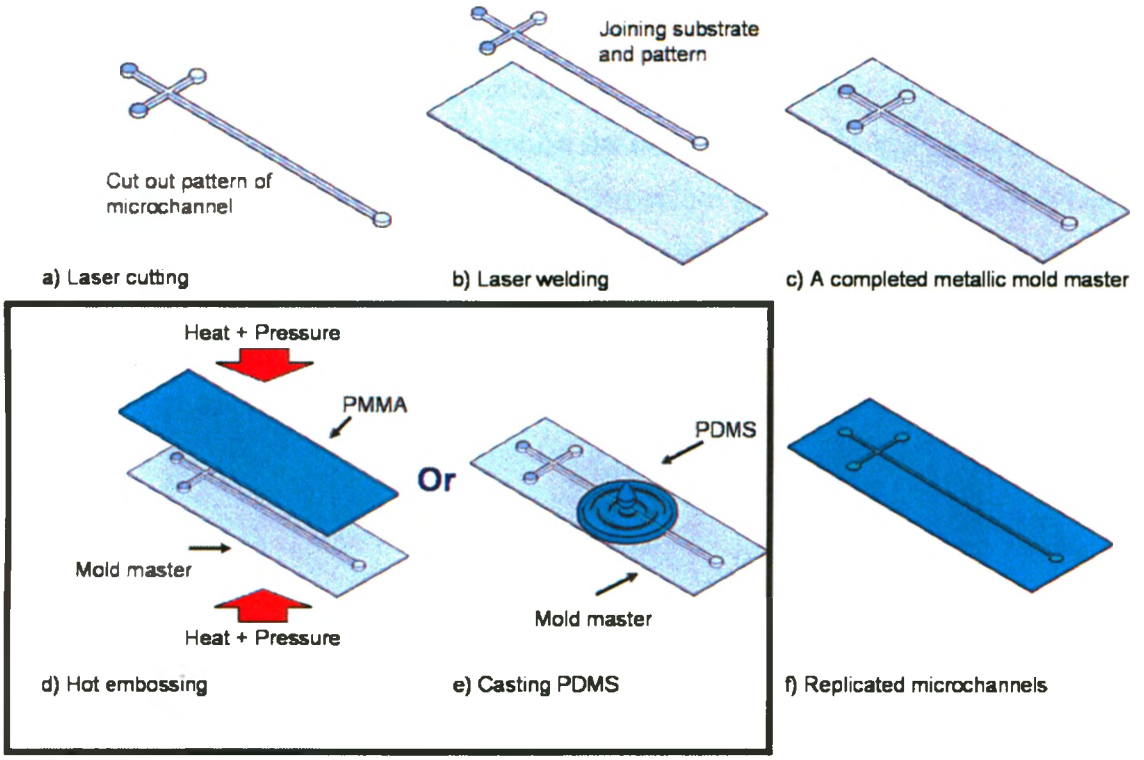

Figure 3.1 LCWM microfabrication process for creating polymeric microfluidic devices: (a) laser micromachining of the microchannel pattern, (b) joining the channel pattern components by laser microwelding onto the substrate, (c) a completed mold master, (d) hot embossing (HE) of PMMA sheet with the mold master, (e) casting elastomer (PDMS) with the mold master, curing, and demolding, and f) the final replicated part.

3.3 Experimental Validation and Results

Several micromold masters were produced to experimentally validate the LCWM method. The desired pattern of the microfluidic channels were first cut in a 50μm thick sheet of low-carbon steel using a laser cutting station equipped with an AVIA UV laser from Coherent Inc., USA. The laser has 3.0 Watts of power at 20kHz with a pulse duration of less than 40 nanosecond at 60kHz. Laser micromachining was conducted under atmospheric pressure and done with air-assistance. Figure 3.2 shows the laser micromachining system, focusing optics, and an X-Y-Z motion stage. Appropriate controller software was used to synchronize the laser cutting and work piece movement. For this study, the laser microwelder was a Starwelder 6002 model from Rofin-Basssel Inc., Germany. The welding process parameters (pulse profile, pulse duration, power level, and spot size) were optimized to produce a smooth surface finish at the weld pool.

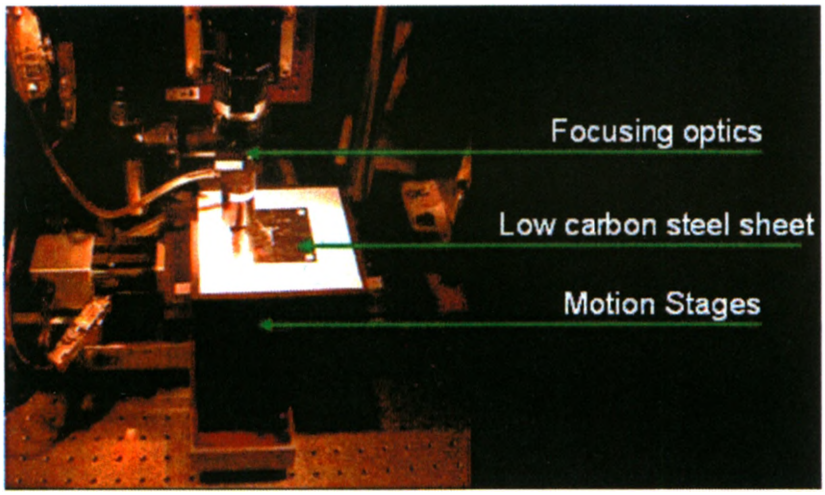

Figure 3.2 Laser micromachining system used in the experiments including focusing optics to accurately deliver the laser beam to the substrate, a concentric gas nozzle to protect the optical system from particles, and a precision motion stage to translate the substrate during microfabrication.

3.3.1 Soft-molding PDMS

The sequence of steps in fabricating the LCWM metallic master and polymer device is shown in Figure 3.3. The microfluidic mixer was originally designed using Mastercam CAD/CAM software. To assist with the alignment of the metallic imprint pattern onto the substrate during the welding operation, the alignment sheet, microfluidic pattern, and the master substrate were all cut from the same 50μm thick low-carbon steel sheet. This reduced the manufacturing time because it would not be necessary for the technician to change materials during the process. It took approximately 25 minutes to laser-cut the Y-channel relief, with 15 passes at 50mm/min cutting speed. The relief was then ultrasonically cleaned in water to remove debris and the ferrous oxide created during the laser cutting process. The time used in laser welding the fluidic pattern onto a substrate was mostly spent on setting up. The laser welding spot took only a few milliseconds.

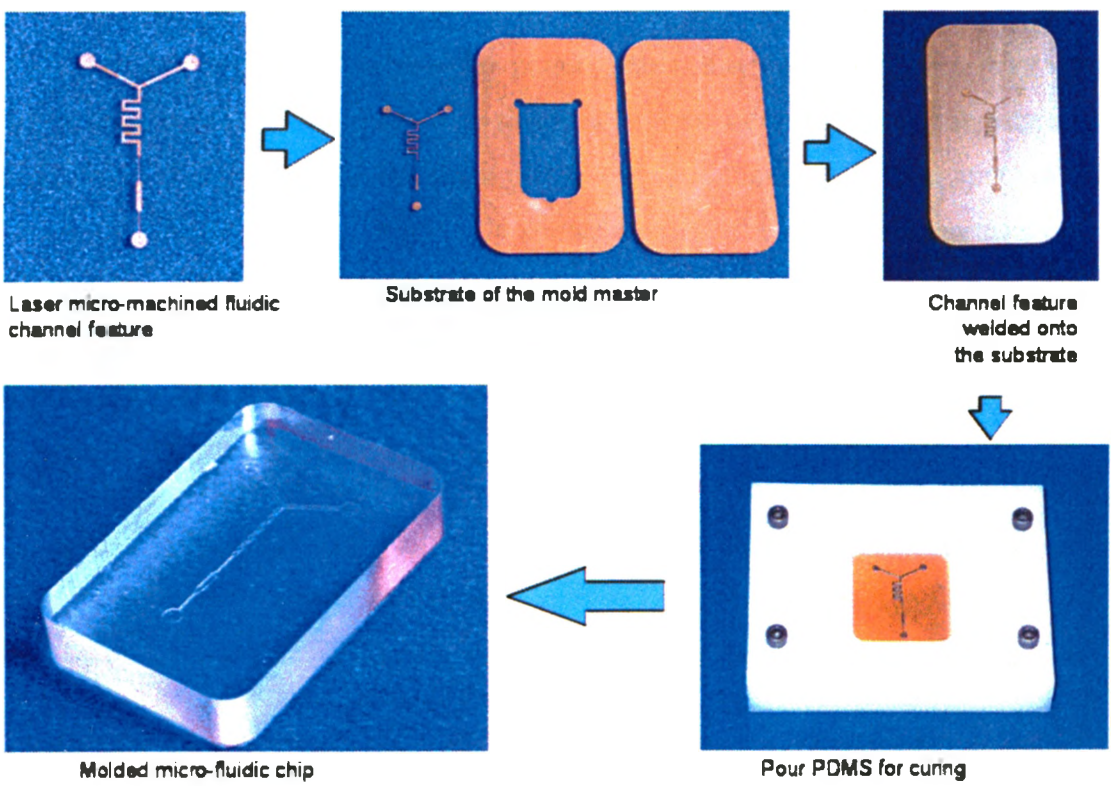

Figure 3.3 The sequence of steps used to produce a micromold master using the LCWM method and an example of the final molded PDMS part.

A number of laser cutting tests were conducted to find optimal parameters for best cut edge quality. Table 3.1 indicates the approximate correlation between roughness and smoother cut edges found in this setup. Equipment settings were as follows: UV wavelength laser, air assisted cutting, 10X beam expander, and 5X focusing objective that delivers the beam diameter to about 10-15μm at focus.

Table 3.1 Laser micromachining process parameters, 15 passes

Power density [W]	Feed rate [mm/min]	Pulse frequency [kHz]	Observed edge quality
0.24	25	1	rough
1.38	25	10	smooth
0.60	40	10	smooth
0.60	50	10	excellent

The cut Y-channel micromixer pattern relief was then welded by laser onto a ~50μm thick stainless steel sheet. The majority of time used in welding the pattern onto the substrate was spent on set up. Once properly aligned the laser welding spot took only a few milliseconds to form. Figure 3.4 shows the optical profiler measurements of the weld pool at the reservoir location of the microfluidic network pattern. The process parameters were: 309J/cm^2 pulse density, shielding gas Argon, 0.66J pulse energy, 1.3ms pulse length, spot welding, and level-and-decline pulse shape. The average surface roughness (Ra) at a weld spot was measured and found to be about 500 nm.

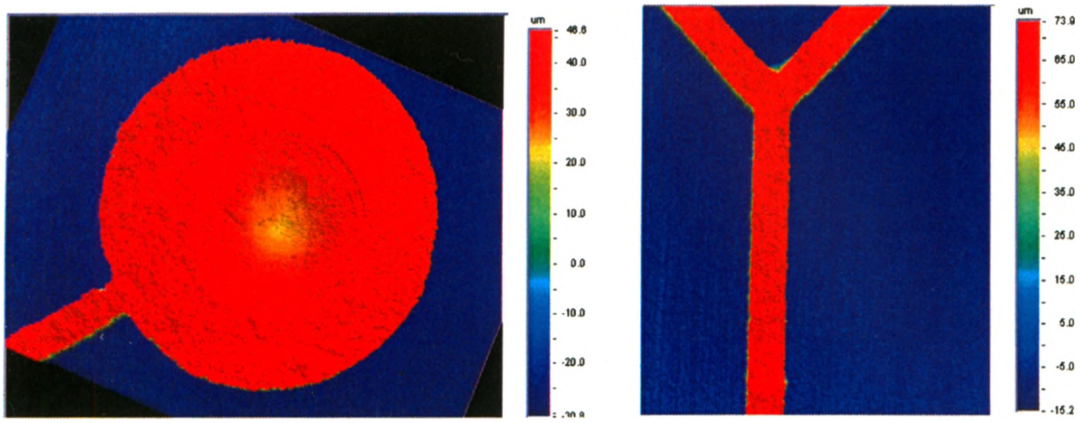

Figure 3.4 Weld pool at the inlet location (left) and Y-channel mold, positive relief (right), taken by an optical profiler.

To assist with the microwelding process a permanent magnet was placed under the stainless steel sheet to provide a magnetic force to hold the Y-channel component tightly to the substrate surface. It was necessary to hold the part firmly because Argon gas, at 20Psi pressure, was supplied into the welding chamber to reduce the impurities formed in the weld pool.

Once completed a thermosetting polymer molding method was used to create the replica PDMS device, Figure 3.5. In this study a Wyko NT1100 optical profiling system from Veeco Instruments Inc., NY, USA, was used to measure the surface roughness and visualize the quality of the 3D features created in the mold master. Figure 3.5(a) provides the optical profiler measurement where the sidewalls of the microchannel are nearly vertical with an average surface roughness Ra that is much coarser than the top of the microchannel relief. The surface finish at the top of the microchannel relief was similar to the metallic sheet material, about 300-600 nm Ra. The rougher surface finishes at the sidewalls of the microchannels are typical for the laser cut surface.

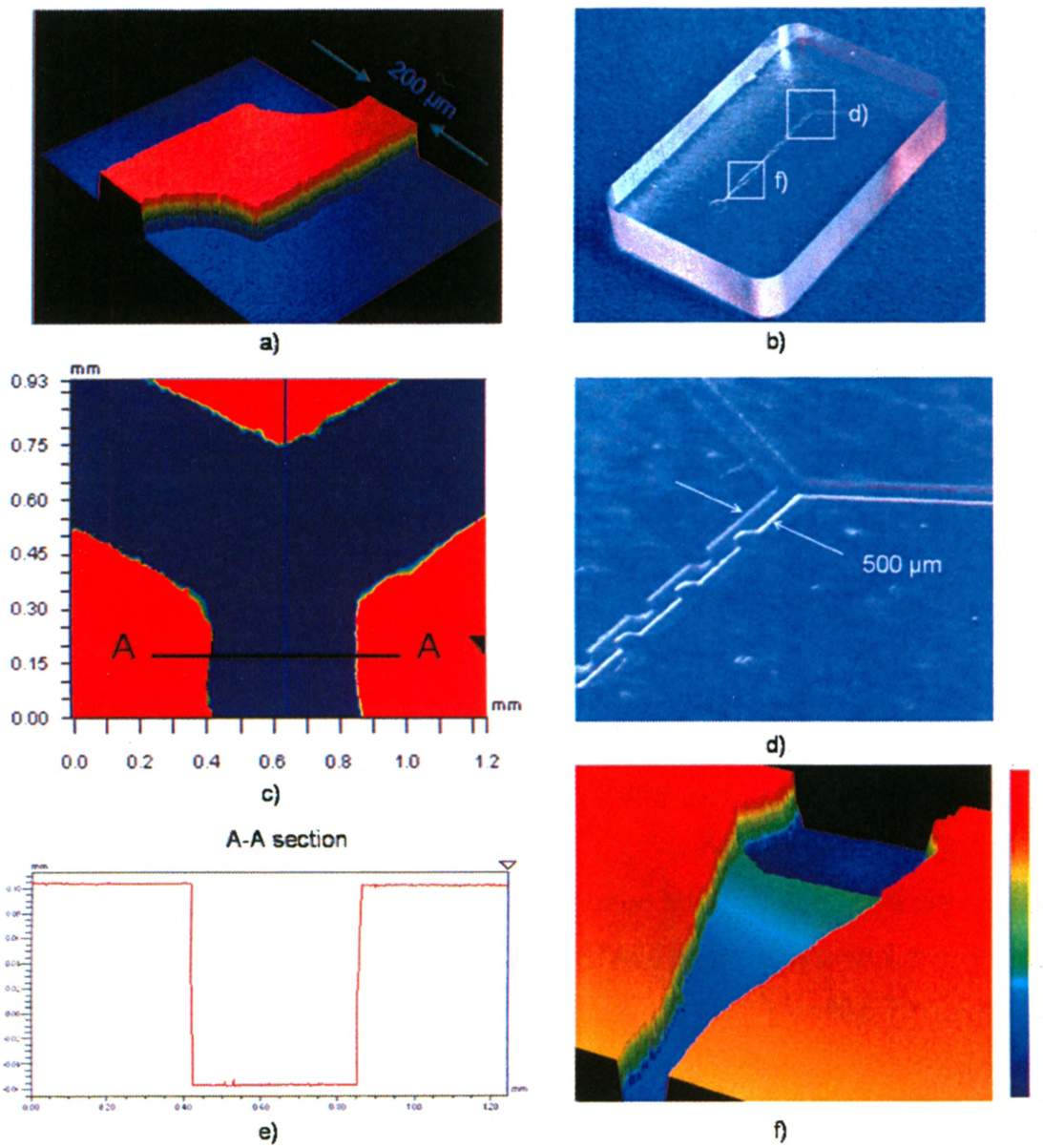

Figure 3.5 (a) LCWM metallic mold master surface roughness, 500nm Ra, rougher microchannel wall surface quality is shown, (b) molded PDMS microchannels, (c) the measurement of optical profiler at the Y-channel junction showing the good "flatness" of the microchannels, (d) a closed-up optical microscopic view of the Y-channel, (e) A-A sectional view of the PDMS microchannel, and (f) optical profiler generated view of the multi-layer molded microchannel.

Figure 3.5(b) shows an example of the PDMS microchannel part produced from the micromold. The white squares on the photo hi-light the locations that are enlarged in Figures 3.5(d) and 3.5(f). Figure 3.5(c) provides a top view of the optical profiler measurement for the molded microchannel. Reasonable "flatness" of molded microchannels is observed and the cross-sectional view also confirms that the replica has a good surface quality. Figure 3.5(d) is an optical microscopic view of the close-up of the molded PDMS microchannel. The optical profiler measurements of a two-level PDMS molded microchannel replicated from a multi-level master is illustrated in Figure 3.5(f). Unfortunately, there is some difficulty in aligning second level to the first level of a multi-level mold master.

3.3.2 Hot-embossing PMMA

Hot embossing process (HE) of thermoplastics using the fabricated mold masters were also investigated to observe the flexibility of the LCWM method. The hot embossing step of the proposed method was conducted using the Multi-purpose Press from GEO Knight & Co. Inc. The press is capable of applying a pressure from 140 to 550kPa (20 to 80Psi) with temperatures from 66 to 220^0C. The LCWM mold master was placed onto a 1.5mm thick PMMA substrate. Process parameters were determined empirically. The parameters included HE temperature about 130°C, HE pressure about 207kPa (30Psi) and HE time about ten minutes and de-embossing temperature at 90°C.

As discussed in Chapter 2, the use of thermoplastics as the substrate for microfluidic devices has a number of advantages, such as low cost of materials, rigid substrate, easily formed during molding, requires a short processing cycle – especially for the injection molding process, and provides a wide range of bio-compatible polymers for different applications. Thus, if the hot embossing molding process could be employed with the LCWM method, the LCWM method could be a robust technique in fabricating mold masters for replication of polymeric microfluidic devices.

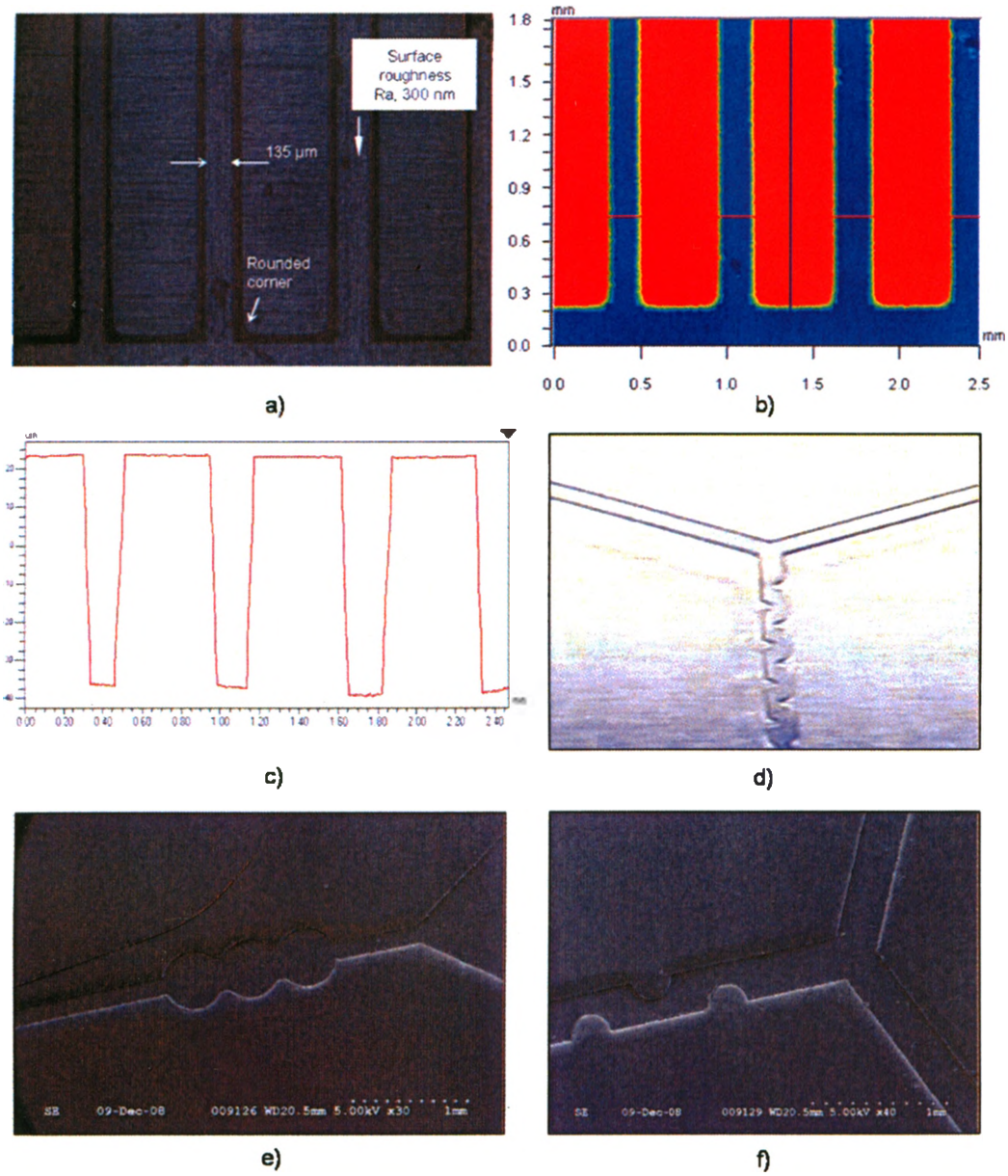

Figure 3.6 (a) The HE PMMA microchannels, Ra about 300 to 400nm, HE temperature at 155°C, de-embossing temperature at 100°C, HE pressure at 40Psi for 10 minutes. (b) Good flatness of the HE microchannels, taken by an optical profiler, (c) cross-sectional view of the PMMA HE microchannels taken by an optical profiler, (d) a microscope view of molded PMMA hot embossed Y-microfluidic channel, (e) an SEM view of a section of the PMMA HE microchannel with draft angle, and (f) an SEM view of the Y-microchannel as shown in (f).

The experimental results demonstrate that it is possible to successfully hot emboss thermoplastics with the LCWM mold master. The metal substrate was about 150μm thick, slightly thicker than the substrate used in casting PDMS. The thicker substrate was necessary to support the structure through the thermal cycle. Figure 3.6 shows a series of views of the results of HE microchannels using the fabricated LCWM master. Figure 3.6(a) shows that a number of various widths of microchannels were hot embossed to identify the suitable process parameters for subsequent tests. The molded corners were slightly rounded which are similar to the results found in the published literatures. The surface quality was observed, about 300 to 400nm Ra, which is slightly better than we found in the PDMS molded microchannels. The better surface finishes of these PMMA molded microchannels than the ones created on PDMS may be explained by the soften polymer having residual forces after the molding pressure was released and forces caused the material regain its equilibrium state. Subsequently, limited soften polymer can smooth out the surface roughness at the nano-scale.

Figures 3.6(b) and (c) show the measurements captured by Wyko optical profiler. HE microchannels had some draft angle and the channel bottoms were not as flat as the molded PDMS microchannels found. As a result of the applied heat and pressure factors the mold master was distorted during hot embossing, it is expected as a higher strength of material of the mold master is required. Subsequently, the microchannel size, thickness and the number of welding spots were increased to strengthen the mold masters. The results found that the damages to masters during hot embossing are reduced. Figure 3.6(d) shows the closed-up optical microscopic view of the PMMA Y-microchannel. Figure 3.6(f) and (e) show SEM views of the PMMA microchannel having tapered shape of cross-sectional microchannels.

Figure 3.7 shows the SEM view of the HE replicated microchannels that has near vertical walls, however, the sidewalls of these replica microchannels were rough due to the soften PMMA adhering to the coarse laser cut edges.

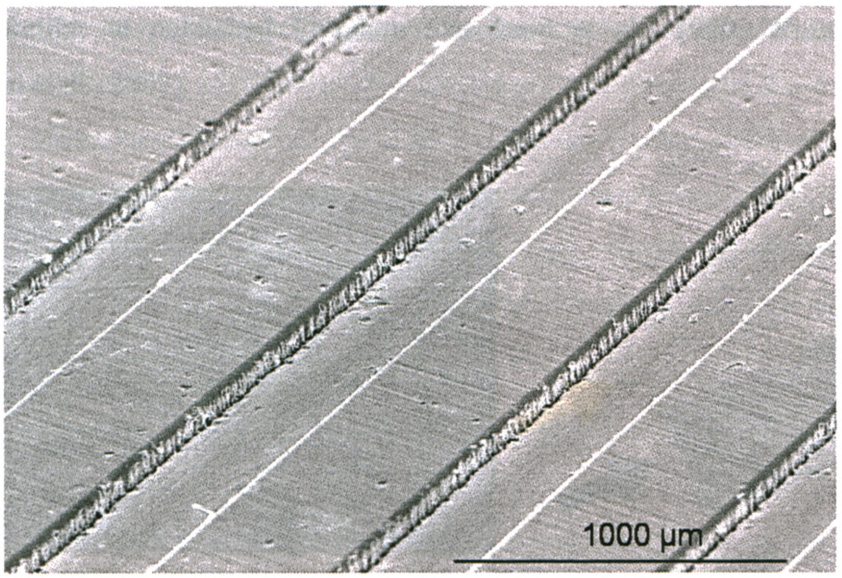

Figure 3.7 An SEM view of the hot embossed microchannels produced by using the LCWM mold master.

3.4 Design and Testing of a Passive Micromixer

A PDMS Y-channel micromixer was created to illustrate the process. The PDMS microfluidic mixer chip shown in Figure 3.8 was injected with colored waters to test the sealing of microchannels and to determine the maximum sustainable pressure in a reversible PDMS-PDMS bonding. The Y-channel micromixer was able to sustain up to 1.2Psi pressure before leaking. If higher fluidic pressure is needed for its intended application, using oxygen plasmas to create permanent sealing of the PDMS chip may be selected.

Typical syringe pump installed with two syringes, blue and yellow colored waters, was used to provide steady streams of fluidic flow injecting into the PDMS microchannels. The flow rate in these flow channels was about from 0.2 to 10µL/min. The observation of the mixing of two colored waters using the fabricated micromixer shows that micromixing fluids is dominated by molecular diffusion under laminar flow

condition similar to published literature (Jacobson et al., 1999; Whitesides, 2006; Vijiayendran et al., 2003).

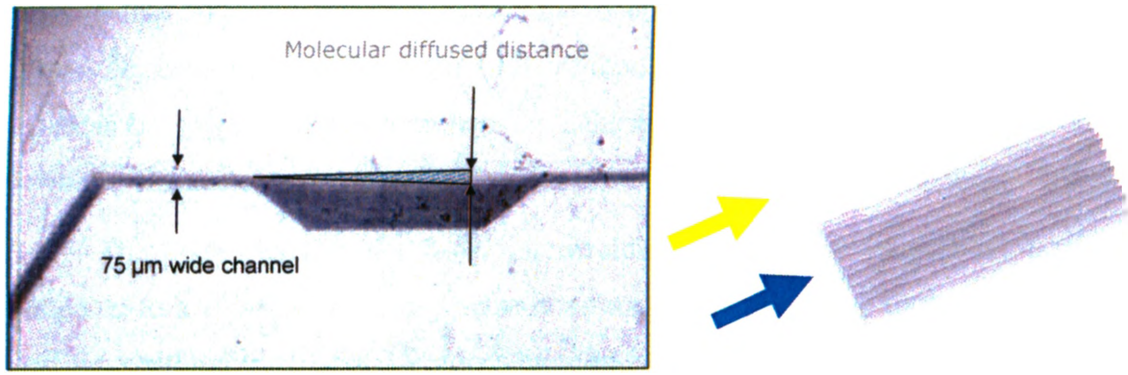

Figure 3.8 PDMS Y-channel micromixer, about 75µm width 50µm height, to observe the sealing. (a) Y-channel micromixer mixing of two colored waters (blue and yellow) and (b) 3D intensity graph observation of the diffusion process between two colored waters.

3.5 Discussion

The experimental results demonstrated that the LCWM mold masters can be successfully utilized for producing polymeric microfluidic devices via casting PDMS elastomers and hot embossing of thermoplastics. This was further illustrated by designing, fabricating and testing a simple passive micromixer. However, a number of critical issues related to the fabrication of the LCWM mold master and replicated parts need to be discussed in greater details.

3.5.1 Fabrication of LCWM mold masters

A key step in fabricating the LCWM micromold master is the assembly and joining of the cut positive relief patterns onto the substrate. One critical aspect of the microfabrication is to ensure a small welding gap because an excessively large gap will cause the material to be vaporized by the laser beam energy. In other words, a large gap will result in a hole being drilled rather than a desirable weld pool being created. Theoretically, the welding

gap should be no more than 5% of the thickness of the thinnest material being welded (Ready, 2001). However, establishing this minimum requirement of the welding gap is very problematic at the microscale. For example, the low carbon steel sheet used in this study is only 50μm thick and, therefore, the theoretical maximum weld gap is 2.5μm. To ensure the success of forming a desirable weld pool and, therefore, to reduce the gap size, a permanent magnet is placed below the substrate to provide magnetic forces holding down the Y-channel component.

The pulse duration for laser microwelding is relatively long about 1 to 2ms, compared to a short laser cutting pulse duration, 10 to 30ns. Due to the lengthy pulses used for welding, the material around the joint is heated for a longer period resulting in dimensional distortions. It is essential, therefore, additional care should be taken by the technicians in selecting the optimal laser welding process parameters in an effort to reduce the effects of the thermal distortion.

The surface roughness of the metallic sheet also directly influences the quality of the final vertical and horizontal surfaces of microfeatures (eg. microchannel). The laser beam interaction with the material during cutting operations determines the surface quality of the resulting vertical walls. Therefore, low carbon steel sheets or stainless steel sheets were used as the substrate because of the good surface finish and the ease in which the material can be laser welded. Furthermore, using low carbon steel and stainless steel in welding minimizes the problems arising from joining dissimilar materials such as material cracking and separation caused by different shrinkage factors in the two materials.

A multi-level mold master was investigated by repeating the same fabrication procedures to create multiple laminated levels. However, the alignment of each additional level became more difficult. For the preliminary experiment, the welding process involved manually in positioning the second level onto the first with a misalignment of approximately 25 to 50μm. This problem may be minimized using post-processes, such as micromilling or microEDM (Electro-Discharge Machining), to alter the final dimensions of mold masters but these additional steps will increase the overall fabrication cost and production time.

3.5.2 Part replication via casting and hot embossing

Replicating passive micromixers by casting of the PDMS is simple and easy, without the need of expensive equipment. It only requires a vacuum chamber to degas the PDMS. In this study, the PDMS micromixers were created by pouring PDMS over the mold and curing the resultant material for 48 hours at a room temperature. The curing speed can be increased by elevating temperatures and the PDMS parts were demolded easily.

Hot embossing (HE) thermoplastics, such as PMMA, also produced good quality results from the LCWM mold master. The successfully replicated microchannels were approximately 150μm wide. The smaller microchannel structures were not able to stand the applying HE pressures and temperatures. The problem may be associated with the excessive filling of PMMA materials that increased the demolding frictions as a result the master was damaged. The laser machining naturally cuts the sidewalls with a slight drafted angle, which was initially thought to be an assisting function for demolding parts, yet it is not the case. One way of improving the sidewall surfaces is to under filled the microchannels where created tapered cross-sections and rounded corners to lower demolding frictions. The experiments demonstrated less damage done by demolding.

Each hot embossing cycle took 30 minutes. Cooling time was the main contributing factor with about 20 minutes because slower natural cooling was used to minimize the residue stresses of the molded parts. If the hot embossing tool was equipped with a better temperature control system, the embossing time could have been optimized and shortened.

3.5.3 Advantages and disadvantages

The advantages of the hot embossing thermoplastics, such as PMMA, can be summarized by the following. The HE process only requires simple and relatively low cost production equipment. It is suitable for either medium or high volume production. A wide range of bio-compatible thermoplastics can be selected for hot embossing the final replicated parts. The material costs are relatively low. Furthermore, using a recyclable thermoplastic is possible (after the removal of bio-hazarded materials). Therefore, the fabrication process

is relatively inexpensive and environmental friendly for creating disposable microfluidic devices.

Casting PDMS to replicate microchannels produces near vertical sidewalls while slight drafted angle ones are produced in HE ones. The selection of HE process parameters is important to control the draft angle which may be beneficial to assist demolding and to prolong the tool life. In addition, near optical quality surface finishes of sidewalls were observed when inclined sidewalls were never in contact with the laser cut surface. This is desirable if the intended application permitted the use of non-rectangular channels.

A similar average surface roughness Ra was observed on both the PDMS and PMMA microchannels, roughly 300 to 500μm. In fact, these values are similar to the metallic sheet surface finishes of the master. However, this is only considering the locations of non-laser welded mark. Each additional weld mark increases the surface roughness. Ideally, increasing the number of welding spots enhances the master strength and, therefore, more durable.

For replicating high accuracy of microchannels, casting PDMS is recommended over HE PMMA. For a shorter cycle time, hot embossing the thermoplastics may be better suit but the PDMS can be cured in 10 minutes at 70 to 80°C. The rapid fabrication of LCWM master reduces the production downtime and, therefore, saves costs. It is relatively low cost to produce the LCWM master, in terms of both materials and labor hours; therefore, a few backup masters can be fabricated in advance. Unique advantages and disadvantages exhibits by the two molding processes tested. Even with these limitations, the LCWM method still is a cost-effective method to build the mold masters for microfluidic devices.

3.6 Concluding Remarks

A nonlithographic technique of fabricating metallic micromold masters was introduced and experimentally demonstrated. The LCWM (Laser Cutting, Welding and Molding)

method is based on the observation that sophisticated microfluidic network designs can be manufactured by stacking and assembling multiple 2D microrelief patterns.

The developed LCWM method can also be used to fabricate metallic masters for either casting soft elastomers or hot embossing thermoplastic sheets. In general, the LCWM process is a simple two-step process that is easy to implement and relatively cost-effective when compared to the more commonly known LIGA method. The use of low-cost materials for creating the LCWM mold master also reduces the total fabrication cost. An additional advantage of the nonlithographic technique is that if the mold master becomes damaged during the actual part production then it can be repaired easily or replaced rapidly, minimizing the expensive downtime.

The prototypes and experimental results validated the notion that it is possible to construct functional and accurate micromold masters by combining laser micromachining and microwelding processes. Although the LCWM method is very simple and quick, the width of the microstructures is limited to about 75μm.

CHAPTER 4

LEDM^2 FABRICATION METHOD (Laser cutting, Electro-Discharge-Machining, and Molding)

4.1 Introduction

The rapid microfabrication technique introduced in Chapter 3, termed LCWM method, has several design limitations including the inability to produce high-quality microchannels that are less than 75μm wide. Although this may be sufficient for many practical microfluidic and LOC applications, it is not ideal for all possible situations. An alternative nonlithographic method for fabricating metallic micromold masters with smaller microfeatures is described below.

The second proposed method of manufacturing micromold masters combines the advantages of rapid and flexible laser micromachining with the capabilities of microEDMs to machine various difficult-to-cut conductive materials. This microfabrication technique is abbreviated as LEDM^2 (Laser cutting, Electro-Discharge-Machining, and Molding). The key innovation is that LEDM^2 enables hardened metallic micromold masters to be directly produced without introducing additional steps that may cause dimensional inaccuracies. In addition, longer tool life is expected because harden steels can be used as the substrates.

4.2 Constructing Metallic Micro-mold Masters using LEDM^2

The construction of a metallic mold master using the proposed LEDM^2 methodology requires two basic steps as shown in Figure 4.1. First, a two-dimensional (2D) mask is created by laser cutting the "negative" relief of the microchannel profiles on a thin brass sheet and the positive microchannel structure is then imprinted on a metallic (brass) substrate by the microEDM die-sinking process. Once completed, the substrate with the patterned relief is used in a poly-dimethyl-siloxane (PDMS) casting process by pouring

the PDMS polymer over the micromold master and allowing the material to cure. Once cured the replicated part is demolded and assembled with the other microsystem components to form the final device.

A very attractive feature of the proposed LEDM^2 method is that the material of the final master is a harden metal that is able to sustain high pressure and temperature in injection molding of thermoplastics for an extensive number of molding cycles. Thus, it makes the LEDM^2 suitable for mass production of microfluidic devices. Any of electrical conductive material can be employed in fabricating mold masters using the LEDM^2 method. This is unlike the LIGA method where only Nickel based materials can be used to create the masters.

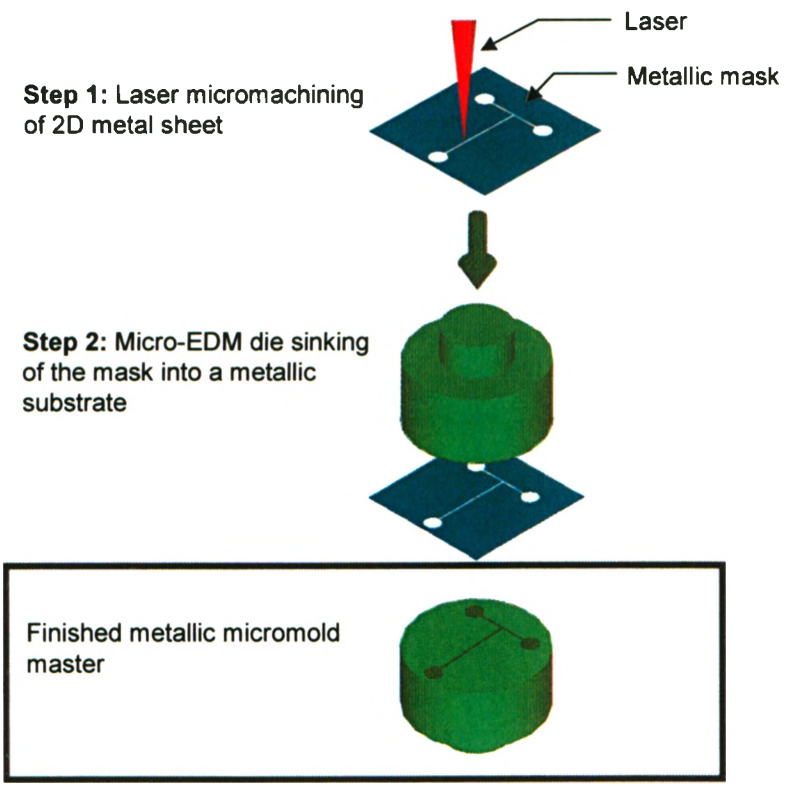

Figure 4.1 The steps used to create a metallic micromold by laser and microEDM machining.

4.3 MicroEDM Fabrication Process

Electro-discharge machining (EDM), or spark eroding, has been proposed as a method of fabricating micro-scale features in metallic substrates. In the late 1960's, Van Ossenbruggen (Van Ossenbruggen, 1969) was one of the first researchers to describe the microEDM process. It wasn't until the 1980s that other researchers used the technology for applications such as drilling 15 to 300μm holes for ink-jet printer nozzles (Sato et al., 1985). More recently Masuzawa et al. (Masuzawa et al., 1989) described how high aspect ratio (10:1) microholes could be drilled using an EDM with a 50μm diameter electrode. The authors further developed the process of microEDM machining where a cylindrical tool electrode, similar to a milling tool, was moved through a contour tool path to fabricate 3D features (Masuzawa et al., 1994). Flescher et al. (Fleischer et al., 2006) introduced a technique for combining both the electric discharge machining and laser ablation to fabricate microstructures. The authors also report an increase in productivity by first machining a large volume block of material via EDM and then performing laser ablation for creating the fine microfeatures.

The EDM process provides several key advantages for creating a micromold master that can be used in large production runs. As the individual features and overall microfluidic network that is patterned on the mold masters becomes smaller, it is necessary that microstructures be produced from a material with very high strength to prevent dimensional distortions during hot embossing or injection molding. Unfortunately, hardened tool steels are very difficult to machine using conventional material removal processes. However, micro-electrodischarge machining (microEDM) is capable of accurately machining any electrically conductive material regardless of its hardness and strength. The material removal mechanism of the microEDM is based on the spark erosion effect that can generate a temperature of nearly 8000 to 12,000°C which causes the targeted material to be removed through melting and sublimation. These sparks are created by separating positive and negative electrodes with a small gap and then applying high voltage.

Micromold features can be created using a very small electrode with a typical length of 50μm and diameter of 5 to 50μm. Although photolithography techniques can

produce smaller sized features, the microEDM approach does permit the creation of dimensional sizes that are sufficient for many practical applications in life sciences which usually in the dimensions of 10 to 100μm width microchannels.

From a design perspective, it may be necessary to rapidly modify mold parameters during the preproduction phase. The geometric dimensions of the patterned metallic mask can also change dramatically after the EDM die-sinking process and, therefore, the mask cannot be reused because of the electrode tool wear. It is important to remember that the same spark that creates the mold will also erode the tool electrodes significantly but at a different rate (Guitrau, 1997). Laser micromachining is selected to minimize the cost of fabricating the metallic masks because laser machining is fast, flexible, and produces consistent and accurate 2D cuts on thin metallic sheets.

4.4 Experimental Prototype

4.4.1 Passive T-mixer design

To validate the proposed manufacturing method a brass master for molding a microfluidic T-mixer device, Figure 4.2, is produced. The brass master is then used to replicate a T-mixing device from PDMS elastomer. Lab-on-chip devices are comprised of several different components such as micropumps, micromixers, separators, filters, reaction chambers, and liquid reservoirs. The microfluidic mixer is particularly important in analytical systems because it permits the controlled mixing of chemicals and bio-reagents.

The suitability of the proposed fabrication method was evaluated by examining the geometric accuracy of the microfeatures and quality of surface finish for both the brass micromold master and the sample device. All the channels of the T-mixer chip in Figure 4.2 are about 50μm wide and interconnect to three reservoirs: two input reservoirs, and an output reservoir. All the reservoirs are 1.5mm in diameter.

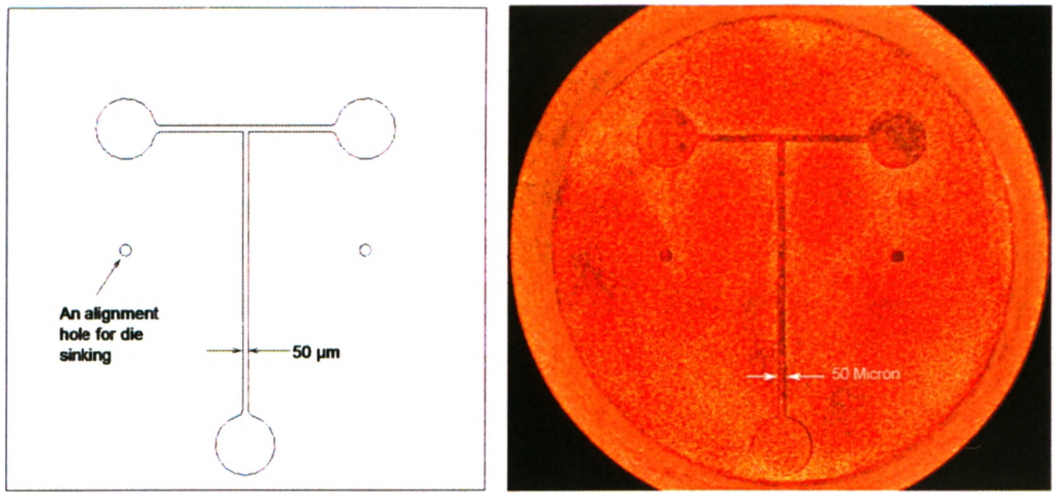

Figure 4.2 The design pattern for the mask T-channel microfluidic mixer and a microscopic view of the fabricated brass micromold master.

4.4.2 Fabrication of prototype

The masks with the microfeatures associated with the channels and reservoirs were initially cut on a 100µm thick brass sheet using the AVIA UV laser from Coherent Inc., USA. The laser had 3.0 Watts of power at 20 kHz. For fabrication purposes, the pulse duration of the laser was set to less than 40 nanoseconds. The laser cutting was conducted under atmospheric pressure and done with air-assistance. The air-assisted condition of laser cutting was used primarily to provide protection to the laser optics. After laser cutting, the mask was cleaned in an ultrasonic bath to remove the debris and oxides from the part. The geometric accuracy of the channels and the reservoirs of the mask were within +/-5µm. The sides of the microchannels were reasonably smooth and within the limits of what can be achieved by nanosecond laser micromachining.

The microEDM die-sinking step of the proposed method was conducted using the MG-NC82 Micro-ElectroDischarge Machining (EDM) system from Panasonic. The voltage was set at 80V with a capacitor of 220pf. The speed of Z-axis die-sinking was set at 1µm/sec. To prepare for the machining process, the mask was immersed in the dielectric oil stage tank, and clamped down. A brass rod of 4mm diameter was mounted

on the rotating shaft and, the brass rod substrate was micro-EDM die-sunken on a flat brass sheet to prepare a parallel surface between the rod and mask for subsequent process. After the parallel surfaces were prepared, the brass rod was microEDM die-sinking to create the final mold master. The die-sinking process took about two days without technician intervention. The substrate was then removed from the system. The ultrasonic bath was then used to clean up the debris deposited on the mold master during die-sinking.

4.5 Experimental Results and Validation

Figure 4.3 shows an SEM view of the T-channel micromixer metallic mold master fabricated via the proposed method. The measured width was about 50μm which is very close to the dimensions of the originally designed mask. The T-intersection of microchannels appears to replicate the sharp corners of the mask fairly well. The SEM view also shows the edges of positive reliefs and that the electro-discharge machined surfaces display no evidence of extreme spark erosion. The debris that was weakly deposited on machined surfaces was largely removed in the ultrasonic bath. Since the debris was easily removed by the ultrasonic bath, it can be concluded that this debris was only weakly deposited during the die-sinking process. Further cleaning would be completed after a few molding cycles.

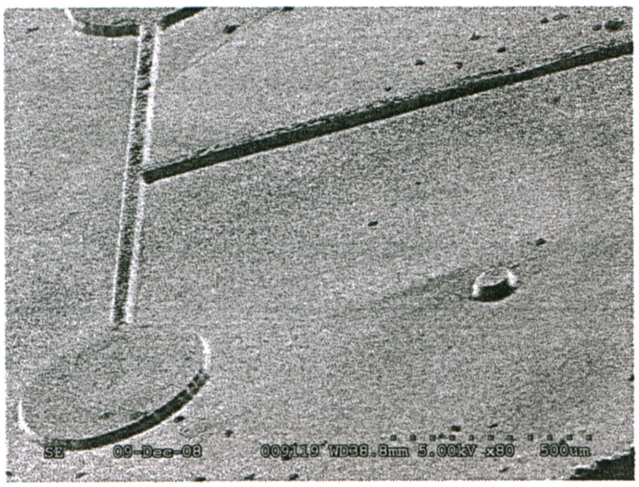

Figure 4.3 An SEM view of the T-micromixer brass mold master.

Figure 4.4 shows the measurement profile of the micromold master captured by Wyko optical surface profiler where the scale of the Z-coordinates has been enlarged. The experimental results show an average surface roughness of 400nm Ra for the finished feature. These measurements indicate that the electro-discharge machined walls of microchannels are slightly inclined which appears to be caused by the electrode wear of the mask tool during the die-sinking process. The inclined microchannel walls also suggest that the level of spark erosion across the positive relief and the wear rate are reasonably stable. One advantage, from a manufacturing perspective, is that the inclined microchannel walls will assist the demolding process by reducing friction between molded polymer and mold master.

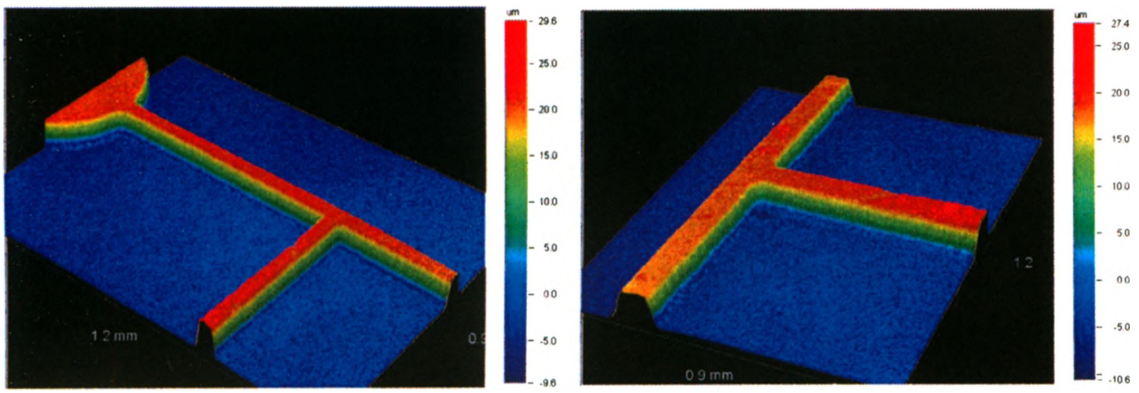

Figure 4.4 Three-dimensional measurements of the T-micromixer mold master taken by the Wyko optical surface profiler.

The cross-sectional views of the mold master, with a 25μm machined height, in the X and Y directions are provided in Figure 4.5. The corners at the peak of the positive microchannel feature are observed to be slightly sharper than at the bottom ones. This was expected because as the die-sinking process continues the tool electrode will wear resulting in a wider opening. This figure also shows that the top surface of microchannels is relatively parallel to the bottom surfaces.

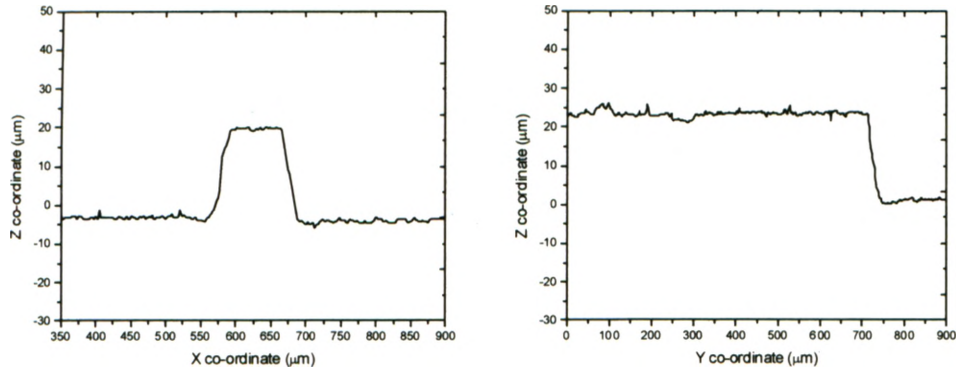

Figure 4. 5 Measured cross-sectional profiles of the brass micromold master along the X-axis and Y-axis, respectively.

A three-dimensional representation of the measured surface finish is provided in Figure 4.6. The surface measurement by the optical profiler shows that a master with a good quality surface finish can be achieved by the proposed LEDM^2 method. Since optical quality surface finishes are not possible with this method, the replicated microfluidic devices created in this manner are more suitable to applications that use electrical or chemical detection methods. The experimental measurement also demonstrates that the spark erosion arising from the electro discharging process was largely uniform across the brass surface.

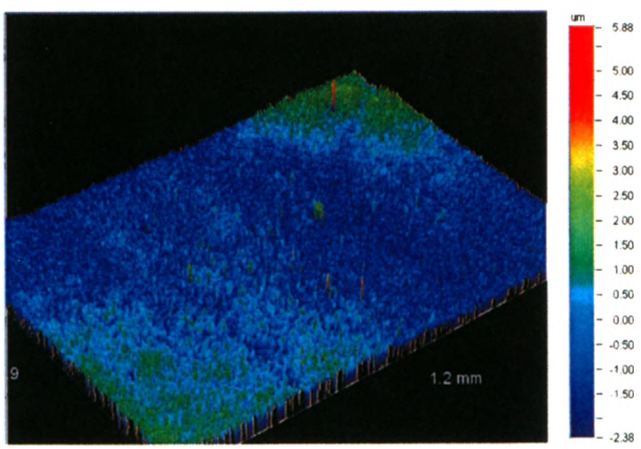

Figure 4.6 Surface finishes of about 400nm Ra after the process of microEDM die-sinking.

Once the metallic master was completed and cleaned with an ultrasonic bath, a pre-mixed and degassed PDMS elastomer was poured over it. The PDMS was left to cure at room temperature for 24 hours and then demolded. Due to the trapezoidal cross-section of the microchannel positive reliefs, demolding was unhindered and no damage the microfeatures were observed in the molded microchannels or the metallic master. The microscopic view of the molded PDMS T-mixer is shown in Figure 4.7. Some weakly deposited debris that attached to the metallic master, during the die-sinking process, was transferred to the molded PDMS channels. Figures 4.8 and 4.9 provide measurements of the PDMS T-mixer device's microchannels via Wyko optical profiler. The depth of the molded PDMS microchannels was slightly less than the height of master, about 5μm less.

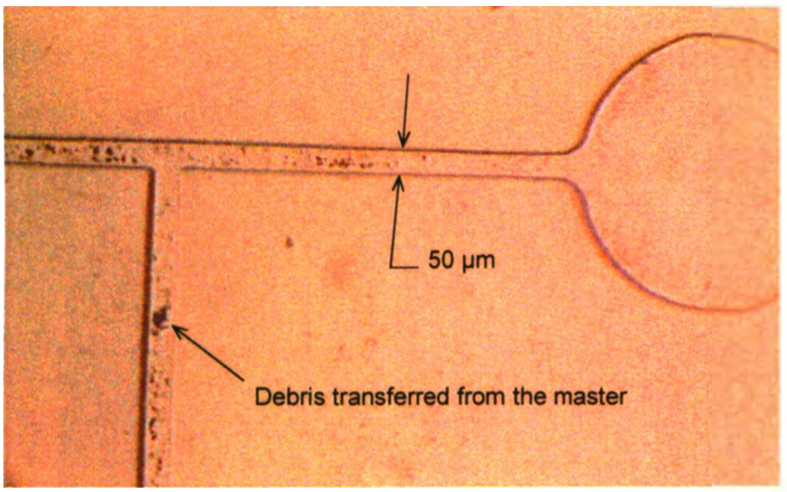

Figure 4.7 The molded PDMS T-micromixer fabricated via the LEDM^2 method.

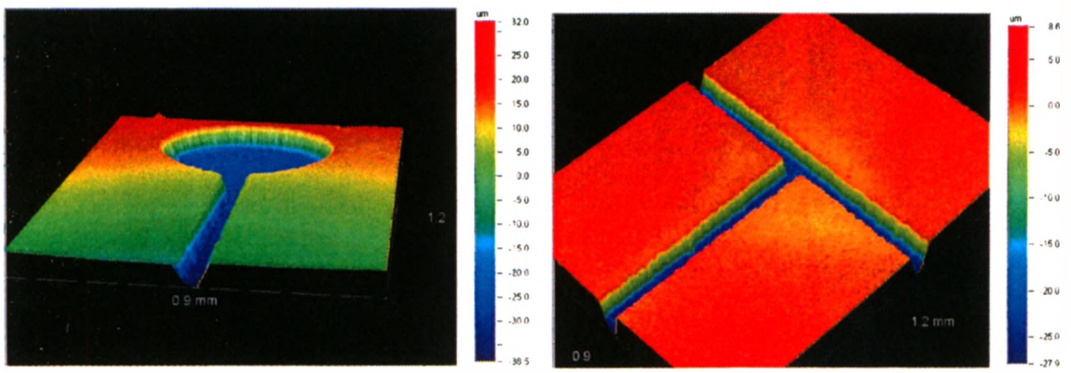

Figure 4.8 Computer generated 3D views of the molded PDMS T-micromixer.

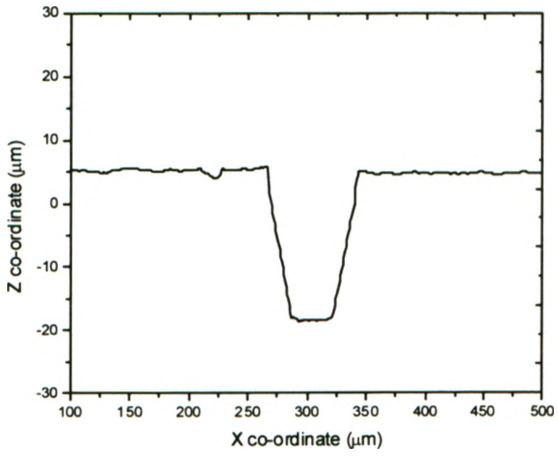

Figure 4.9 Measured cross-sectional profile of the molded T-mixer along the Y-axis.

The surface finish of the molded T-mixer is nearly identical to the surface quality of the mold master. Experimental measurements, Figure 4.10, confirm that the molded part has a similar surface finish to the master, with a surface roughness (Ra) around 350 to 400nm.

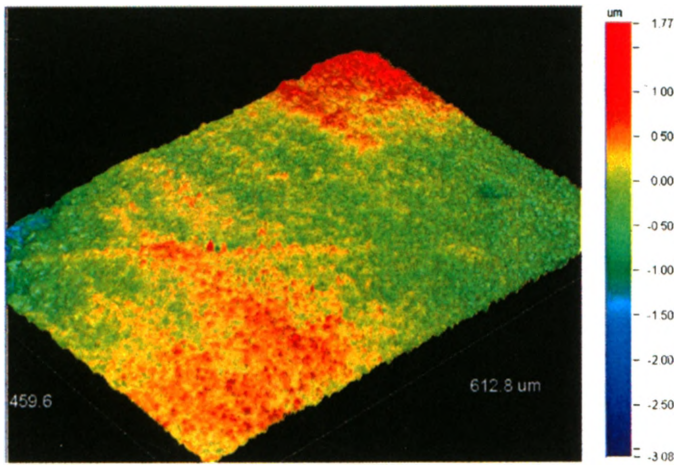

Figure 4.10 Surface finish of the molded T-mixer measured by the optical profiler, around 350 to 400 nm Ra.

4.6 Fabrication of Microstructures with High Aspect Ratios

To explore the capability and flexibility of the LEDM^2 fabrication method in producing micromold masters with high aspect ratios, a Y-micromixer and a more complicated microfluidic network were created. Due to the high degree of laminarity of the fluid flow in microchannels the proper mixing of different fluids is often difficult to achieve in short microchannels (Whitesides, 2006). For a simple Y-micromixer, molecular diffusion is the primary mechanism and its rate of diffusion, or efficiency, depends on the size of interfacial areas between the two mixing fluids. Therefore, high-aspect ratio microchannels provide a large interfacial area that is desirable for micro-mixing applications. Figure 4.11 shows an SEM view of the Y-channel micromixer mold master with aspect ratio of about 4.

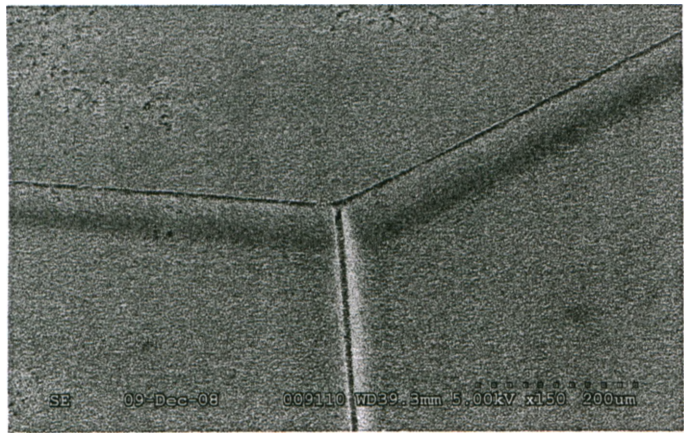

Figure 4.11 An SEM view of the Y-channel micromixer mold master with an aspect ratio about 4.

Figure 4.12 shows the SEM views of a micro-EDM mold master with a more complicated fluidic network pattern. The smallest width of the microfeatures produced using this method was 10 to 20μm. Any microstructures smaller than 10μm were found to be damaged by the debris igniting irregular patterns of spark erosion. Observations also supported the higher aspect ratio microstructures could be produced by optimizing flushing debris during die-sinking.

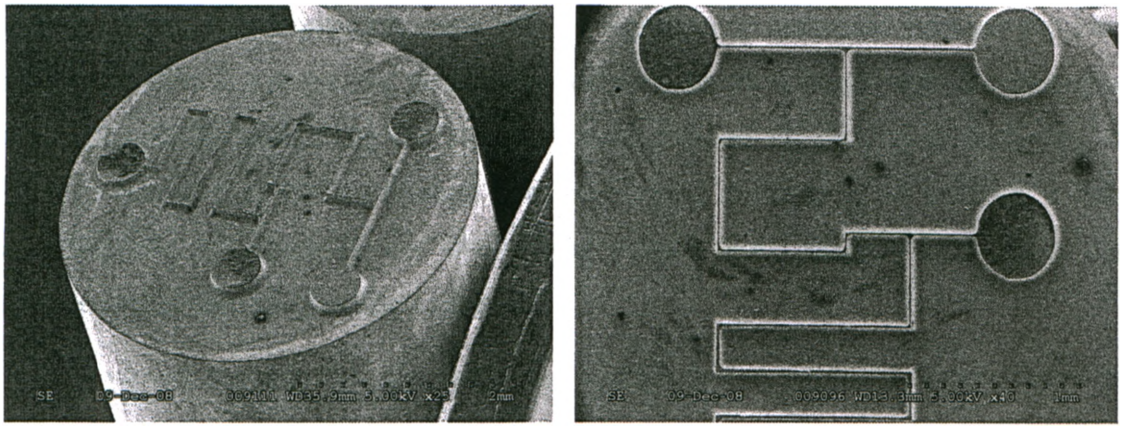

Figure 4.12 SEM views of a mold master with a more complex microchannel network.

4.7 General Observations and Discussion

Although the quality of the surface finish for both the metallic master and replicated PDMS T-mixer microchannel layer is noticeably less than optical grade, it remains adequate for many fluidic applications where a surface finish of 300 to 400nm Ra is acceptable. It may be possible to improve the quality of surface finishes through different combinations of tool electrode and substrate materials, and selecting optimal process parameters of microEDM die-sinking. However, this requires further investigation and detail study.

Furthermore, it is essential that a quick and cost-effective solution be found to fabricate the electrode mask because these electrodes experience excessive wear during the micro-EDM die-sinking process and must be replaced after a single use. To reduce the machining time as much as possible, the LEDM^2 approach presented in this chapter uses a high-power laser to cut the contour of microfluidic network on a planar brass sheet. The T-mixer electrode tool was cut in less than 20 minutes. For certain types of microfluidic network designs that require masks with deep channels and reservoirs, it may be difficult to accurately cut through the thick substrate material without distorting the template channel walls. In these applications, an electrode tool milled directly on a block of conductive substrate by a laser may create the desired geometry but the

machining time and fabrication costs will be significantly increased because the laser milling operation is a sequential process. In addition, the cut through technique presented in this Chapter for machining the electrode mask assisted the process of removing, or flushing, debris from the cut-through openings during die-sinking. In contrast, a fully laser machined 3D electrode tool would require more debris flushing of the holes and microstructures than the proposed method.

To lower the unit cost of a single microfluidic device, the mold masters should be built to sustain a large number of molding cycles before a replacement is needed. With this method, various conductive metals can be used as the substrate material. Tool steels that can be machined via microEDM process are particularly attractive. Not only can mold masters from higher strength metals be fabricated using this method but also lower cost off-the-shelf metals can be easily purchased and used. Brass sheets and substrates were selected in this study to demonstrate this economical aspect of the $LEDM^2$ method.

Furthermore, the resultant metallic mold master has sufficient high strength that it can be used for either hot embossing or injection molding. Hot embossing and injection molding are common techniques for mass production and, therefore, contribute to the reduction in cost per device replicated. The proposed method is also relatively environmental friendly due to the minimal use of chemicals in the process except dielectric oil. From a product life-cycle perspective, the cost of disposing chemicals used in manufacturing is minimal.

One disadvantage of using the die-sinking process to fabricate the mold master is that it requires about 24 to 48 hours. However, unlike the more common electroplating process to produce metallic mold master, the $LEDM^2$ method has only a few operational steps. Another concern about the proposed methodology is that surface wear on the electrode tool mask resulted in significant dimensional variations, as measured from the peak-to-bottom, in microfeatures with high aspect ratios. This suggests the aspect ratio is limited by a combination of electrode and work piece materials. If high aspect ratio microstructures are desirable, then, a thicker electrode mask should be employed.

4.8 Concluding Remarks

A method of creating metallic micromolds with features that have high-aspect ratios was described in this chapter. The proposed manufacturing process utilized laser micromachining to cut the negative two-dimensional profiles of the desired microfeatures and fluidic network patterns on a 100μm thick brass sheet. The positive relief of the cut pattern was then created through die-sinking the metallic mask onto a brass substrate by using electro-discharge micromachining (micro-EDM). The final substrate with the desired relief pattern became the molding tool used for either elastomer casting or thermoplastic hot embossing.

To validate the proposed fabrication methodology and evaluate the quality of surface finishes, a brass mold master of a T-channel micromixer (50μm width, 25μm height) was developed and multiple replicas of the device were cast on this mold using polydimethylsiloxane (PDMS). The surface finish of both the original micromold master and final molded channels on PDMS were measured by an optical profiler and found to have a roughness of approximately 400nm Ra. The ability of the proposed fabrication technique to create accurate features with high-aspect ratios was illustrated by manufacturing a Y-channel micromixer with an aspect ratio of 4 and microchannel widths smaller than 75μm.

CHAPTER 5

CONTACTLESS LHEM FABRICATION METHOD (Laser cutting, Hot-Embossing, and Molding)

5.1 Introduction

The LEDM^2 method described in the previous chapter for manufacturing metallic micromold masters has several key advantages including being able to make a mold from any harden conductive material. The microfabrication technique is, however, a very lengthy process, requiring 24 to 48 hours to complete. In addition, the final surface finishes of the microEDM mold master is not near optical grade quality, with a surface roughness of around 400nm Ra. In general, any metallic micromold will require some form of post-processing to cleanup debris and smooth the surfaces.

It is important to realize that the surface quality of the mold master will determine the final surface characteristics of the microfeatures on the molded part. If the microfeatures on the mold master can be fabricated using minimal tool contact then all post-processing steps necessary to reduce the roughness of the surface can be eliminated. These practical limitations have led to the development of another less expense nonlithographic microfabrication technique for producing polymer mold masters that have microstructures with near optical quality surface finishes. The proposed method is also based on laser micromachining, but unlike the LEDM^2 method, the microEDM die-sinking process is replaced with the direct hot embossing of a thermoplastic. Although polymer micromolds are less durable than metallic mold masters, they can be used effectively for small-and-medium batch production.

The micromold fabrication technique termed LHEM (Laser micromachining, Hot Embossing, and Molding) is similar to the manufacturing approach used by a number of researchers to create polymer microlenses (Shen et al., 2002; Ziolkowski et al., 2003; Pan et al., 2004). Since hot embossing can be used to mold high-quality optical microlenses

from a variety of thermoplastics, like polymethylmethacrylate (PMMA), the same basic manufacturing process can be used to produce functional polymer micromold masters with optical grade surface finishes.

5.2 Laser Cutting, Hot Embossing and Molding (LHEM)

The key steps in producing the PMMA micromold master and soft-molded PDMS microfluidic device using the LHEM microfabrication method are summarized in Figure 5.1. The metallic mask with the desired microchannel structure (eg. microchannels, reservoirs) is initially machined by an industrial laser. This metallic mask and a thermoplastic, polymethylmethacrylate (PMMA), substrate were then placed into the hot press. Constant pressure and heat are applied for a predefined period of time to create the mold master. The process parameters are carefully chosen to avoid the extruded microfeature reaching the top of the mask. Subsequently, the heat element is turned off allowing the extruded microfeatures and the substrate to cool below the glass transition temperature (T_g) of the PMMA material. Once cooled below the transition temperature, the PMMA substrate is carefully removed from the mask and the mold master is completed. Finally, the fabricated mold master is used in soft-molding the PDMS-based disposable microfluidic devices.

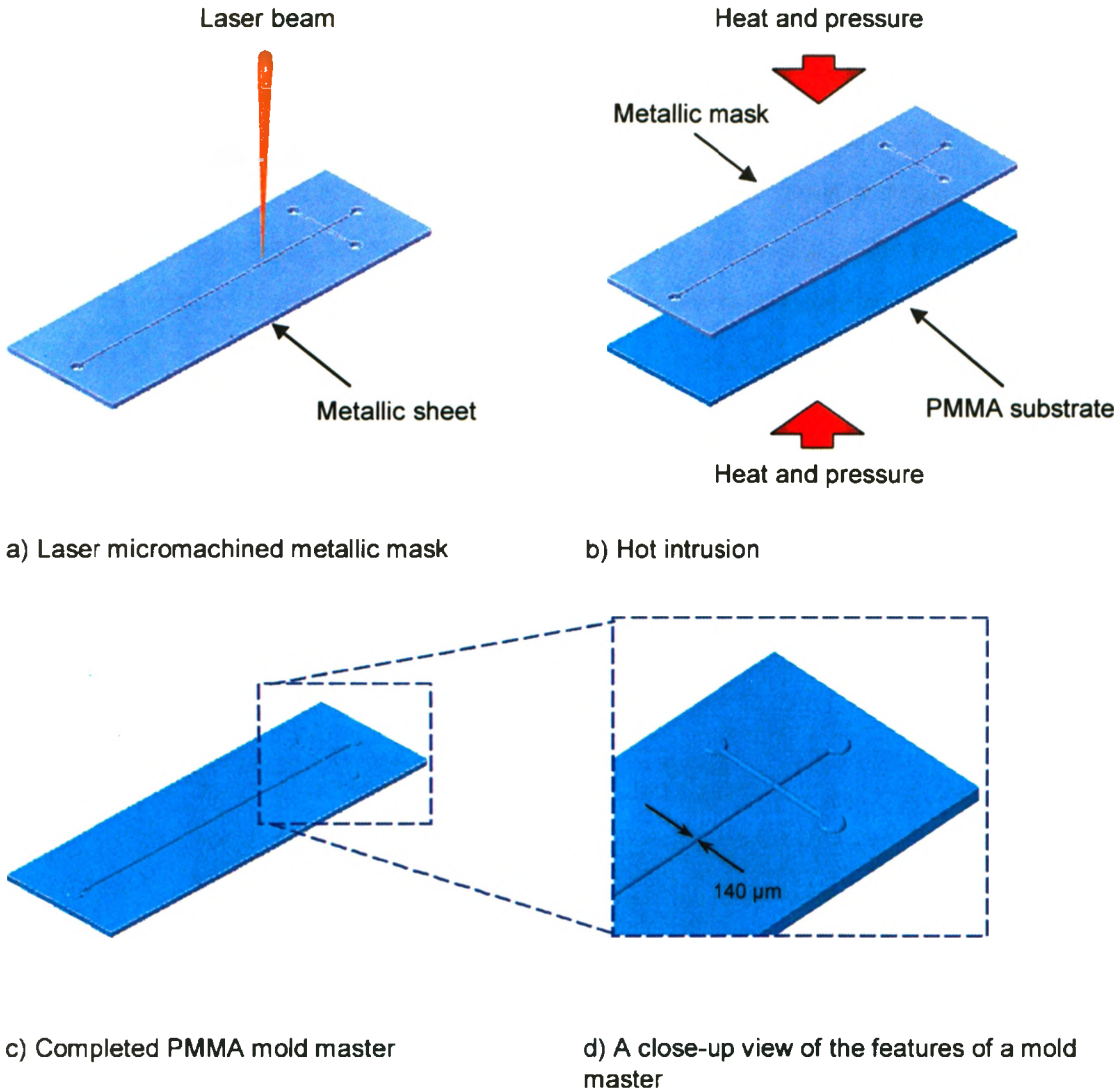

a) Laser micromachined metallic mask

b) Hot intrusion

c) Completed PMMA mold master

d) A close-up view of the features of a mold master

Figure 5.1 Various steps used to fabricate a PMMA micromold master by the LHEM method. The illustration is for a micro capillary electrophoresis (CE) device.

Figure 5.2 shows cross-sectional view of the proposed fabrication method. An important observation is that the cross section of the extruded relief on the micromold master is non-rectangular. The non-rectangular shape is a result of the partial hot embossing process (hot intrusion) using the mask where the relief is extruded during the process without allowing the molten material to contact the walls of the mask. The shape of the microfeature is, therefore, determined by the physical process of the free flow of the softened material into the negative channel openings of the mask. The non-rectangular shape of the microchannels is a desirable feature for many biomedical applications (Lee et al., 2007; Chen et al., 2003). The PMMA substrate with the microrelief features is then used as a micromold master for molding the microchannel structure in suitable materials, such as the polydimethylsiloxane (PDMS) elastomer.

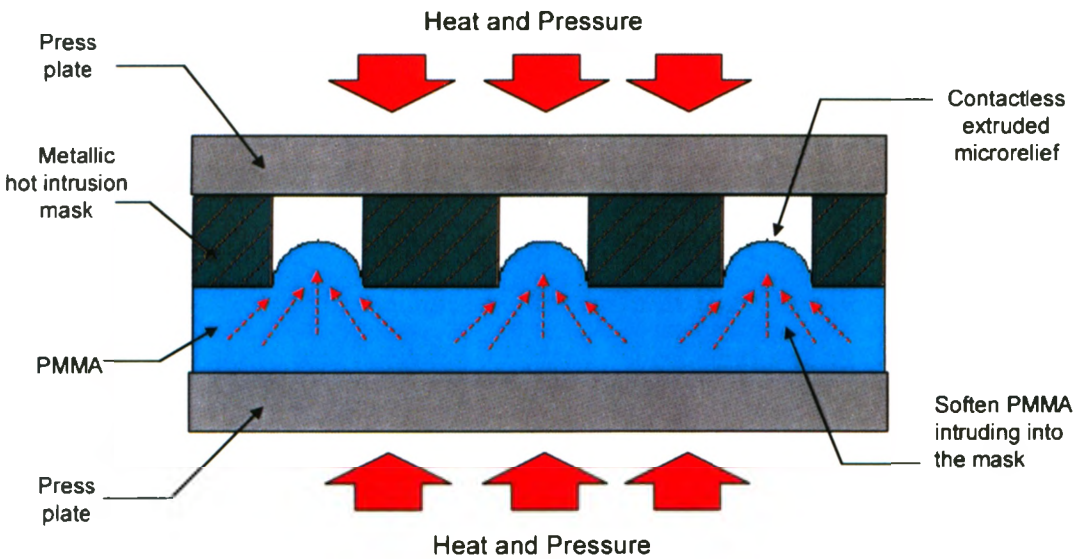

Figure 5.2 Cross-sectional view of the hot intrusion process showing "contactless" formation of the microrelief.

The process of molding a final microfluidic device from the PDMS elastomer, as described in Chapter 4, involves pouring the material over the micromold master, allowing the material to cure and then demolding it. The fabricated microfluidic part is

then assembled with other components to form the LOC or μTAS. The complete process of producing the mold master is rather simple and involves only two major steps: laser micromachining and hot embossing. This simplicity makes the method easy to implement and potentially very cost-effective.

Another very attractive feature of the LHEM method is that a single mask can be used to produce several identical mold masters for several machines that operate in parallel. Furthermore, a very high quality micromold surface finish is created because the relief patterns on the PMMA master are formed by the free flow of softened material into the negative relief of the metallic mask (without touching its walls).

It should be noted that the mold master can be produced from materials other than PMMA; the only requirement of this method is that the material is suitable for hot embossing. Similarly, the mold master can be used for molding disposable microfluidic devices from materials other than PDMS, as long as the mold master material can sustain the process temperatures without deforming.

A similar method that used hot embossing as the key process was used to fabricate microlenses (Pan et al., 2004; Chang et al, 2007). The main difference with the techniques proposed in this chapter is that hot embossing was used to mold the final parts (microlenses) and not the mold master. In Pan and Chang's work (Pan et al., 2004; Chang et al, 2007), the mold master is produced via conventional electroplating processes.

5.3 Experimental Results and Validation

To validate the proposed method, a PMMA master was produced for molding a double-T shape micro capillary electrophoresis (CE) device as shown in Figure 5.3. CE devices are commonly used in bio-analytical systems for DNA analysis (Chen and Ren, 2004; Korvink and Paul, 2006). In this study, the purpose was to fabricate a PMMA master and use it to mold a sample CE device from PDMS elastomer. Once completed, the suitability of the proposed method for the fabrication of micromold masters was assessed on the basis of the geometric accuracy and surface finish quality of both the PMMA master and the molded sample device.

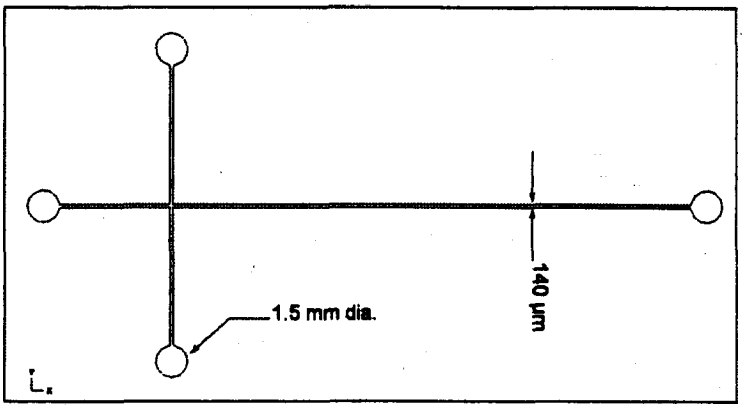

Figure 5.3 The channel and liquid reservoir layout of a micro capillary electrophoresis (CE) device.

All the channels of the CE chip in Figure 5.3 are approximately 140µm wide and used to interconnect to four reservoirs: sample reservoir, buffer reservoir, injection reservoir, and waste reservoir. All the reservoirs are 1.5mm in diameter. First, the mask was fabricated by laser cutting the microchannel patterns and reservoirs structure of the CE device in a 100µm thick sheet of low-carbon steel. Laser cutting was done using the AVIA UV laser from Coherent Inc., USA (as described in Chapter 3). The laser has 3.0 Watts of power at 20kHz, pulse duration of less than 40 nanosecond at 60kHz. The laser cutting was conducted under atmospheric pressure and air-assisted condition. The air-assisted laser cutting was used primarily to provide protection to the laser optics.

After laser cutting, the metallic mask was cleaned in an ultrasonic bath to remove the debris and oxides from the part. The geometric accuracy of the channels and the reservoirs structure of the mask were within +/- 5µm. The sides of the microchannels were reasonably smooth, within the limits of what can be achieved by nanosecond laser micromachining. The actual surface finish quality of the sides was not measured as it is not critical for the proposed method because the sides of the mask do not come into direct contact with the molten PMMA material during the hot embossing process.

The hot embossing step of this method was conducted using the Multi-purpose Press from GEO Knight & Co. Inc. The press is capable of applying a pressure from 140 to 550kPa (20 to 80Psi) with temperatures from 66°C to 220°C. The mask was placed onto a 1.5mm thick PMMA substrate. The parameters of the press were set to 125°C temperature and 207kPa (30Psi) pressure. The press was preheated to the target temperature before placing the mask onto the PMMA substrate. After the target temperature was reached, the sample was placed in the press. The pressure was applied and held for 10 minutes. Then the heater was turned off while maintaining the applied pressure, fan was employed in assisting the cooling until the de-embossing temperature, 95°C at about 1°C/minute, was reached. The slow cooling rate was designed to reduce thermal stress in the material caused by rapid cooling. After that, the mask and substrate were removed from the press. Further cooling to the room temperature was completed in about 5 minutes. Then the mask was removed from the substrate and the mold master was completed.

The quality of the surface finish of the mold master was evaluated through optical microscopic images, SEM (scanning electron microscopy), and a white light optical profiler. Figure 5.4 shows an optical microscope image of the Au-coated mold master. Figure 5.5 shows SEM views of the intersection of the microchannels positive relief on the master.

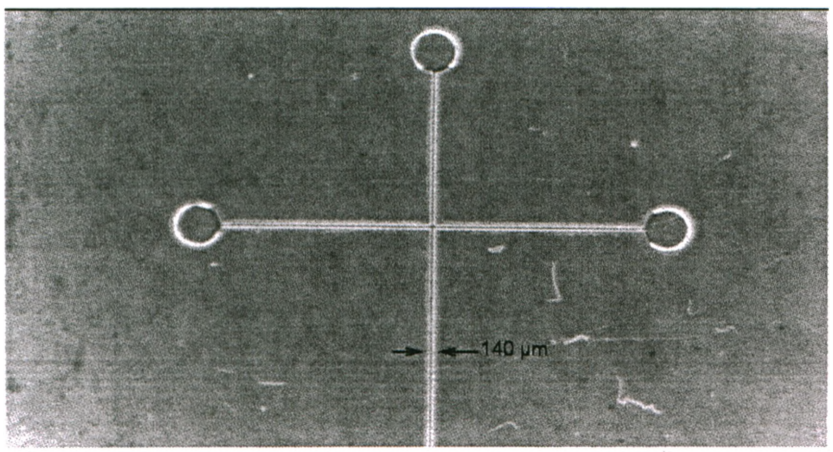

Figure 5.4 A microscopic view of the PMMA master after it was coated in Au.

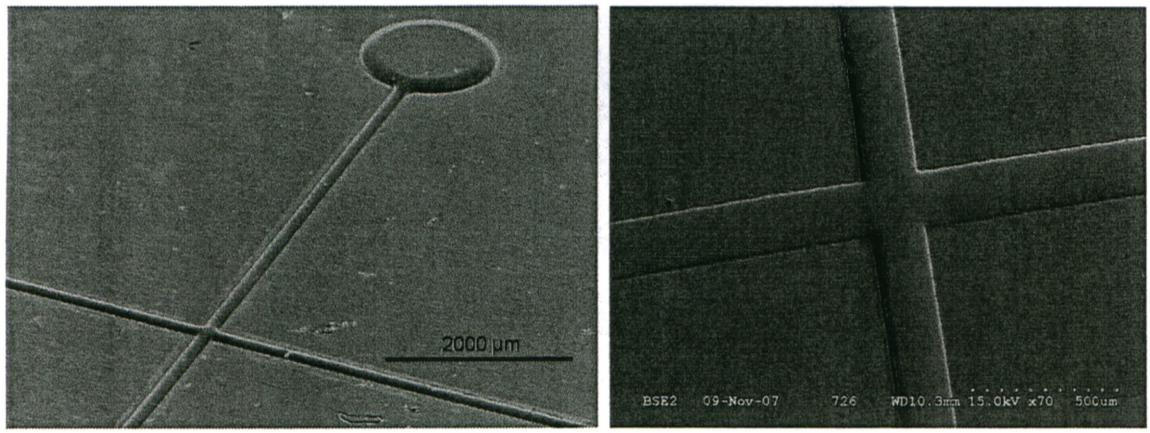

Figure 5.5 SEM views of the PMMA master for molding of PDMS CE devices.

Figure 5.6 shows an SEM picture of the extruded surface finish along the flat surface of the microchannel to compare the high quality of the surface finish of the extruded microrelief and the rough surface finishes that made contact with the mask. Figure 5.7 shows an optical microscopic view of a smooth transition from the microchannel to reservoir of the master. The high quality surface finish of the microfeature is attributed to the fact that the relief is created by a "contactless" hot embossing process where the molten PMMA did not touch the sides of the cut-through slots on the mask. Thus, the free flow of the softened material moved unimpeded into the slots of the mask and the surface tension of the material produced a very smooth surface of the relief.

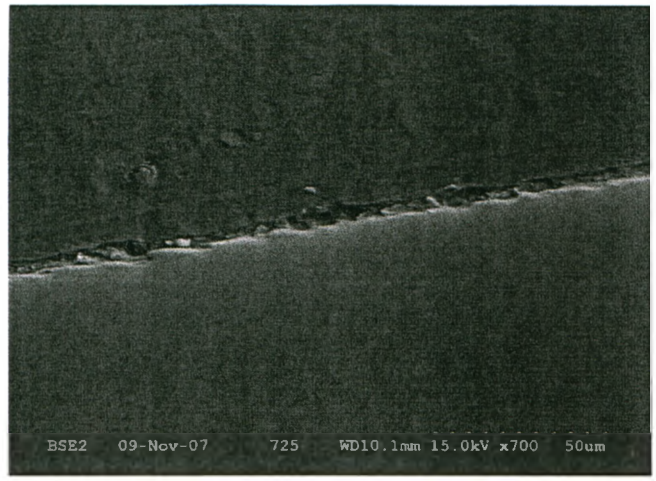

Figure 5.6 SEM close up of the surface finishes for both the flat surface (top side) and extruded profile (bottom side).

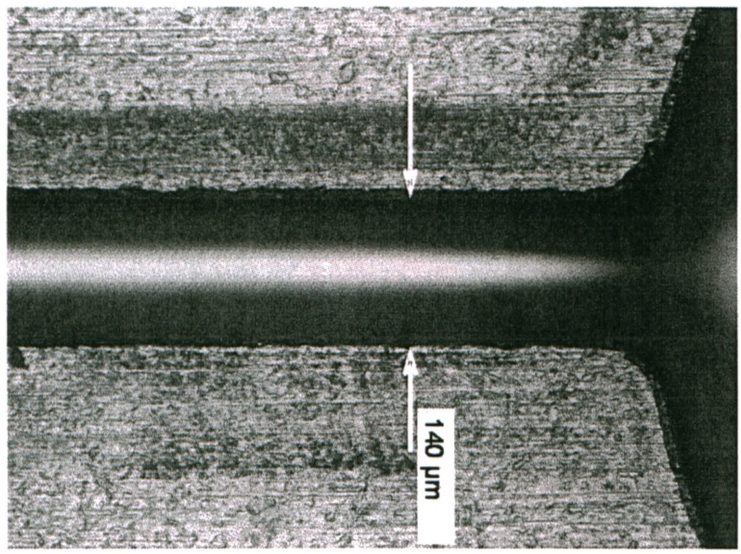

Figure 5.7 Microscopic view that reveals the high contrast between the two surface finishes produced on the PMMA master.

Figure 5.8 shows the cross-sectional profile of the relief formed on the PMMA master. The profile was measured using the Dektak^{3}ST surface profile measuring system from Veeco, Sloan Technology. The actual measured width of the extruded channel

relief was slightly (10-12μm) larger than the width of the slots in the mask. This non-rectangular profile of the relief indicates that "contactless" between the sides of the mask slots and the softened material during the hot embossing process was occurred.

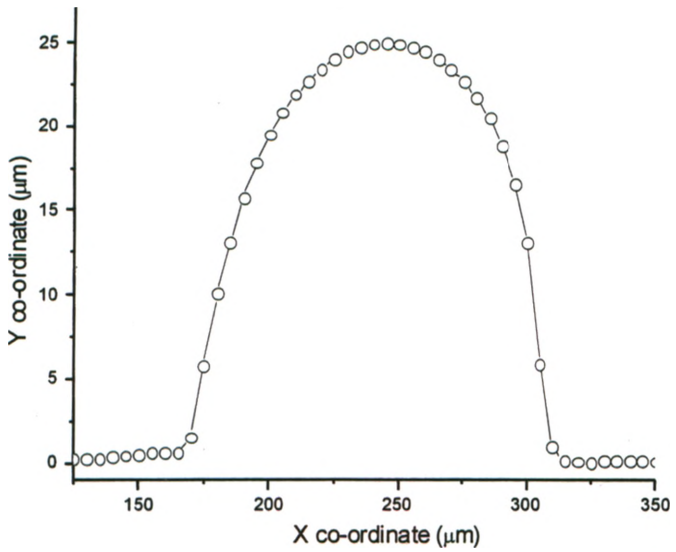

Figure 5.8 Cross-sectional profile of the extruded microrelief on the PMMA master.

Figure 5.9 shows a microscopic view of the polished cross-section of the PMMA master. It has a similar extruded profile as seen in the profiler measurement of the surface. To measure the surface finish (average roughness, Ra) of the PMMA master, the Wyko NT1100 optical profiling system from Veeco Instruments Inc., USA, was used. The results show the proposed method can produce an extruded channel relief with a surface finish of 10nm Ra. Furthermore, a few measurements were taken in different locations at the PMMA master and the results showed the Ra to be around 10 to 100nm, near optical quality.

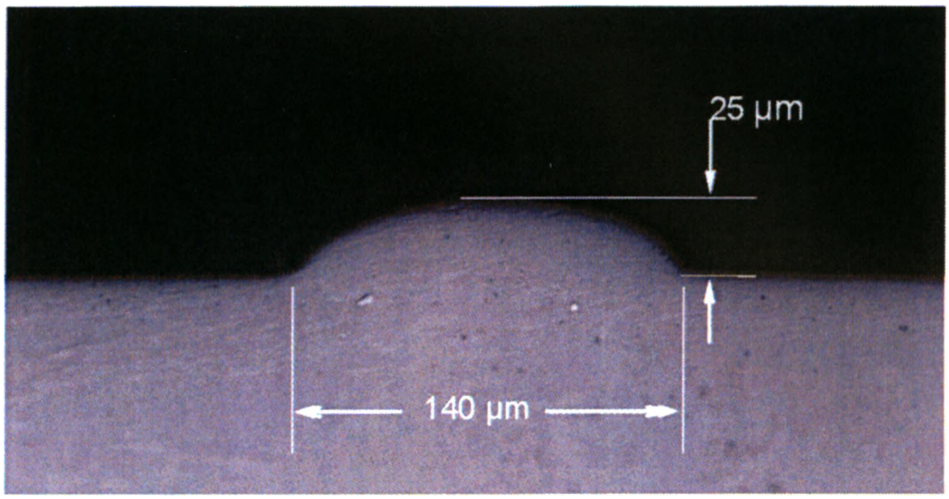

Figure 5.9 Metallographical view (cross-section) of the extruded microrelief.

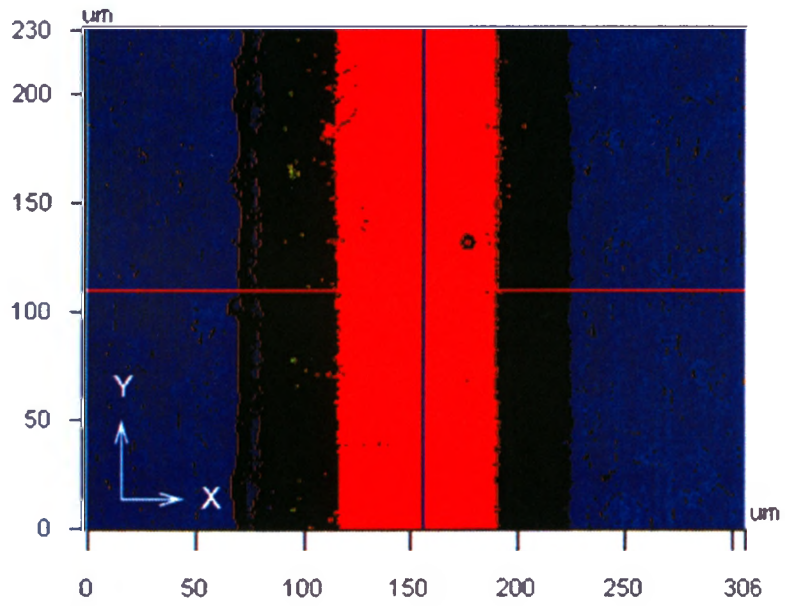

Figure 5.10 Image of the extruded microrelief as measured by Wyko optical profiler.

The optical profiler has a limitation in that it cannot capture data when measuring a surface which is too steep (percentage of light was reflected away too much to be captured by the detector). This limitation is shown in Figure 5.10 as the black colored area (no data was captured by the optical profiler). Figure 5.11 shows that the measured surface finish by Wyko optical profiler is about 10nm Ra.

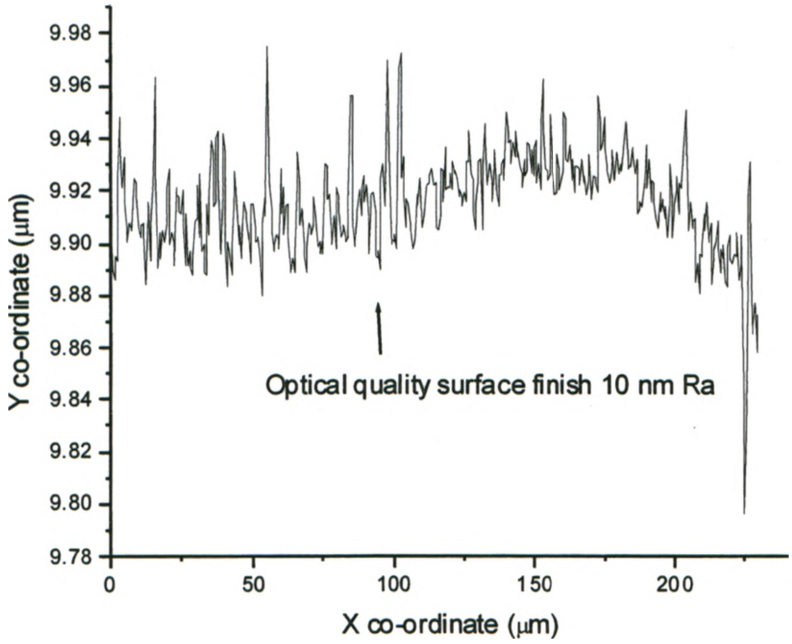

Figure 5.11 The surface finish of the PMMA master along the Y-axis as measured by the optical profiler.

Once the PMMA master was completed, a sample PDMS microfluidic CE device was molded. The PMMA master was placed on a horizontal surface and the PDMS elastomer poured over it (PDMS elastomer was degassed prior to this step). The material was left to cure at room temperature for 24 hours, and then demolded (peeled off). Due to the non-rectangular profile of the microchannel relief, demolding was easy and caused no damages to the molded microchannels or the PMMA master. The resulting PDMS part was then bonded onto a flat piece of PDMS material to complete the CE device.

SEM views of the molded PDMS CE device's microchannels are given in Figures 5.12 and 5.13. The intersection of the molded microchannels show the quality of the surface finish of the final part. An optical microscope view that illustrates the contrast between the surface finish of the molded microchannels and the surrounding flat surface of the original substrate is provided in Figure 5.14. These SEM and microscopic images demonstrate the high quality surface finishes that can be accomplished by the LHEM method and near identical quality of the mold master and final polymer part.

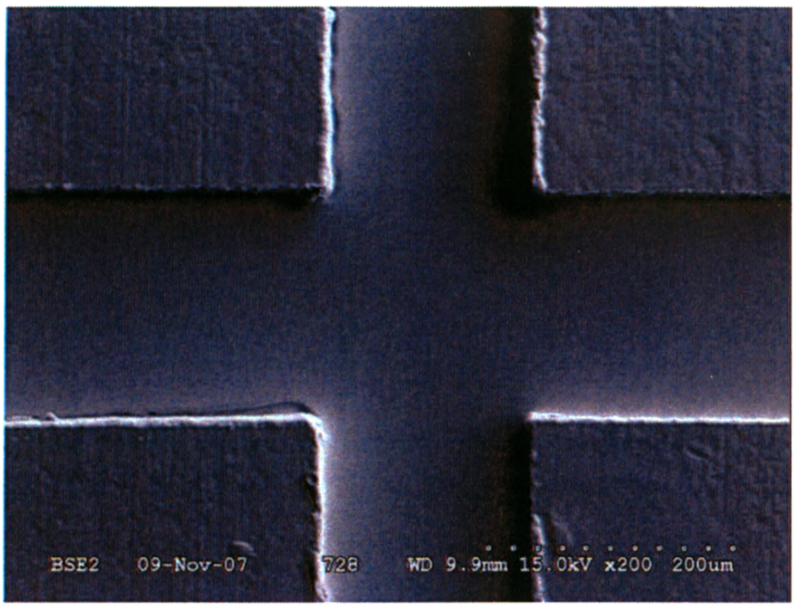

Figure 5.12 SEM view of the intersection of two microchannels in the CE device.

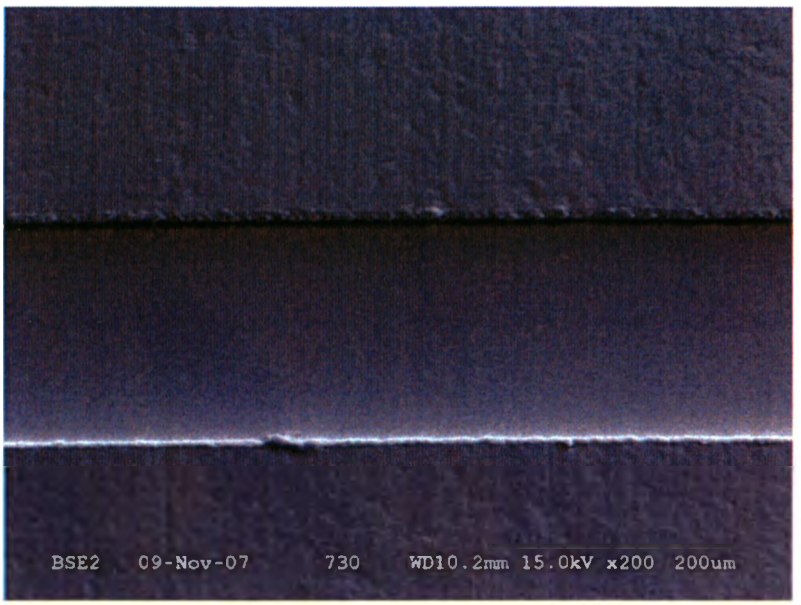

Figure 5.13 SEM view of the CE microchannel.

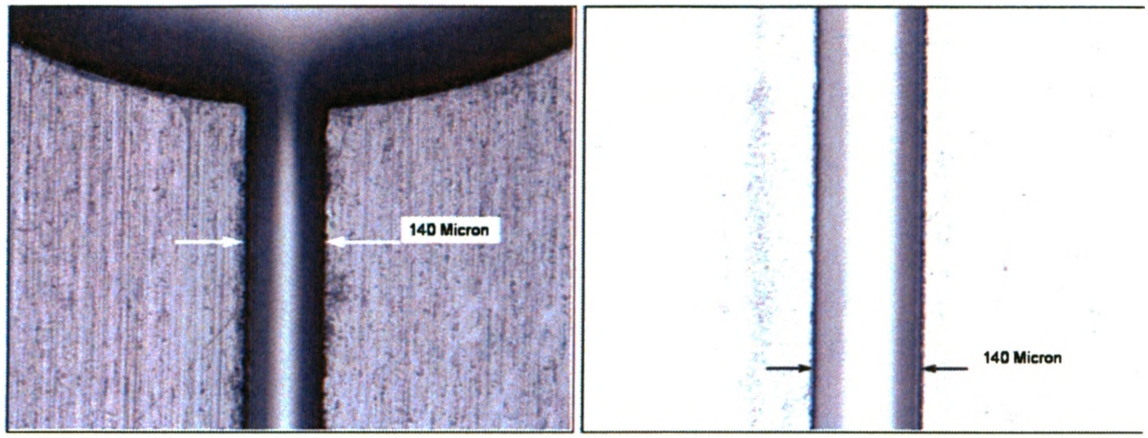

Figure 5.14 Smooth transition from the microchannel to the reservoir of the CE device (left), and a microscopic view showing higher contrast of the microchannel and flat surface around the CE detection section (right).

Figure 5.15 presents a cross-sectional profile of the CE microchannel as measured by surface profiler. Figure 5.16 shows an optical microscopic view of the cross-section of the microchannel. Figures 5.17 and 5.18 show the data as captured by the Wyko optical profiler. The experimental results confirm that the result surface is of high quality with a roughness value around 40nm Ra.

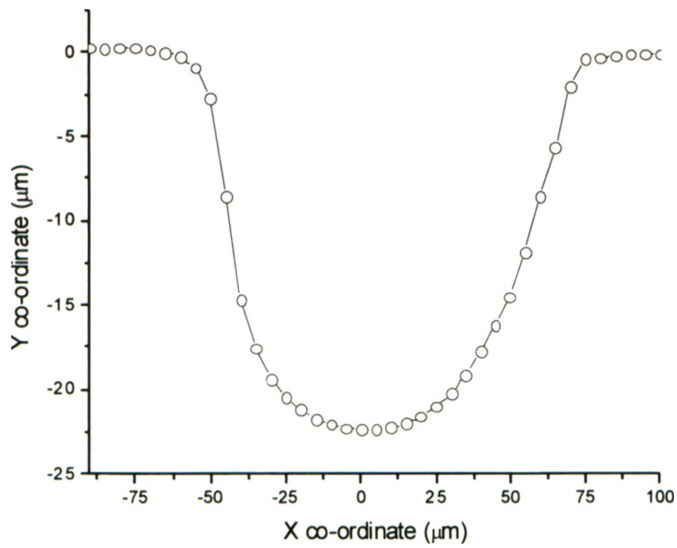

Figure 5.15 Cross-sectional profile of the molded CE device's microchannel as measured by a stylus profiler.

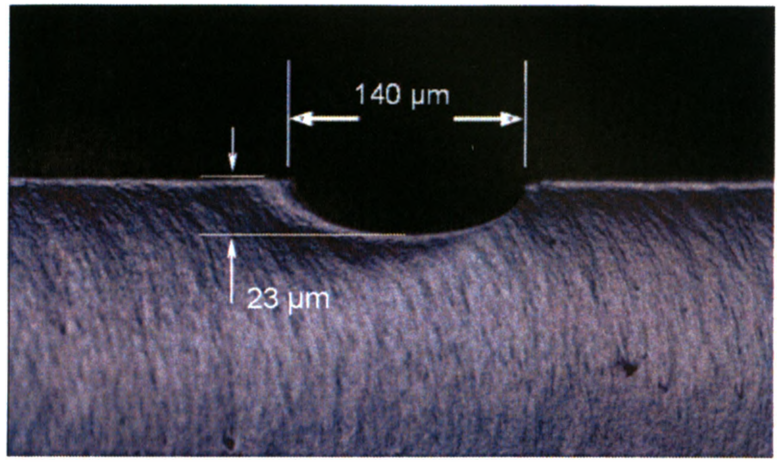

Figure 5.16 Microscopic view of the cross-section of a microchannel on the final CE device.

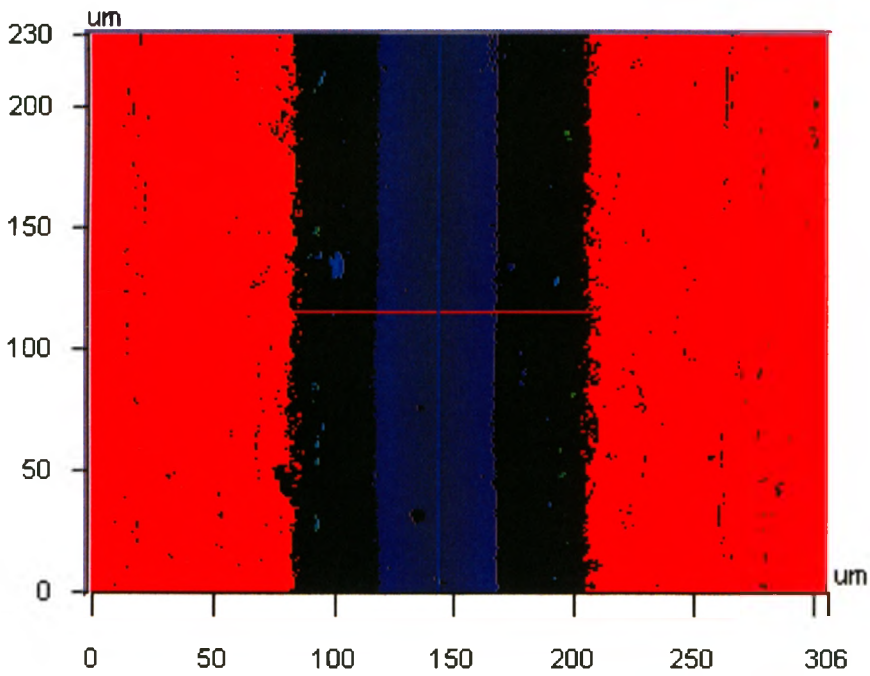

Figure 5.17 Pseudo-coloured image of the CE device as taken by Wyko optical profiler.

To evaluate the replication fidelity of the molded microfluidic device, measurements using surface profiler for both of the extruded microrelief of the mold master and soft-molded microchannel of the CE device were combined and illustrated in

Figure 5.19. Approximately 10% shrinkage of PDMS molded microchannels was observed.

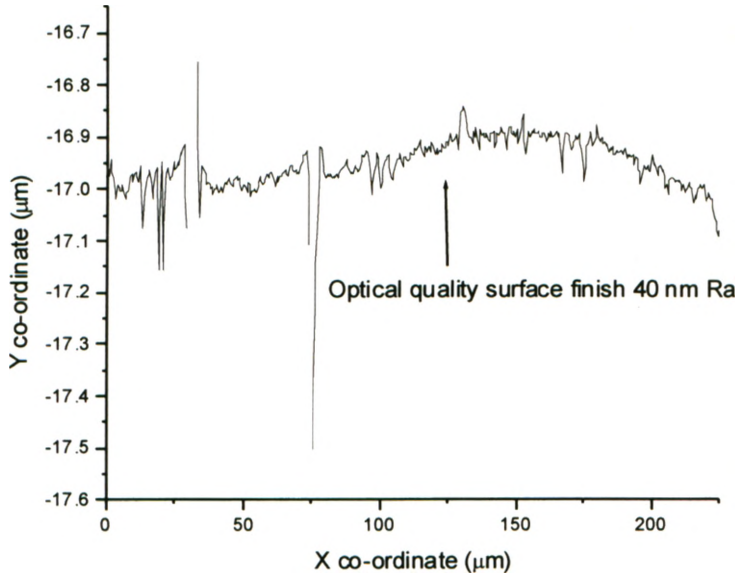

Figure 5.18 Surface roughness of the CE device along the Y-axis as measured by the optical profiler.

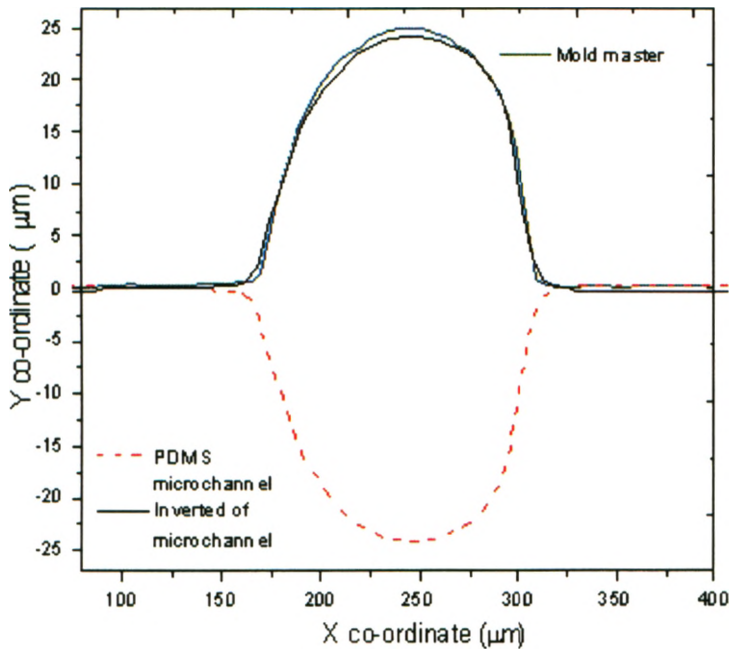

Figure 5.19 Cross-sectional profiles of the PMMA mold master and the molded PDMS microchannel. Minor shrinkage (approximately 10%) is observed between the mold master and final replicated microfeature.

5.4 Discussion

The observed quality of both the PMMA master and the fabricated CE device indicates that the proposed nonlithographic method for creating a polymer mold master is adequate for the intended applications. The quality of the surface finish of the fabricated microchannels is notably near optical grade. Pan et al. (Pan et al., 2004) described a novel method for fabrication of microlenses, a method that, like the LHEM method described in this thesis, uses hot embossing as a key step in the fabrication process. The primary difference of their work is in the use of hot embossing to manufacture a final functional part (microlenses) and not a tool such as a micro-mold master. One relevant and useful result presented by Pan et al. (Pan et al., 2004) is that a very high quality surface finish can be achieved in polycarbonate (PC) molding (Ra around 1-5 nm was reported). This suggests that PC material may be an even better option than the PMMA for creating polymeric mold masters. However, the required hot embossing temperature and embossing times for PC material were higher than those used in the PMMA process reported in this thesis. This would require additional studies in the future.

The experiments also confirmed that the complete process of fabricating a mold master and the desired fluidic device is both quick and inexpensive. The most time-consuming step of the process is the PDMS curing (24 hours under the room temperature in our experiments). This can be significantly reduced if curing is conducted under elevated temperature, at roughly 75°C for 15 minutes on a standard temperature controlled hot plate.

A limitation of the proposed LHEM method is that the mold master can only be made from materials suitable for hot embossing. Furthermore, the mold master can only be used to mold materials whose processing temperature is below the glass transition temperature of the mold master. Even with these limitations, the proposed method appears to be a high quality and cost-effective solution for a wide range of microfluidic applications. To make the method more readily usable, a practical method is needed for choosing suitable process parameters (primarily the hot embossing parameters) for a given design of the microfluidic device.

5.5 Concluding Remarks

This chapter presented an innovative method developed in this research project for rapidly fabricating polymer mold masters for replicating polydimethyl-siloxane (PDMS) microfluidic devices. The method involves only two major steps: laser micromachining to create a metallic mask, and hot embossing the microchannel features onto a PMMA substrate. Fabrication of microfluidic devices then involves pouring the PDMS elastomer over the PMMA mold master and curing it at a suitable temperature.

The main advantages of the proposed method are that fabrication of the metallic mask is quick and inexpensive, and the mask can be re-used to fabricate a large number of micromold masters for parallel replication of PDMS microfluidic devices with high quality surface finish of microchannels but non-rectangular profile, yet low cost and biocompatibility. Furthermore, the process involves the minimal use of harmful chemicals. Critical limitations of the LHEM method relate to the soft polymer material that must be used for hot embossing the micro mold and the inability of the proposed technique to fabricate rectangular channels.

CHAPTER 6

COMPARISON OF NONLITHOGRAPHIC MICRO-FABRICATION METHODS (LCWM, LEDM^2, and LHEM)

6.1 Introduction

In the previous three chapters, several nonlithographic microfabrication techniques were introduced to create functional mold masters that would permit the cost-effective manufacturing of disposable microfluidic devices for a variety of biological and chemical analysis. Extensive characterization of their capabilities and identification of their limitations for mass production requires further studies. The focus of this thesis research has been on introducing these unique rapid microfabrication methods and demonstrating the potential for the microfluidic design and manufacture. To this end, each proposed method is now analyzed and evaluated in terms of the potential to make an impact on creating low-cost high quality microfluidic and LOC devices.

The evaluation methodology used to assess the three techniques is outlined in Section 6.2. A summary of key advantages and disadvantages of each are provided. Section 6.3 discusses how the three developed methods measure up with each identified criterion. Section 6.4 presents the conclusions drawn from the assessment and identifies which proposed microfabrication technique will be developed in greater detail in Chapter 7.

6.2 Evaluation Methodology

The advantages and disadvantages of each method are listed in Table 6.1 and the comparison of each method is listed in Table 6.2. To assist with the assessment, the sequence of operations for the three developed methods introduced in this thesis is

summarized in Figure 6.1. The LCWM, LEDM^2, and LHEM techniques will be evaluated against the following seven criteria:

1. *Quality of surface finishes* - Excellent surface finishes with low Ra values are required to avoid adhesion of bio-molecules to microstructures and to achieve optical detections.
2. *Environmental impact of microfabrication process* – Modern manufacturing process must make minimal use of toxic chemicals and utilizes processes that leave a minimal harmful impact on the environment. Some of the chemicals used in micromachining are carcinogenic. For example, chlorobenzene is a carcinogenic compound that frequently used in dissolving PMMA photoresists.
3. *Technology readiness* – A commercially viable production technique must exploit technologies that have been established or proven effective. Using a technology in a commercial manufacturing process that is not ready will result in excessive cost over-runs and production time delays. Therefore, developed microfabrication technologies in this research project should be compatible with the existing micromachining technologies to reduce the uncertainty of new product developments.
4. *Fabrication steps* - The fewer fabrication steps involved in producing a part the higher the quality parts would be (avoids misalignment during setup or a failed processing step ruins the final parts.) and it lowers costs due to handling and machine operations.
5. *Total fabrication time* - Added production time translates into higher overall costs.
6. *Ease of tool replacement* – Quick and ease replacement of tools, such as micromolds, will reduce production downtimes.
7. *Scalability* – The ability to scale-up micromold master fabrication (ie. making multiple identical micromold copies) will enable the manufacturer to meet higher production volumes by running parallel molding processes.

Table 6.1 Advantages and disadvantages of the LCWM, LEDM^2, and LHEM methods.

Fabrication Method	Advantages	Disadvantages
LCWM	a) Only few processing steps: laser cutting and welding b) Direct fabrication of metallic mold masters c) Rapid fabrication, less than 1 hour in the demonstrated master d) Material cost relatively low, stainless steal or low-carbon steel e) Material strength of mold masters: high strength metals can be used. f) Environmental friendly: involved minimal chemicals	a) Smallest channel width of about 75μm b) Non-optical surface finishes without a post polishing process
LEDM^2	a) Only few processing steps: laser cutting and microEDM die-sinking b) Direct fabrication of metallic mold masters c) Able to machine conventionally difficult-to-cut materials such as tool steels d) Minimum channel width of about 25μm e) Fabrication of high aspect ratio microstructures f) Environmental friendly: involved minimal chemicals - only dielectric oil is needed. g) Material strength of mold masters: very high strength metals such as tool steal can be used as substrates.	a) Non-optical surface finishes without a post polishing process b) Relatively long fabrication time, 24 to 48 hours of microEDM die-sinking process
LHEM	a) Only few processing steps: laser cutting and hot embossing b) Rapid fabrication, 1 hour for the 1st demonstrated master, 30 minutes for an additional master c) Near optical grade surface finishes d) Minimum channel width of about 25μm (smaller width is possible with an improved process control system.) e) Environmental friendly: involved minimal chemicals	a) Low aspect ratio (height/width), less than 0.5 aspect ratio b) Non-metallic mold master c) Material strength of the mold master: strong enough for casting of PDMS or hot embossing a thermoplastic that has a lower glass transition temperature than PMMA.

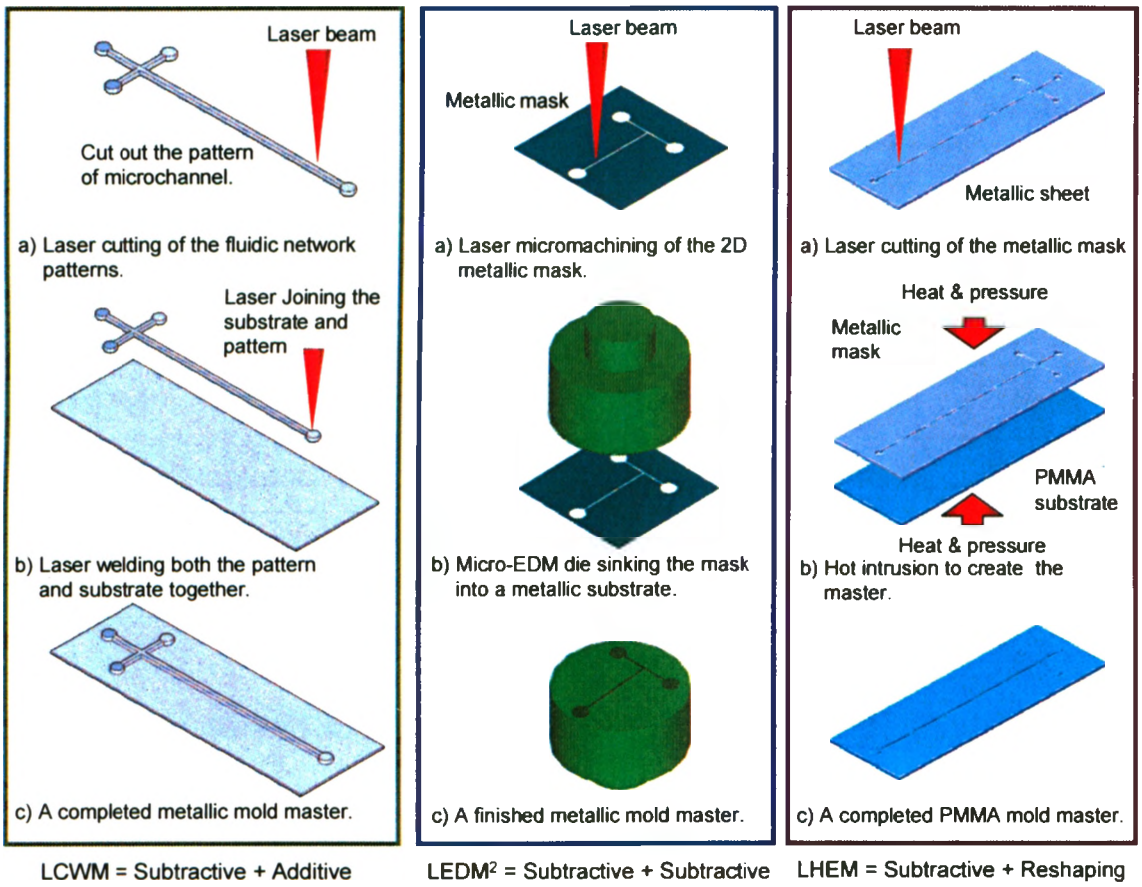

Figure 6.1 The sequence of fabricating micromold masters using LCWM, LEDM^2, and LHEM methods.

Table 6.2 Comparison of LCWM, LEDM^2, and LHEM method.

	LCWM	LEDM^2	LHEM
Quality of surface finishes	Good	Poor	Excellent
Environmental impact	Very Low	Low	Very Low
Technology readiness (compatible)	Acceptable	Acceptable	Good
Fabrication steps	2 steps	2 steps	2 steps
Total fabrication time	Short	Long	Short
Ease of tool replacement	Easy	Medium	Very easy
Scalability	Medium	Low	High

6.3 Discussion of the LCWM, LEDM^2, and LHEM Methods

6.3.1 Quality of surface finishes

To avoid adhesion of bio-molecules or provide optical detection of the samples to be analyzed, it is necessary to produce surface finishes of optical quality. Based on the experimental studies, polymer CE devices molded using the LHEM technique exhibit near optical grade surface finishes. As discussed in Chapter 5, the surface finishes of these mold masters and molded channels are near 10nm Ra. Further, this near optical grade of surface finishes may be useful for incorporating "integrated optics," such as microlenses, along the microchannels. For example, the LCWM molded Y-channel micromixer shows reasonable optical quality for optical detection. The mixing of two colored waters was easily observed under the microscope as shown in Chapter 3.

In contrast, the LEDM^2 mold masters have surface finishes of 300 to 400nm Ra which is not suitable for optical applications. Under microscopic observation, the molded *PDMS T-micromixer produced using the LEDM^2 metallic mold master showed poor* optical transparency even though PDMS is a transparent material. These molded

microchannels may still be used for optical detection applications if the covering layer is transparent. However, this solution would allow only one side available for optical sensing.

6.3.2 Environmental impact of microfabrication process

To reduce the environmental impact of the manufacturing process, as discussed in Chapter 1, it is essential that a minimal use of chemicals be required during mold and part fabrication. The LCWM and LHEM methods use essentially no harmful oils or etching chemicals in the fabrication process. However, the LEDM^2 method requires the use of dielectric oil which under certain circumstances may be replaced with de-ionized water when machining certain materials. The stated objective of developing a microfabrication method that uses minimum chemicals is accomplished. In addition, the substrate materials used in the LCWM, LEDM^2 and LHEM mold masters are recyclable – LCWM and LEDM^2 are metal and LHEM is PMMA thermoplastic polymer.

6.3.3 Technology readiness

Fabrication methods that are compatible with the established and readily available micromachining technologies could potentially increase its impact on industry because of numerous exciting MEMS devices developed have been created by combining various micromachining techniques and processes such as the photolithography, E-beam lithography, thin-film deposition, wet bulk micromachining, dry etching, and more.

The LCWM and LEDM^2 methods do not appear to be compatible with the established micromachining technologies. In contrast, the LHEM method appears to be highly compatible with the established micromachining technologies. With some modification of the process such as depositing a thin polymer film on a silicon wafer via spin coating and used the LHEM method to transfer the microfluidic pattern or fabricating polymer micro-optics. However, these suggestions require further investigation.

6.3.4 Fabrication steps

The number of fabrication steps required for each of these methods is essentially two: LCWM-laser cutting and laser microwelding; $LEDM^2$ – laser cutting and microEDM die-sinking; and LHEM – laser cutting and hot embossing. Both the LCWM and LHEM techniques require nearly no preparation of the substrate prior to laser cutting. However, the $LEDM^2$ requires a longer setup time for the technician to prepare the material for the microEDM process.

6.3.5 Total fabrication time

$LEDM^2$ requires the longest fabrication time, about a few days. The microEDM die-sinking contributes the most to the overall fabrication time and this time is a direct correlation of the required aspect ratio for the microstructures. If a low aspect ratio structure is acceptable for the application, then the fabrication time can be shorten significantly.

Both the LCWM and LHEM require only about one hour of fabrication time for creating the mold masters used in this study. When an additional master is needed, the LCWM requires re-cutting the metallic microfluidic network patterns, every time sequentially, which means no reduction of the fabrication time for additional masters.

Once a metallic mask for the LHEM method has been cut, the mold masters can be replicated by hot embossing in about 30 minutes for a complex pattern of microfluidic network – in fact, the fabrication of LHEM mold masters is a rapid replication process that can mass-produce masters, which makes the process easily scaling up according to the production demands.

6.3.6 Ease of tool replacement

Damage to the mold master can occur frequently during the part production because of the improper use by the manufacturing personnel. For example, if non-optimal process parameters are used to shorten the production cycle-time, such as increasing injection

pressure and temperature, then the mold master will experience higher stresses that lead to premature failure. Therefore, to reduce the production downtimes due to damaged mold masters it is necessary to have a quick, relatively low-cost method of making replacement molds.

The LEDM^2 mold masters are the most difficult to replace because the method requires the technician to repeat the complete fabrication sequence for every additional master produced. Similarly, the LCWM method also does not allow any significant reduction in fabrication time for creating additional masters.

Replacing LHEM mold masters can, however, be quick because the fabrication of LHEM mold masters is, in fact, a replication process. Once the hot embossing mask is fabricated, any number of additional LHEM mold masters can be easily replicated.

6.3.7 Scalability

As discussed in Section 6.3.5, the production scalability is desirable attribute for mass-producing large volumes of disposable microfluidic devices. Fabricating multiple identical mold masters makes parallel production possible and the simplicity of the technique for fabricating functional mold masters ensures that basic designs can be easily varied to respond to customer demands. In addition, the issue of scalability is closely related to the total time needed to fabricate the mold masters and the ease of replacing discontinued or damaged mold masters.

In terms of the LCWM and LEDM^2 techniques, the unit cost of a mold master for any additional masters created by the LHEM technique are easily replicated in large volumes once the metallic hot embossing mask is fabricated. This allows numerous parallel production lines to be used to manufacture very high volumes of PDMS polymer microfluidic devices. The PDMS can be quickly and easily cured under elevated temperatures. It only requires simple heating units such as an industrial hot plate with temperature control. One researcher at Harvard University (Whitesides, 2006) suggests that using PDMS to replicate microfluidic devices has the potential to become the future standard material for developing a wide range of microfluidic devices.

6.4 Concluding Remarks

This chapter provided an evaluation of each developed method against seven criteria for design and manufacturing. It is important to recall that the overall objective of this research is to develop innovative microfabrication methods for creating functional micromold masters that use a minimal number of processing steps, are compatible with the proven micromachining technologies, minimize negative impact on the environment, permit scalability as production demands increase, and ensure reproducibility of the mold master. The rapid fabrication process must also produce complex mold masters with accurate microfeatures and high quality surface finishes. Only the LHEM method has met all these requirements. The LCWM and LEDM^2 method have the advantage of direct fabrication of metallic mold masters but it falls short of the scalability, compatibility, and surface finishes, when compared it to the LHEM method. Because the LHEM method appears to be highly compatible with the established micromachining technologies and measures up well to all seven evaluation criteria, further investigations for this method should be taken.

CHAPTER 7

CHARACTERIZATION AND MODELING OF THE LHEM PROCESS

7.1 Introduction

This chapter presents the experimental characterization and development of an empirical model for the hot intrusion process (HI) of the LHEM microfabrication technique. The hot intrusion process is, in fact, a partial hot embossing method where the microrelief features are formed on the polymer substrate without the soften material making direct contact with the walls of the cut features in the embossing mask. This "contactless" process means that the rough wall surfaces formed during laser cutting will not impact the surface quality of the extruded microfeatures. The objective of the characterization and mathematical modeling is to better understand the physical relationship between the hot intrusion process (HI) parameters and the resultant geometric microfeatures. The selection of "optimal" process parameters is necessary to make LHEM a viable production methodology.

Mathematical modeling of the contactless hot intrusion process for parameter selection has been the subject of several previous studies (Ziolkowski et al., 2003; Shen et al., 2002; Pan et al., 2004). Typically, these researchers describe a hot-intrusion method in which an array of microlenses is fabricated by pressing a metallic mask onto a heated polymer substrate. Ziolkowski et al. (Ziolkowski et al., 2003) developed a model for fabricating contactless-embossed plastic microlenses that exploits the Laplace equation to describe both the surface tension and contact angle between the mask wall and the surface of the resultant microlens. This model is used to estimate the height and radius of the resultant PMMA microlenses. Pan et al. (Pan et al., 2004) reported the fabrication of the PC (polycarbonate) microlenses via the hot-intrusion and used an Arrhenius-type function to model the changes of viscosity with respect to temperature.

Shen et al. (Shen et al., 2002) modeled the hot-intrusion process of the fabrication of PC microlenses using the activation energy function and surface tension of the melt polymer to approximate the height and radius of curvatures of the microlenses. The authors of the latter two studies (Shen et al., 2002; Pan et al., 2004) used an empirical curve fitting technique to determine the values of constants in their proposed models.

Since the hot-intrusion process can be interpreted as a partial hot embossing (HE) process (Cameron et al., 2006; Lei et al., 2005; Luo et al., 2006; Worgull et al., 2006), previously published studies in modeling HE are also relevant to the current research. Cameron et al. (Cameron et al., 2006) empirically optimized the process parameters for hot embossing lithography of microfluidic devices by varying the embossing force, embossing temperature, embossing time and de-embossing temperature. Lei et al. (Lei et al., 2005) used contact stress analysis to model hot embossing of PMMA microchannels, and showed that the numerical prediction of wall profiles compare favorably with experimental results for channel widths, pressures, and temperatures. Luo et al. (Luo et al., 2006) employed the visco-elastic model to describe the hot embossing of PMMA microchannels. Finally, Worgull et al. (Worgull et al., 2006) applied non-linear transient thermo-visco-elasticity constitutive equations to model the hot embossing process. These researchers often used finite element analysis software to simulate the process (Luo et al., 2006; Worgull et al., 2006).

7.2 Experimental Characterization of Hot Intrusion

A primary objective of the LHEM method is to produce PMMA mold masters that have extruded microrelief patterns with near optical quality surface finishes. The previously published work of creating plastic microlenses via hot intrusion process (Ziolkowski et al., 2003; Shen et al., 2002; Pan et al., 2004) showed that the surface quality of the pillar microstructures located below the microlenses, which were formed in contact with the mask, was directly depended upon the surface finish of the masking tool. In the LHEM method, the laser micromachined surface of the mask is less than mirror quality and, therefore, the formation of the pillar microstructures during the hot intrusion process should be avoided in the LHEM method. As a result, the optical quality of microchannel

features on the PMMA master can be produced at the best quality possible. Experimental characterization reported in this chapter will focus on the formation of the extruded profiles without extended pillar microsturctures.

To quantitatively analyze the fabricated geometric features of these extruded microreliefs of the PMMA mold master, a metallic mask of microchannel features with various widths (25 to 200μm) was designed and laser cut. The mask was then used to fabricate mold masters on 1.5mm thick PMMA substrates under various HI process conditions. The geometric attributes of the extruded microreliefs were then measured.

7.2.1 Experimental setup

The key process parameters for the experiments are the pressure, temperature, and time profile of the hot-intrusion process. The geometric features of the extruded microreliefs used to replicate microchannels are width, height, curvature, and aspect ratio. Figure 7.1 shows a typical cross-sectional profile of an extruded microrelief. The range of process parameters used to fabricate the test samples are based on limitations of the experimental setup and the properties of the substrate material (PMMA), and the prior experimental observations in Chapter 5 (Shiu et al., 2008).

The metallic mask used for the hot-intrusion (HI) experiments was laser micromachined using a 3.0W (at 20 kHz) AVIA UV laser from Coherent Inc., USA (as described in Chapter 3). The pulse duration is set to less than 40ns at 60kHz. The hot intrusion (HI) mask is cut from a 75μm thick sheet of brass. The molding mask features a matrix of 9X3 machined slots. Each slot is about 2 mm length and the widths of the nine slots in each row vary from 25 to 200μm. The widths of the slots in the three rows are designed to be same in order to test the consistency of geometric properties of the fabricated microchannels. The slots are set 500μm apart from one another to ensure that they do not affect each other during the molding process.

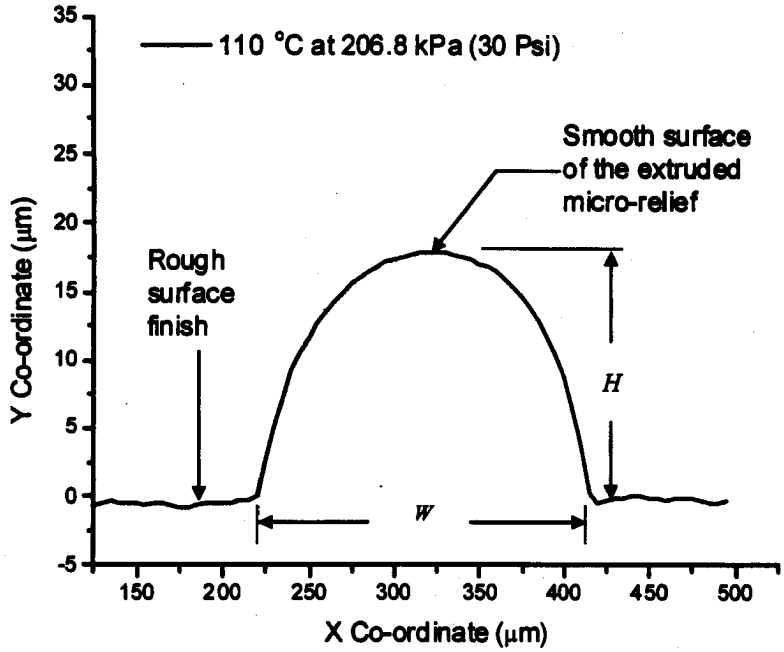

Figure 7.1 Typical cross-sectional profile of the extruded micro-relief (height H, radius R, and aspect ratio $AR = H/W$).

The minimum width of the slots is chosen to be 25μm because of the inherent limitations in the laser system that was used to produce the HI mask. Although the diameter of the focused beam of the laser is about 10μm, the cutting process was observed to be more stable in the 25μm range. The maximum width of 200μm is a typical upper limit for microfluidic applications.

Once the machined hot-intrusion mask is completed, it is then used to fabricate the test mold masters from PMMA material. PMMA material is widely used in hot-embossing and hot-intrusion processes for microfluidic applications. In addition, PMMA has good mechanical and optical properties. Its glass transition temperature (T_g) allows faster curing of elastomer PDMS molding material at an elevated temperature. The process parameter values selected for these tests are summarized in Table 7.1.

Table 7.1 Hot intrusion process parameters used in this study.

Hot-intrusion pressure p **[Psi (kPa)]**	**Hot-intrusion temperature** T **[°C]**	**Hot-intrusion time** t **[min]**	**Width of the intrusion base** W **[μm]**
30 (206.8)	T_g +10 = 110	2	25
40 (275.8)	T_g +25 =125	5	to
50 (344.7)	T_g +35 = 135	10	200
60 (413.7)	-	15	-

The minimum molding pressure (p) is chosen to be 2.07×10^5 Pa (30Psi) because the pressure distribution produced by the hot press below this value was observed to be uneven, a potential source of error. The maximum value of hot-intrusion pressure is selected to be 4.14×10^5 Pa (60Psi) in order to prevent the extruded profiles from reaching the top surface of the metallic mask.

The hot intrusion step was performed under air, and the phenomenon of air trapping was not noticeable in the fabricated mold masters when observed under microscope. In general, air trapping in the LHEM method can easily be avoided by providing "bleeding holes" in the upper press plate to let the air escape, since the softened material never touches the upper plate. In the experiments, the bleeding holes were not necessary, as the clearance between the mask and the press plate was sufficient to prevent air trapping.

In addition, a minimum temperature of 110°C is selected because this value is 10°C above the glass transition temperature (T_g) of the PMMA substrate material. The upper limit of the temperature is set at 135°C to prevent the value of Young's modulus of the PMMA to increase (Lei et al., 2005). Figure 7.2 shows that the Young's modulus of this material varies with temperature.

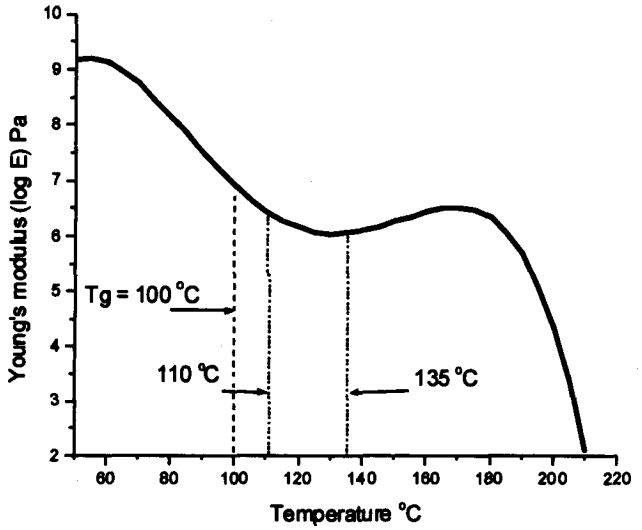

Figure 7.2 Young's modulus of PMMA material as a function of temperature (Lei et al., 2005).

In the experiments, the "HI time" is varied between 2 and 15 minutes. When the maximum duration of HI time is reached, the heater of the press is turned off and the fabricated part is left to cool down by natural air-cooling. The natural cooling (observed 1.5°C/min) is sufficiently slow to avoid build up of the thermal stress in the molded master. The demolding temperature is set to 90°C which is slightly below the PMMA glass transition temperature.

An SEM view of typical extruded microreliefs produced in this study is shown in Figure 7.3. The corresponding cross-sectional profile of a single extruded microrelief was previously given in Figure 7.1. The profile measurements were recorded using a surface stylus profiler Dektak^{3}ST with the X-coordinates of the profile measured at 5μm intervals. The average surface roughness (Ra = 10nm) of these microreliefs was measured using Wyko NT1100 optical profiling system from Veeco Instruments Inc., NY, USA.

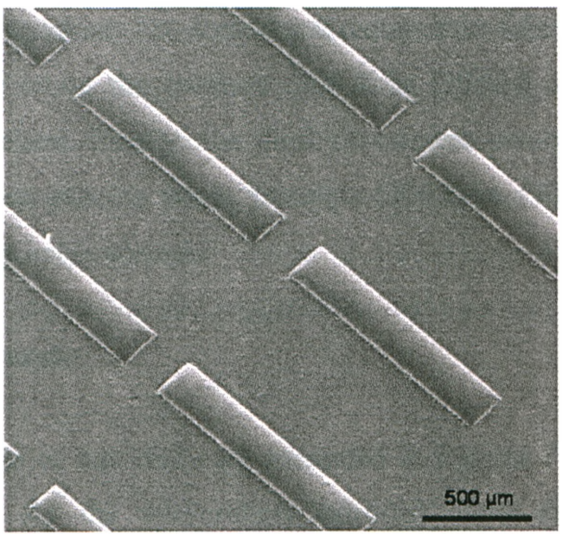

Figure 7.3 Observed features of the PMMA mold master produced in the experiments (HI temperature 125°C, HI pressure 413.7kPa (60Psi) for HI time 10 minutes): an SEM view of the extruded microreliefs showing consistent geometric features and high-quality surface finishes.

The radius R of an extruded profile can be estimated several different ways. For example, the Laplace equation was used by Ziolkowski et al. (Ziolkowski et al., 2003) to estimate the radius of extruded microlenses from surface tension and contact angle of the microlenses. R may be estimated using a simple equation based on the assumption that the cross-sectional profile of the microrelief is a circular arc. Knowing that the chord length of the circular arc is equaled to the width of the profile base (W) and knowing the height of the arc (H), it is possible to calculate the radius from basic geometric relationship:

$$R = \frac{W^2}{8 \cdot H} + \frac{H}{2} \tag{7.1}$$

To investigate the relationship between the geometric features of the microreliefs produced by the LHEM method and the hot-intrusion (HI) process parameters, three sets of experiments were conducted. The first experiment involved varying the HI pressure over a predetermined range while the temperature (125°C, T_g + 25°C) and intrusion time

(10 minutes) were held constant. The second test required the HI temperature to be varied over the desired range while the pressure (206.8kPa (30Psi)) and intrusion time (10 minutes) remained constant. Finally, the third experiment involved changing the time duration of the intrusion process while pressure (206.8kPa (30Psi)) and temperature (125°C, T_g + 25°C) were held constant.

7.2.2 Experimental results

The experimental results of this study are presented in Figures 7.4 to 7.6. The height-width (*H-W*) diagram for the microreliefs extruded under the "varying pressure" conditions is shown in Figure 7.4. The diagram shows an approximate linear relationship between height *H* and width *W*, with the slope of the plot being a function of the applied HI pressure. At a HI pressure of 4.2 x 10^5 Pa (60Psi), the height of several extruded microreliefs reached the top of the metallic mask, thereby, causing the top of the microrelief to be flattened during the fabrication process. These samples were removed from the data presented in the figure.

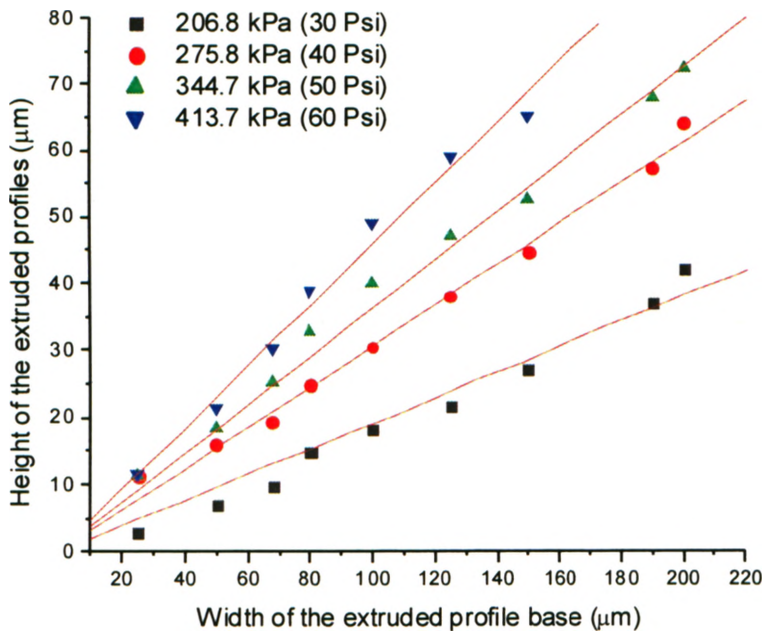

Figure 7.4 *H-W* diagram for the *"Varying HI Pressure"* experiments. Constant parameters: temperature T_g + 25°C (125°C) for 10 minutes.

Figure 7.5 shows the *H-W* diagram for the micro-reliefs extruded under the "varying temperatures" conditions. Similarly, an approximate linear relationship is observed between the extruded heights and widths, with the slopes dependent on various HI temperatures. Note that the slopes of the lines are steeper for higher temperatures. This shows that the Young's modulus, which is temperature dependent in the elastic region, is inversely proportional to the heights of the extruded micro-reliefs.

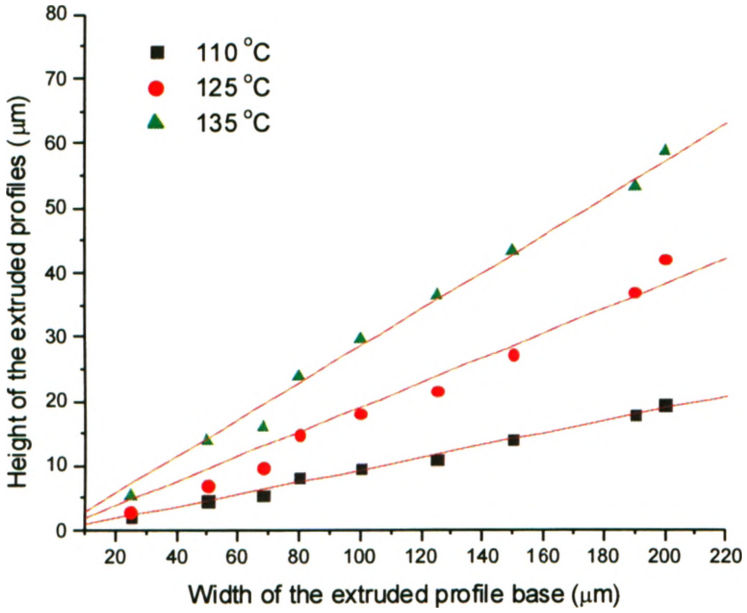

Figure 7.5 *H-W* diagram for the *"Varying HI Temperature"* experiments. Constant parameters: HI pressure 206.8kPa (30Psi) for 10 minutes.

The *H-W* results collected from the "varying time" experiments are given in Figure 7.6. In this case, there is also a linear relationship between *H* and *W*, but the slopes of various HI time durations appear to be independent of the HI time over the range investigated in this study.

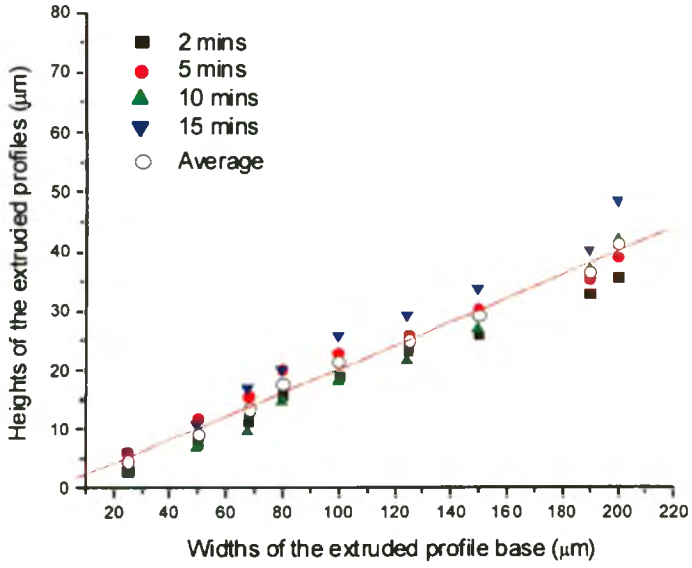

Figure 7.6 *H-W* diagram for the *"Varying Time"* experiments. Constant parameters for the experiment include a temperature of 125°C and HI pressure of 206.8kPa (30Psi).

Once H and W are measured, the aspect ratio (AR) of the extruded microrelief is calculated as: $AR = H/W$. Table 7.2 summarizes the range of values of AR calculated from the experimental data and the values of the estimated R of the extruded microreliefs calculated using Eq. (7.1) with the measured values, H and W. A comparison is shown in Figure 7.7 and it indicates a reasonably good agreement between the two. A power function model that appears to better describing the cross-section of these extruded microreliefs is investigated and is presented in later sections.

Table 7.2 Aspect ratio (AR) and calculated radii of the extruded profiles.

-	**Varying HI pressure**	**Varying HI temperature**	**Varying HI time**
AR (H/W) Min	0.09	0.09	0.17
AR (H/W) Max	0.46	0.28	0.22
Radius (μm) Min	12.56	16.96	15.62
Radius (μm) Max	140.8	269.11	157.96

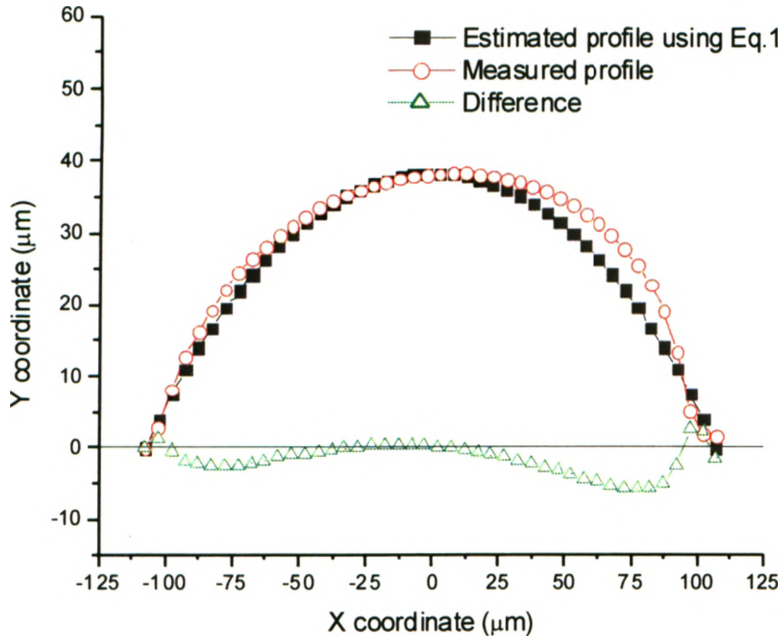

Figure 7.7 Comparison between the measured and estimated profile at 2.1×10^5 Pa and T_g + 25°C.

The widths of the extruded profiles were also measured and found, on the average, to be about 21% larger than the widths of the machined features in the HI mask. This appears to be a result of the deformation of the mask during the hot-intrusion process, caused by the lateral forces generated from the intruding soften polymer to the mask.

To examine the reproducibility of the extruded profiles, the mold master was re-fabricated under the process conditions of 125 °C, 207 kPa, and 10 minutes, and the *H-W* measurements were repeated. The difference in measurements on the two mold masters was small (average standard deviation: W: 5.1 μm and H: 0.77 μm), indicating reasonable reproducibility of the extruded profiles.

7.3 Development of an Empirical Model

In this section, an empirical model is derived from the experimental data to describe the relationship between the HI process parameters and the geometric features of the extruded microrelief. The data distribution in Figures 7.4 to 7.6 clearly indicates a linear relationship between height (H) and width (W) of microchannel profile that can be described as:

$$H = a \cdot W, \tag{7.2}$$

where a is the dimensionless parameter.

To determine the values of the "a," Eq. (7.2) was fit into the data given in Figure 7.4 using the least-squares method, with 95% confidence. This was done using Origin 6.0 software package from OriginLab, Massachusetts, USA. The resulting values are:

$$\begin{aligned} &\text{for } p_1 = 207 \text{ kPa}, \quad a(p_1) = 0.1904 \\ &\text{for } p_2 = 276 \text{ kPa}, \quad a(p_2) = 0.3063 \\ &\text{for } p_3 = 345 \text{ kPa}, \quad a(p_3) = 0.3628 \\ &\text{for } p_4 = 414 \text{ kPa}, \quad a(p_4) = 0.4587 \end{aligned} \tag{7.3}$$

The root mean square (RMS) errors of the linear fits were from 1.74 to 2.34, and root-square (R^2) values were from 0.986 to 0.992. The parameters given in (7.3) were used to plot Figure 7.8. Since it shows an approximate linear relationship between the parameter a and pressure p, the relationship can be described as:

$$a(p) = C_1 + C_0 \cdot p \tag{7.4}$$

where C_0 is a constant determined empirically with the unit of Pa^{-1} and C_1 is a dimensionless constant. Fitting this model to the experimental data using the least-squares method (RMS = 0.01715), results in: $C_0 = 1.25 \times 10^{-6}$ [Pa^{-1}], and $C_1 = -5.81 \times 10^{-2}$.

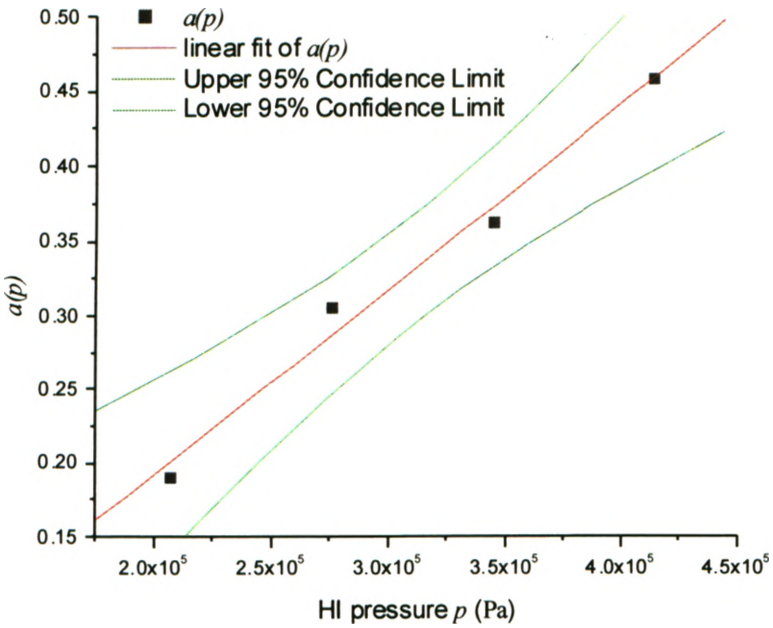

Figure 7.8 Linear relationship between *a(p)* and the HI pressure *p*.

Substituting Eq. (7.4) into Eq.(7.2) yields:

$$H = (C_1 + C_0 p)W \tag{7.5}$$

which holds under the "varying HI pressure" conditions: $p \in [207, 414]\ kPa$, $W \in [25, 200]\ \mu m$, $T = 125\ ^0$C, *Time* = 10 minutes, and substrate material is PMMA.

Recall that the extruded heights of the microrelief were shown to be inversely proportional to the HI temperature in Figure 7.6. This observation is consistent with the fact that the Young's modulus is a function of temperature (Lei et al., 2005). Therefore, Eq. (7.5) can be extended as follows:

$$H = \frac{C_T(T)}{E(T)}(C_1 + C_0 p)\, W \tag{7.6}$$

Note that $C_T(T)$ is a temperature dependent constant of the PMMA, which must be found empirically, and $E(T)$ is the Young's modulus of the material. To make both (7.5) and (7.6) hold, it is necessary that $C_T(125\ ^\circ C) = E(125\ ^\circ C)$.

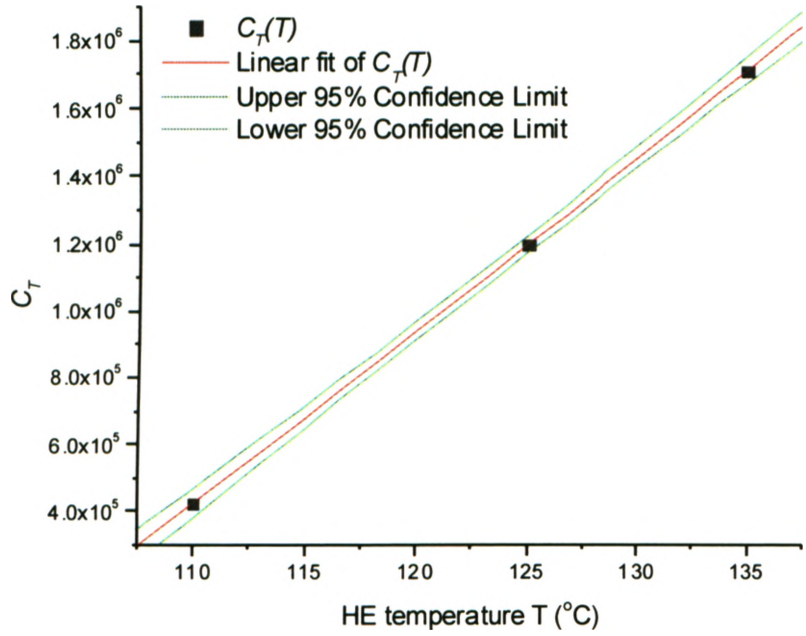

Figure 7.9 Linear relationship between C_T and the HI temperature T.

Lei et al. (Lei et al., 2005) conducted an experimental study to determine the Young's modulus of PMMA material under various temperatures. The experimental data were fitted with the following polynomial curve:

$$\log E(T) = -1.3909\times10^{-7}T^4 + 6.5716\times10^{-5}T^3 - 0.0107T^2 + 0.6707T - 4.9704 \quad (7.7)$$

The values for $C_T(T)$ at other temperatures can be estimated by fitting data shown in Figure 7.9 into the linear model:

$$C_T(T) = C_3 + C_2T \quad (7.8)$$

by using the least square method (R^2 = 1.0, RMS = 1540.3). The resulting values are: C_2 = 5.16x10^4 [$Pa/^oC$] and C_3 = -5.24x10^6 [Pa].

With these values, it is possible to obtain a final empirical model for the extruded height H:

$$H = \frac{1}{E(T)}(C_3 + C_2T)(C_1 + C_0p)W \quad (7.9)$$

which holds for: $p \in [207, 414]\ kPa$, $W \in [25, 200]\ \mu m$, $T \in [110, 135]\ ^{o}C$, $Time$ = 2 to 15 minutes, and substrate material is PMMA.

7.4 Model of a Cross-Sectional Profile

7.4.1 Mathematical representation of an extruded micro-profile

In previous sections, the experimentation and empirical model, Eq. 7.9, used to describe the relationship between the key hot intrusion process parameters with the width and height of the extruded profile were presented. The shape of the extruded profiles was estimated based on the assumption that the extruded profile can be represented as an arc curve. This section illustrates a more accurate mathematical model representation that describes the extruded profile shape and verified using the experimental data with statistical analysis. The extruded profile width W is measured at the base of the extruded profile and the height h is measured from the profile base to the peak of the profile, Figure 7.1. Based on the experimental observations, 2D profile of extruded microreliefs appears to be approximated well by a power function:

$$y = A \cdot |x|^{B} + C \tag{7.10}$$

where x and y are the coordinates of a profile and A, B, and C are real parameters. The extruded profiles are symmetric from observations in experimental data in Section 7.2, therefore, half width of a profile can be described as $W/2 = p$.

The boundary conditions of the power function are when ($x = 0$, $y = h$), and when ($y = 0$, $x = p$. By substituting these conditions into Eq. (7.10), the real parameters of A and C were found when $x = 0$, $y = h$, and therefore, $C = h$, and when $x = p$, $y = 0$, we have

$$A = -\frac{h}{|p|^{B}}$$

By substituting the A and C into Eq. (7.10):

$$y = -\frac{h}{|p|^B} \cdot |x|^B + h \tag{7.11}$$

Now B is the only remaining unknown in Eq. (7.10). To estimate B, it is possible to fit the measured points of an extruded profile into Eq. (7.11). To simplify the process, the x and y coordinates are normalized by dividing by p and h, respectively.

$$X = \frac{x}{p}, Y = \frac{y}{h} \tag{7.12}$$

This step makes all curves of extruded profiles having the same unit length of height and half-width. Thus, Eq. (7.13) is obtained by substituting X, and Y into Eq. (7.11):

$$Y + 1 = |X|^B \tag{7.13}$$

Parameter B can now be estimated by linear fit the curve in the plot Log$(Y+1)$ vs. Log X using the least-squares method. The conditions for the model to be valid are summarized in below:

a) $B > 1$ is physically possible given the experimental observations in Section 7.2. Figure 7.10 shows the effects of various B values onto the shape of extruded profiles,

b) the extruded profiles are assumed to be symmetric about the Y-axis,

c) the absolute value of X and $Y+1$ are required to make Eq. (7.13) valid for the logarithm function.

Through the above derivation, it has been shown that the three parameters (p, h, and B) can represent the extruded microprofiles. The model is then validated using the experimental data presented in Section 7.2. B values of the extruded profiles will be determined with the same experimental data.

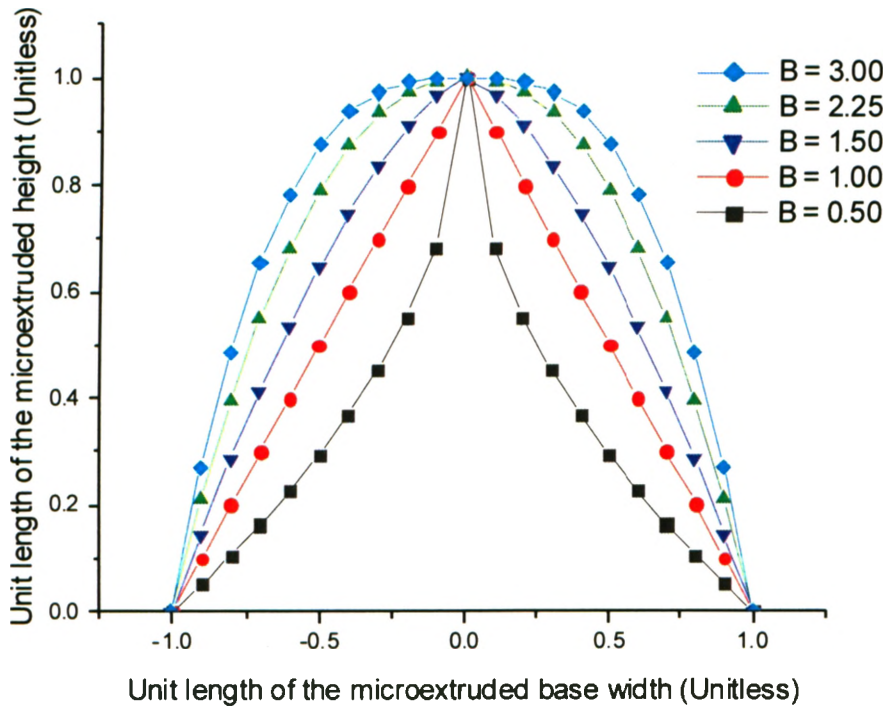

Figure 7.10 Effect of the parameter *B* on the shape of the micro-relief profile.

7.4.2 Results of the power-function model

The visual comparison between the modeled and measured profiles appears to be in good agreement. Figure 7.11 shows a typical plot of the coordinates of a measured profile and a modeled profile. Figure 7.12 shows a typical *B* values of an extruded profile calculated by linear fit the log-log plot of the coordinates of a measured profile using least-squares method, $R^2 = 0.99$. In a typical profile, a slight variation of *B* values from both sides was observed. These two *B* values were averaged to represent a *B* value of a profile.

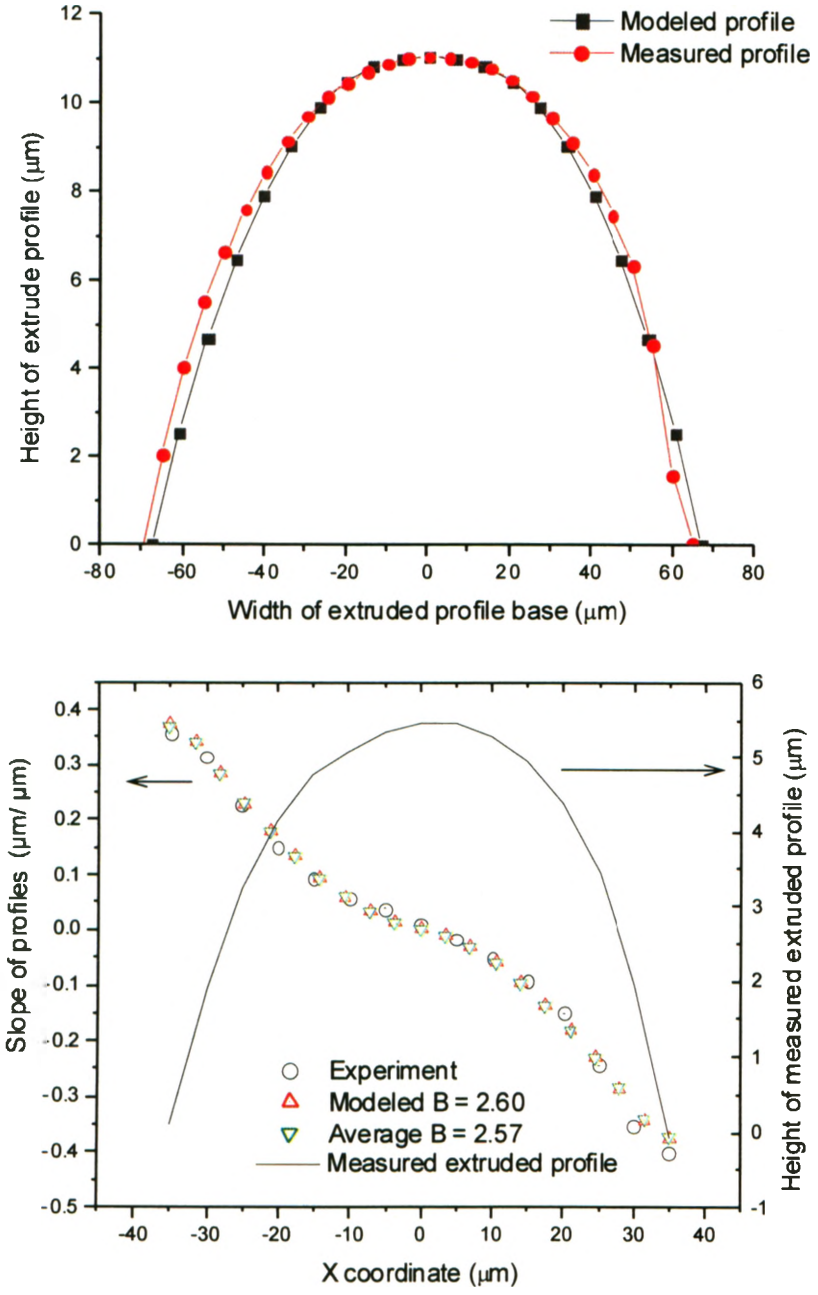

Figure 7.11 Comparison between the modeled and measured extruded profiles. The shape of slopes (top) and process parameters (bottom) where: 110°C, 207 kPa (30 Psi), and 10 minutes.

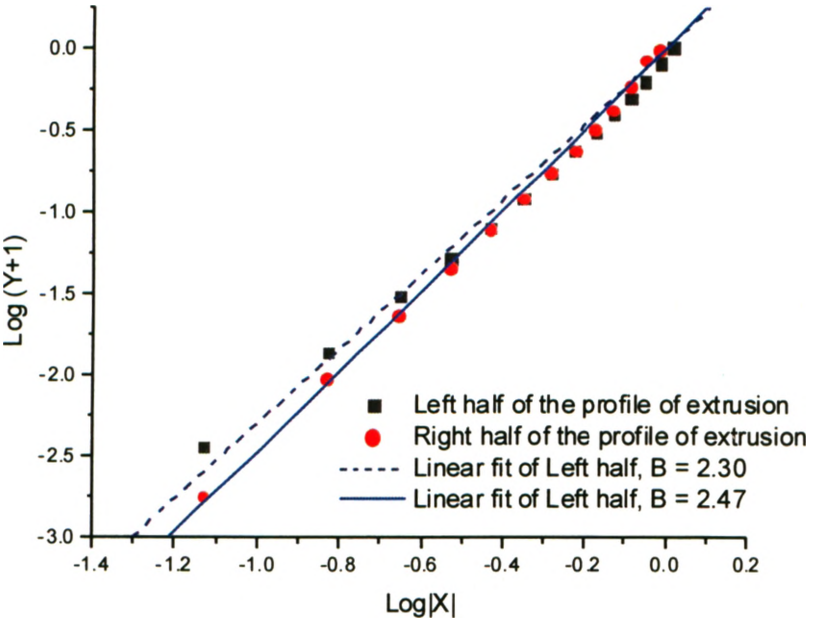

Figure 7. 12 *B* value of an extruded profile estimated by linear fit of the log-log plot.

Figures 7.13 to 7.15 show these computed *B* values under three different process conditions such as HI pressure, temperature and time. These values appear to be distributed randomly but mostly concentrated around 2.35 to 2.75. Figure 7.16 show the distribution of the *B* values and average value is around 2.57. Figure 7.17 shows the areas under the curve (extruded profiles) of both modeled and measured profiles and indicated less than 2% of difference in areas.

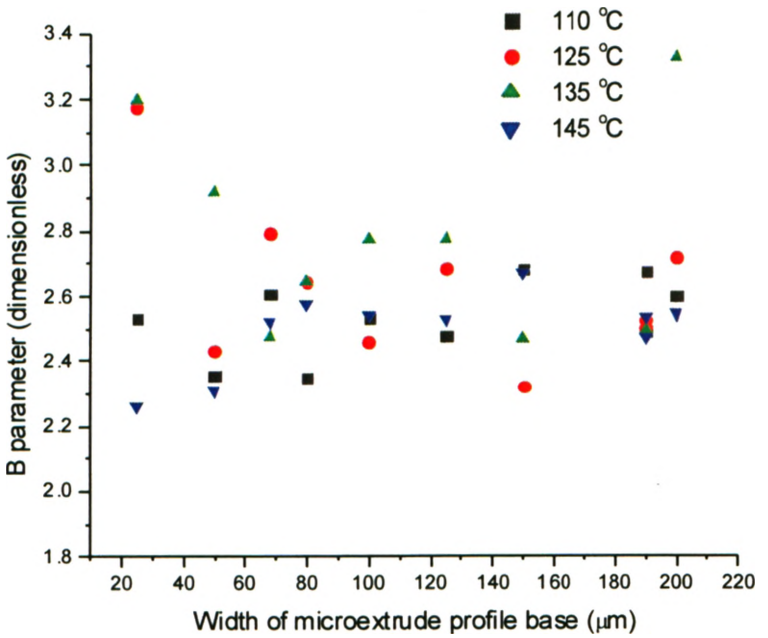

Figure 7.13 *B* values at various hot intrusion temperatures.

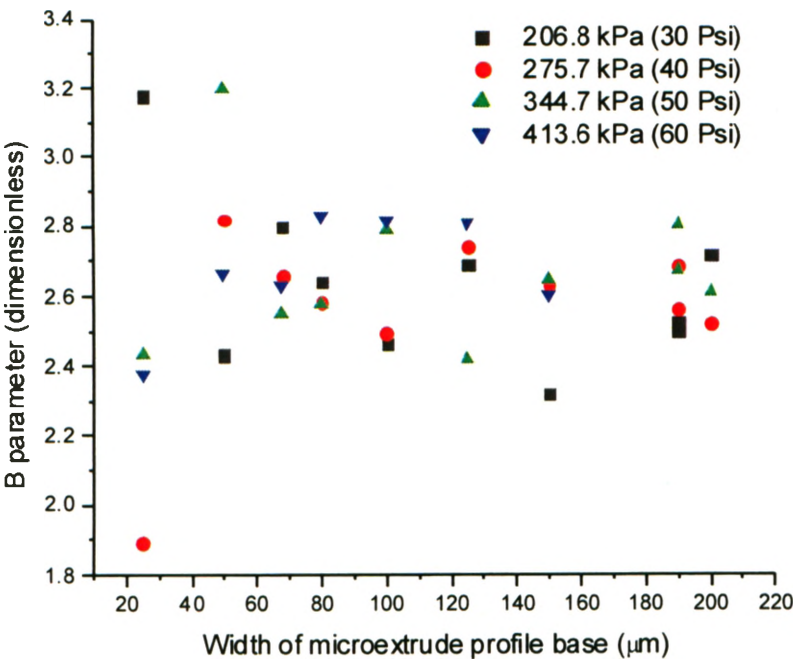

Figure 7.14 *B* values at various hot intrusion pressures.

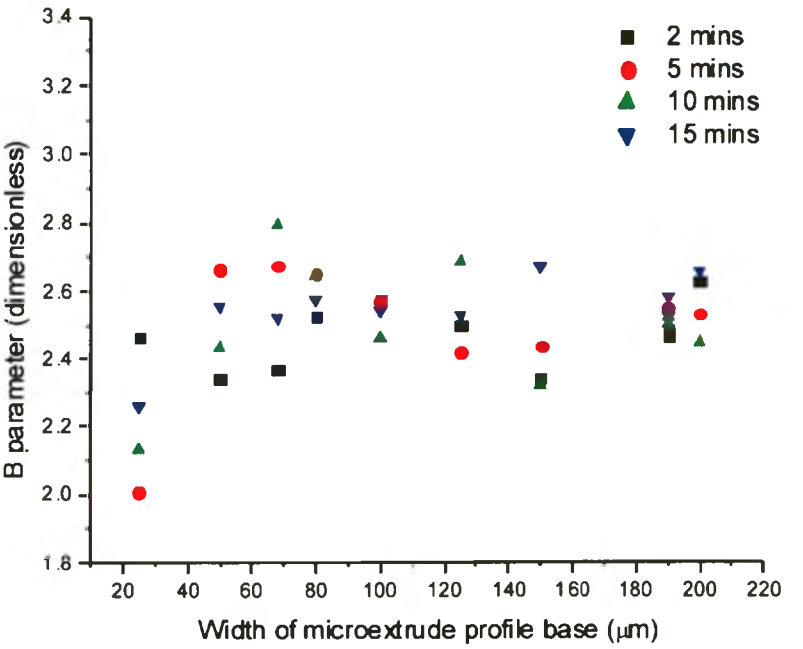

Figure 7.15 *B* values at various hot intrusion times.

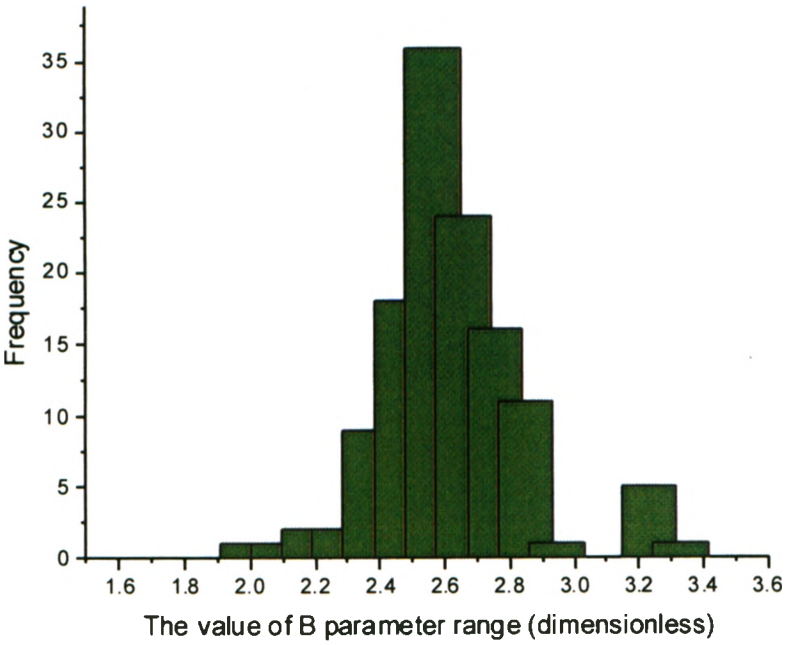

Figure 7.16 Distribution of *B* values concentrated around 2.45 to 2.75.

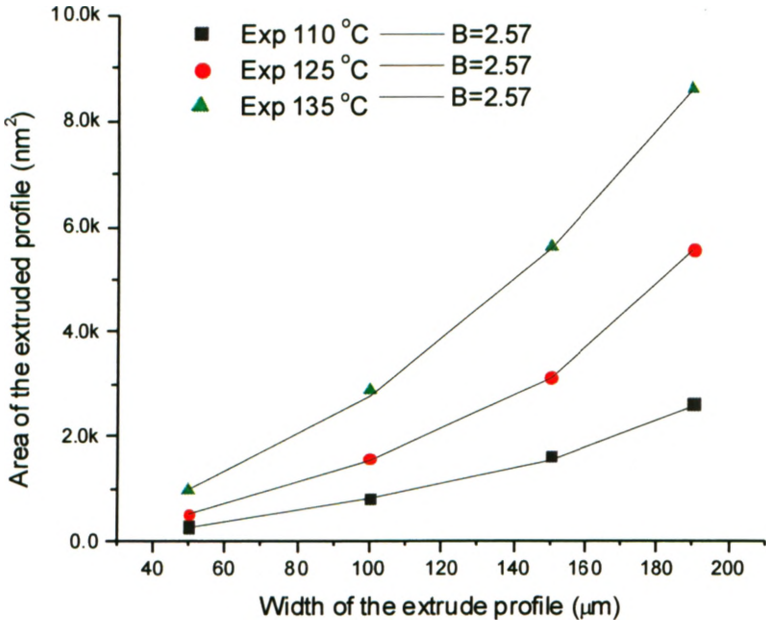

Figure 7.17 Comparison of area under the profile curves of the extruded microprofiles between measured and modeled ($B = 2.57$) profiles.

7.5 Discussion of the Results

The developed empirical model given by (7.9) can be used as a simple tool for estimating the height of the micromold reliefs fabricated by the LHEM method. It establishes the relationship between the height of the extruded microrelief and the designed width of extruded profile and key process parameters (pressure and temperature). Being a simple algebraic equation, the model is easy to use and provides the estimate feature dimension without the need for computationally intensive finite element analysis.

As shown in Figure 7.6, the hot-intrusion time in the investigated range does not have a significant effect on the height H, and therefore can be set within the bounds defined above. This is in line with the previously published results (Cameron et al., 2006) where longer hot embossing time was shown to have little effect on the filling of microchannel cavities.

The model is valid within the bounds of the key parameters defined by (7.9), and when PMMA is used as the substrate material. PMMA features good mechanical and

optical properties and is a widely used material in micromolding of microfluidic devices. As such, it was chosen for this study; other materials (such as polycarbonate) will be considered in the future work.

For the power function that models the extruded microprofile shape, the results of the modeling using Eq. (7.13) indicated that the modeled profiles describe the measured extruded profiles in an average of only 1.62% difference in cross-sectional area. Therefore, the profiles generated using the proposed model appears to be a good approximation of the microprofiles. The relationships between the B values and HI process parameters (hot intrusion pressure, temperature and time) under our considered process conditions were examined based on statistical analysis techniques. The results suggest that B values are uncorrelated to the process parameters experimented in this study.

7.6 Concluding Remarks

This chapter presented the experimental characterization and an empirical model describing these heights of the extruded microreliefs as a function of key process parameters for the LHEM method. The fabricated heights of microreliefs are a nonlinear function of temperature and pressure. The height of the extruded microreliefs ranged from 5 to 75μm and aspect ratio from 0.1 to 0.46. The model was derived by fitting experimental data using the least-squares method, and is offered as a simple tool for choosing hot-intrusion parameters for the LHEM method. The cross-sectional profiles of the extruded microreliefs were modeled using a simple power function and an average value of 2.57 was found to represent well the profile shape across various hot intrusion process parameters in the experimental conditions.

CHAPTER 8

MODELING THE HOT INTRUSION PROCESS USING FINITE ELEMENT METHOD

8.1 Introduction

An empirical model used to describe the formation of contactless extruded microreliefs, created by hot intrusion process (HI), was presented in Chapter 7. The derived model was based on the experimental observations and measurements of key process parameters that influence the profile shape of the extruded microreliefs. This empirical model does not, however, explain the physics behind the formation of the extruded microreliefs as the softened material flows through the cut features of the mask.

A *finite element method* (FEM) model is introduced in this chapter to describe the formation of the cross-sectional profile of the extruded microrelief features during the HI process. This FEM model was generated by applying first principals to develop a deeper understanding of how the extruded microreliefs are physically created. The FEM model and analysis is developed using the commercial software package called Comsol Multiphysics 3.2.

8.2 Mechanical Properties of PMMA

As discussed in Chapter 2, polymmethacrylate (PMMA) behaves as a hard, rigid and optical clear material at ambient temperature. However, as temperature increases the mechanical properties of PMMA undergoes significant changes. Some amorphous polymers such as PMMA become "rubber like" or "solid-rubber" state when the temperature is increased to a value above its glass transition temperature (T_g). At this transition state, the molecules of the heated polymer tend to align themselves in the direction of stress. If the material is then cooled below its T_g, while maintaining the

applied pressure, the polymer hardens at that state. The material stress characteristics of the glass transition property exhibited by amorphous polymers makes it possible to describe the formation of the extruded microreliefs using a stress-strain model. Often a shrinkage factor is included in the design to compensate the expected percentage shrinkage. However, in this application the shrinkage percentage is expected to be difficult to observe because the extruded microreliefs are created "contactlessly".

8.3 Finite Element Method (FEM) Modeling

8.3.1 FEM model of PMMA

The intent of the FEM model is to describe the cross-sectional profiles (2D) formed through hot intrusion. With the known stresses and PMMA substrate's Young's modulus value at it's elastic region, Hooke's law can be applied to calculate strains at the given process temperature, provided the assumption of that the polymer behaves elastically when it is above T_g and below the melting temperature (T_m), and the polymer solidifies under a constant pressure when polymer cools below its T_g. As previously discussed, an amorphous polymer becomes a soften polymer at its "solid-rubber" state when it is heated above its glass transition temperature (T_g), and does not exhibit typical plastic stress-strain behavior. Therefore, once the stress is known and the strains are related to Young's modulus E and the Poisson ratio v, the following stress-strain equation can be used:

$$\varepsilon_x = \frac{1}{E}(\sigma_x - v\sigma_y) \quad , \quad \varepsilon_y = \frac{1}{E}(-v\sigma_x + \sigma_y) \tag{8.1}$$

The displacement can be calculated via the strain-displacement relationship (Budynas, 1999). The Poisson ratio is assumed to be independent from temperature, v = 0.4. Young's modulus value of the PMMA polymer is dependent of the processing temperature as reported by Lei et al. (Lei et al., 2005). For the FEM model, the temperature condition of PMMA material at the processing temperature under hot

intrusion is assumed to be constant. Young's modulus value *E(T)* for PMMA material is computed using an empirical equation, Eq. (8.2), that derived from curve fitting experimental data (Lei et al., 2005),

$$\log E(T) = -1.3909\times10^{-7}T^4 + 6.5716\times10^{-5}T^3 - 0.0107T^2 + 0.6707T - 4.9704, \quad (8.2)$$

where *E(T)* is Young's modulus (Pa) of the PMMA polymer at a hot intrusion (HI) temperature T(°C). Experimental observations in Chapter 7 have shown that the differences in the final geometries of the fabricated microfeatures from 2 to 15 minutes of HI time are small, and, therefore, the hot intrusion (HI) time condition in this FEM model is considered as a static condition if the HI time remains within 2 to 15 minutes. A static analysis case provided by the FEM software package is used in all models.

The exact melting temperature of PMMA is relatively less definite than the glass transition temperature (T_g). The melting temperature of PMMA material (T_m) starts at around 130 to 140°C. This heated polymer may be in the state of between "solid-rubber" and "rubber-liquid." Therefore, the FEM simulated results at 130°C and above may have deviated predictions of the extruded heights of the microreliefs.

8.3.2 Computational issues

The implementation of the FEM model and analysis were done using Comsol Multiphysics 3.2 (previously known as FEMLAB) FEM commercial software package. The CPU time to process and solve each condition was approximately 10 to 20 minutes computational time on a 1.6 GHz PC having 1 GB RAMs. The simulated FEM results are then compared with the experimentally determined and measured data taken from Chapter 7. This FEM model is valid only under the following processing conditions: hot intrusion (HI) pressures range from 207 to 414kPa, HI temperatures are between 110 to 135°C, widths of the microfeature base are from 25 to 200μm, and the process times of the PMMA substrate material are within the range of 2 to 15 minutes. FEM model run conditions were based on the experimental observations unless otherwise mentioned.

The element type used in the finite element method (FEM) was Lagrange-Quadratic. The principle of virtual work was also used in the implementation by the software package. The continuum application mode for plane-stress structural mechanics was employed in this FEM model. The 2D extruded microreliefs were assumed to behave as a thin plate problem. The CAD model generated in Comsol consisted of two structural steel sheets lying on top of a PMMA polymer substrate. The FEM mesh of the fabrication process is shown in Figure 8.1.

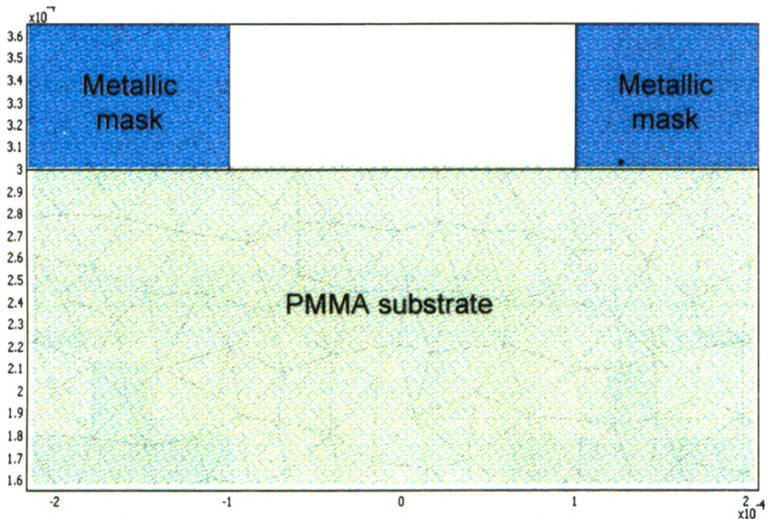

Figure 8.1 Two-dimensional layout of the meshes of the FEM model. The walls of the metallic mask are shown at the top of the PMMA substrate.

The static analysis case was selected to simplify this FEM model because the heated and soften PMMA was assumed to align along the direction of the applied stress and the applied stress was maintained until the heated PMMA cooled below its glass transition temperature. At this state the shape of the PMMA polymer would be frozen. The polymer and metallic mask were assumed to be at a same processing temperature throughout the hot intrusion molding process. This assumption in the FEM model helped to simplify the complexity of modeling exercise because the conditions of heat transfer such as conduction, convection, and radiation were neglected.

Figure 8.2 shows the FEM simulated result of the extruded profile arising from the hot intrusion pressure applied on a heated PMMA substrate. This figure also illustrates the deformed shape of the PMMA substrate which closely resembles the measured profiles taken by the surface profile Derkat[3]ST. The distribution of stress applied onto the mask and PMMA substrate are mostly concentrated at the corners where the metallic mask makes direct contact with the PMMA substrate. Furthermore, by varying the input values of process parameters in the FEM model, the FEM simulated extruded profile appears to be similar to that found in the metallographical cross-sectional view captured by the optical microscope, see Figure 8.3. Careful systematic FEM simulations were conducted. The next section describes several tests used to compare the FEM simulated and measured data.

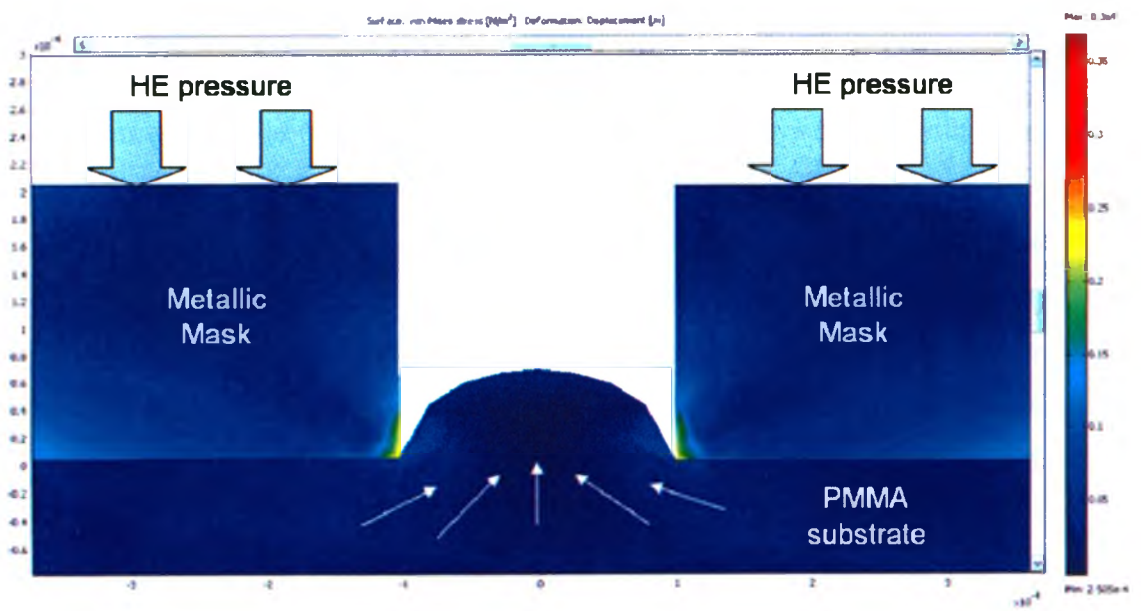

Figure 8.2 FEM simulated result of the formation of a PMMA extruded profile by the hot intrusion process.

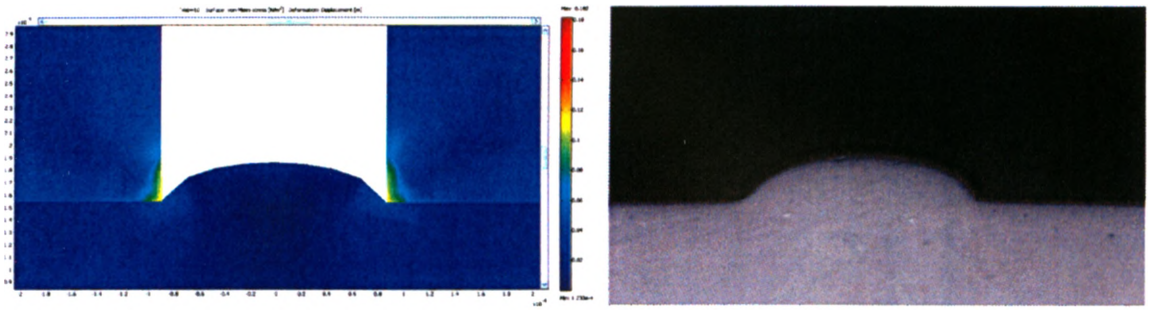

a) b)

Figure 8.3 The extruded profiles generated by FEM simulation under varying the key process parameters (a), and metallographical cross-section of the extruded profile found in experimental results (b).

8.3.3 Simulation results and comparative analysis

Figures 8.4 to 8.6 show the FEM simulated results of the heights of extruded profiles under various HI pressures and were compared with the experimentally measured results. The FEM results were consistently lower than the measured results but with very similar tendencies. Subsequently, the HI pressures were increased by 30% and the FEM simulated results were in close agreement with the measured data at HI temperature of 110 to 125°C. However, the FEM model was further under predicted the extruded heights of microreliefs at the HI temperature 135°C. Subsequently, Young's modulus value of PMMA substrates was adjusted at this HI temperature. A good agreement between the FEM data and measured data was found when the modulus was reduced by 25%.

Figure 8.6 shows the differences between the widths of the mask openings and of the extruded microreliefs at the base. This figure validated the measured results in experiments presented in Chapter 7 that the extruded microreliefs have a wider base width dimension than the mask openings because of the mask suffered deformation caused by the lateral forces generated by the soften polymer intruding into the mask during hot intrusion. FEM simulations were re-run under the condition of both with and without the constraint of horizontal direction of the metallic mask.

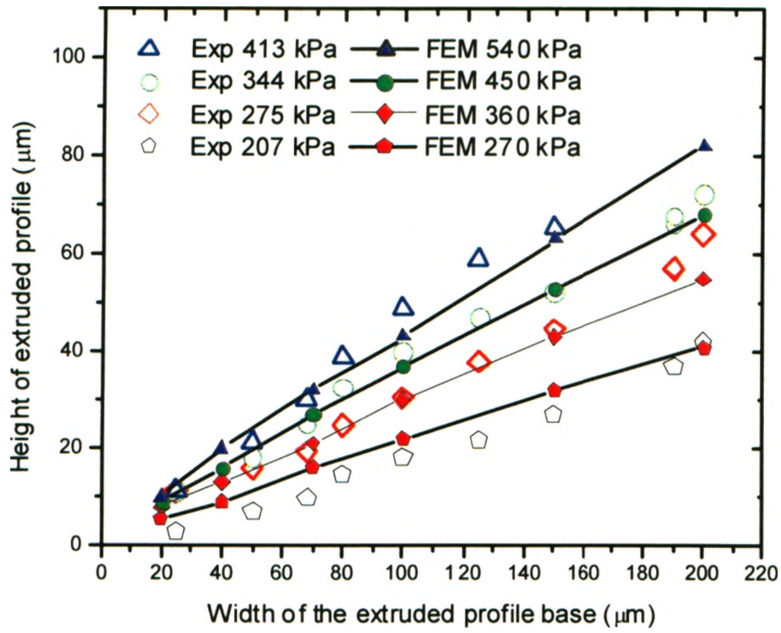

Figure 8.4 Comparison of heights of extruded profiles between measured and FEM simulated data under various HI pressures at 125°C HI temperature.

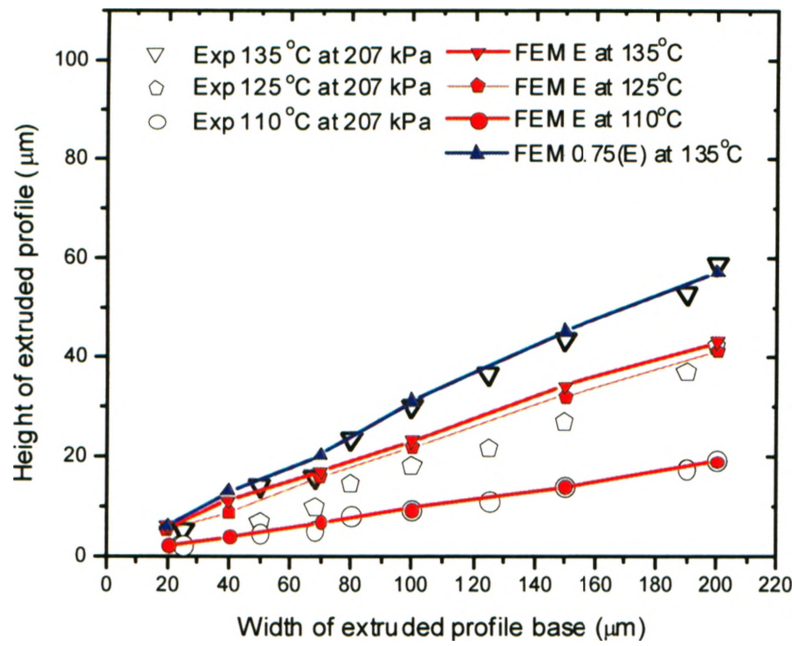

Figure 8.5 Comparison of height of extruded profiles between measured and FEM simulated data under various HI temperatures at 207kPa HI pressure.

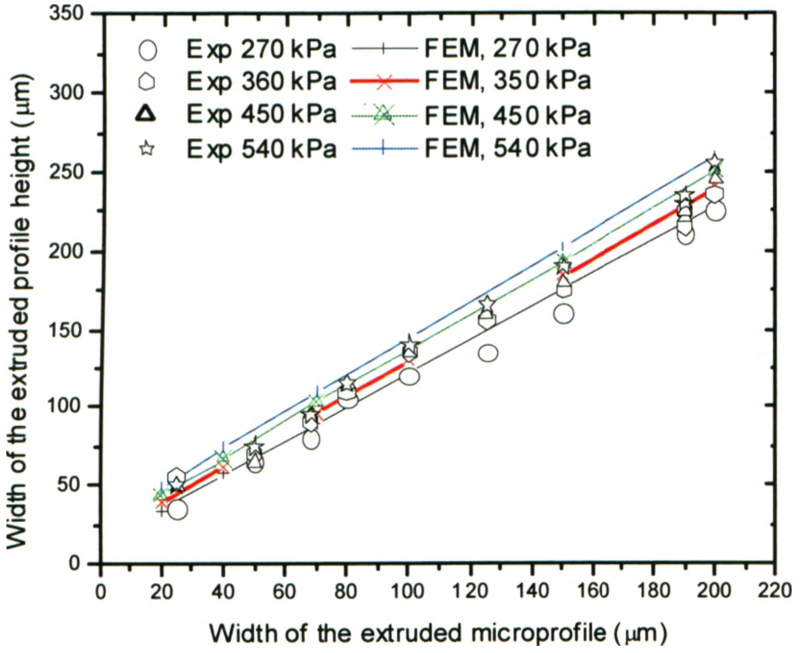

Figure 8.6 Comparison of widths of extruded profiles between measured and FEM simulated data under various HI pressures at 125°C HI temperature.

8.4 Microfeatures with Near Optical Quality Surfaces

Based on the FEM predictions described in this chapter and experimental measured results in Chapter 7, there is a strong positive correlation between the extruded height H and width W of the extruded profiles at a given hot intrusion process conditions. The implication of this correlation is that, if used innovatively, the LHEM method can be employed to fabricate 3D microfeatures. This section, therefore, illustrates the potential of the LHEM method for fabricating several micromold masters with complex microfeatures such as a 3D micronozzle.

Figures 8.7 to 8.13 show several examples of these 3D microfeatures produced by the LHEM method. Figure 8.7 provides a microscopic photograph of a 3D microchannel mold master that was formed by a mask with three connected circular holes. The profile of the microchannel measured by optical profiler along its axis is given in Figure 8.8. Continuous varying heights of microstructure are clearly visible. Figure 8.9 shows

another example of a 3D microchannel mold master and its profile is illustrated in Figure 8.10. A more complex microchannel with varying (3D) profile is given in Figure 8.11.

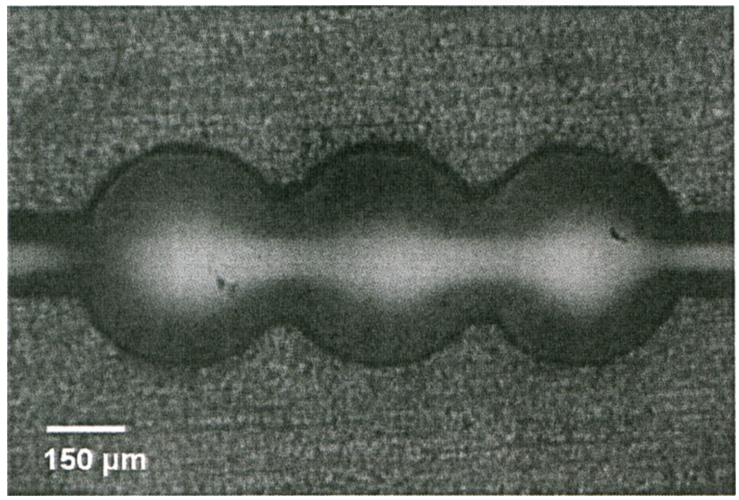

Figure 8.7 Microscopic view of the microfeatures of microlens/microchannels of the PMMA mold master.

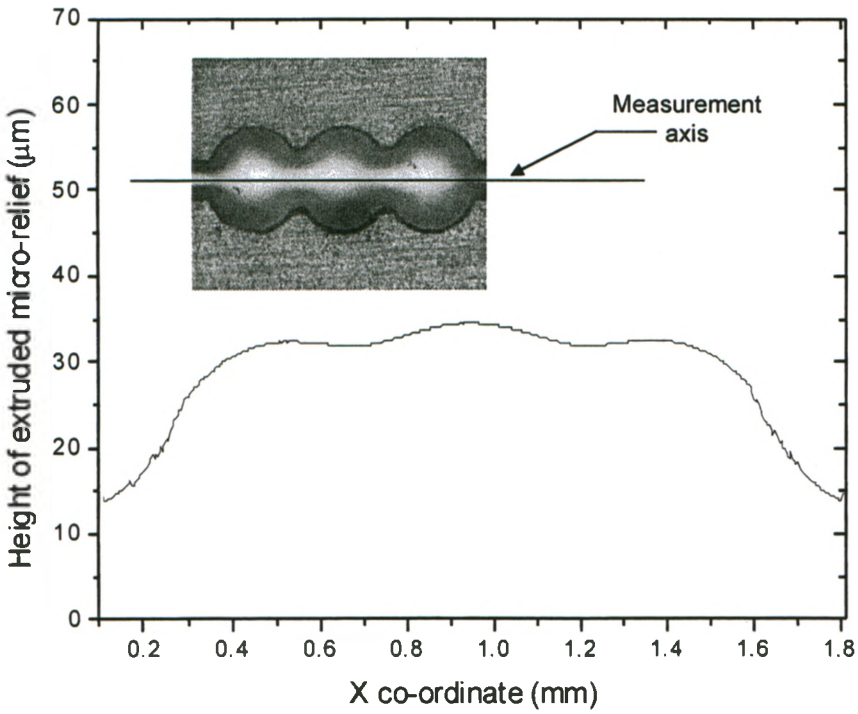

Figure 8.8 The measurement of the PMMA mold master taken by the Wyko optical profiler, shown in Figure 8.7.

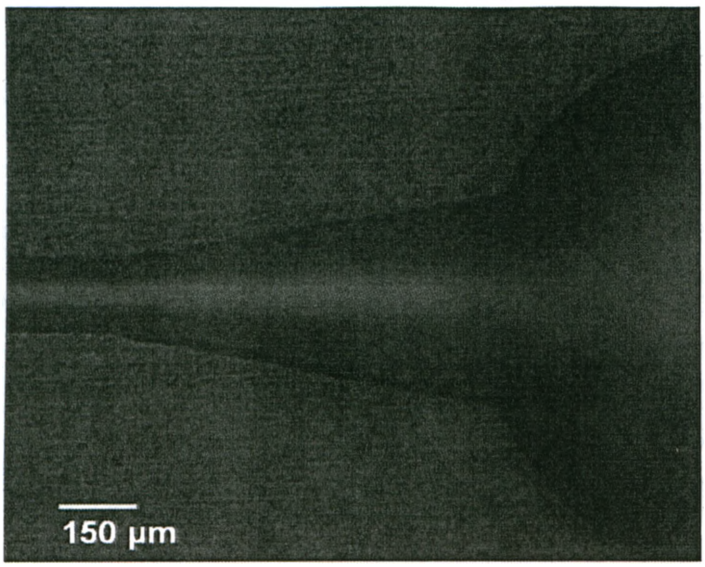

Figure 8.9 Microscopic view of the 3D nozzle microfeatures connected to a reservoir, fabricated using the LHEM method.

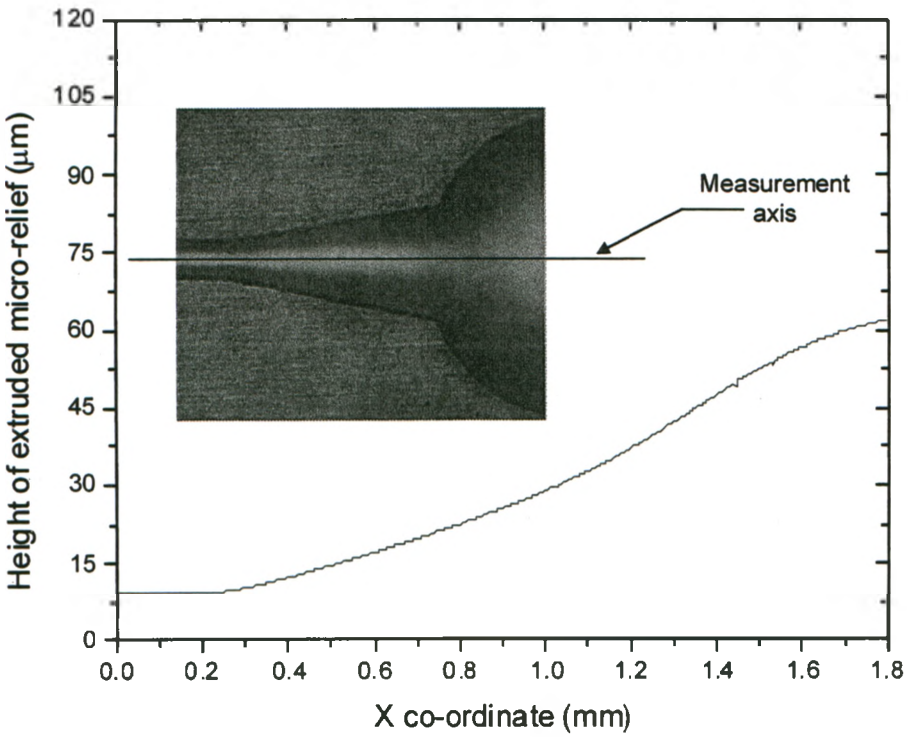

Figure 8.10 The measurement, taken by the Wyko optical profiler, of the 3D micronozzle feature of the PMMA mold master shown in Figure 8.9.

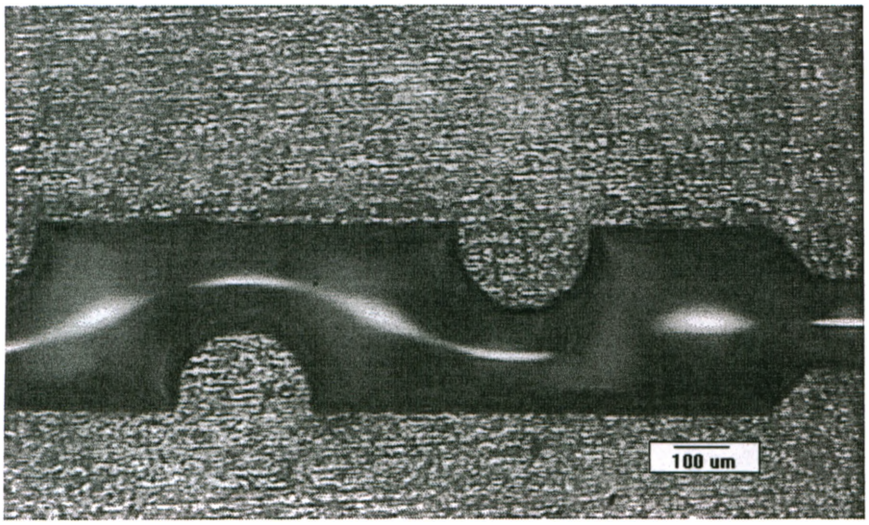

Figure 8.11 Microscopic view of a section of the 3D microchannel PMMA mold master.

The surface finish quality in all examples was measured using the Wyko optical profiler and the measurements were Ra = 10 to 40nm. This means that the fabricated microchannels have walls with near optical quality finish. Figures 8.12 and 8.13 show two cases where the top of the microchannels were flattened when the softened material reaches the top press plate. This can be achieved by choosing appropriate process parameters and can be useful in some applications.

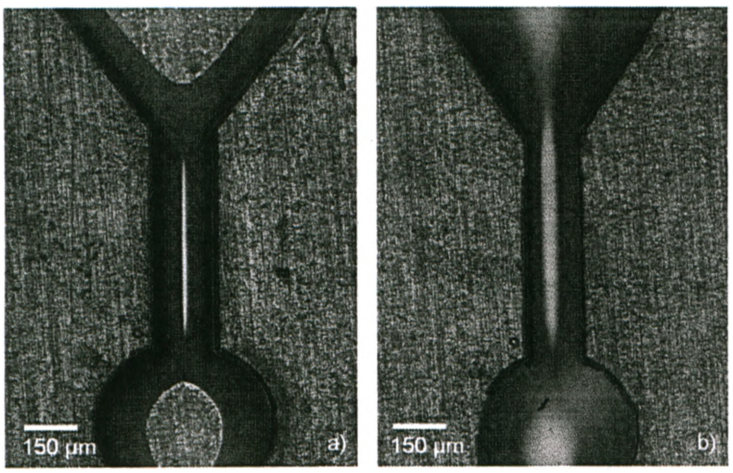

Figure 8.12 Two microscope views of microchannels of the master fabricated under different process conditions: (a) applied a higher pressure, and (b) applied an optimal pressure to produce near optical finishes.

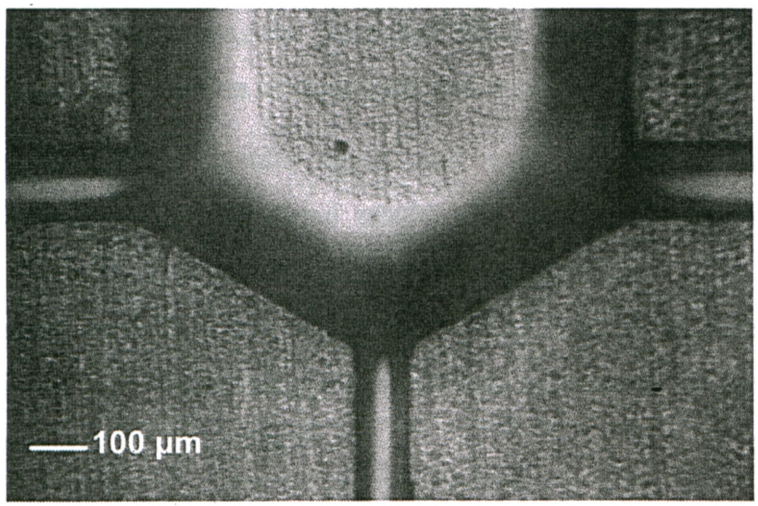

Figure 8.13 Microscopic view of a PMMA mold master had large flatted surface connected to three microchannels.

8.5 Discussion

The FEM simulated results agree well with experimental data at HI temperature above PMMA's glass transition temperature (T_g) and below its melting temperature (T_m). This suggests that the proposed model for describing the formation of cross-sectional shape of microfeatures (2D case) produced via the hot intrusion process of the LHEM method is adequate in a specific temperature range. Initially, the consistent offset of the FEM prediction of the extruded heights of microreliefs at HI temperature from 110 to 125°C by 30% lower HI pressure suggests that the model that only considers a 2D case may contribute to the deviation. Once this HI pressure values were increased by 30%, the simulated FEM results and measured data at HI temperatures from 110 to 125°C are in good agreement. Further investigation is needed to confirm the reasons of this deviation of the FEM simulation.

At 135°C HI temperature, the FEM model further under predicted the extruded heights of microreliefs. At a 25% reduced Young's modulus of PMMA at 135°C, a good agreement was found between the FEM and measured data. Because of the melting temperature of PMMA is around 130 to 140°C, PMMA at 135°C may be in a "rubber-liquid" state rather than in a "solid-rubber" state. This "rubber-liquid" condition suggests

that at higher HI temperatures, the proposed FEM model may not be suitable to completely describe the formation of these extruded microreliefs.

The simulated FEM results agree well with the experimental observation presented in Chapter 7. The simulated results also confirmed that the hot intrusion distorts the mask openings; as a result, the extruded features have wider widths than the mask. This was further verified by re-running the FEM simulations under the conditions of non-constraining and constraining the horizontal movements of the metallic mask during the formation of the microreliefs.

Thermal shrinkage effects due to the thermal cycle applied on the PMMA were neglected in the FEM model because of the microreliefs were created in a contactless manner. The simulated FEM heights of extruded reliefs were initially expected to be higher than the measured data to account for the thermal shrinkage effects. In result, the shrinkage effect can be estimated. However, the required increase of 30% HI pressure adjustment prevented the FEM model from estimating the shrinkage effect arising in this process.

Because the extruded microfeatures were not in contact with the mask walls, the friction condition that commonly occurs during demolding was not a critical factor that needed to be modeled. The low friction condition occurs because of the naturally created parabolic profile and the near optical grade surface finish that assists with demolding - unlike the impact that friction has on the processes of hot embossing or injection molding. FEM models for hot embossing and injection molding must take demolding friction into consideration (Worgull et al., 2006).

Finally, the 2D FEM model demonstrated that the hot intrusion process of the LHEM can be adequately modeled when the PMMA processing temperatures are above PMMA's glass transition temperature and below its melting temperature. Furthermore, 3D microchannel features can be fabricated based on the strong positive correlation observed between extruded heights and widths of these LHEM method produced features.

8.6 Concluding Remarks

This chapter presented a finite element model (FEM) study to predict the extruded microrelief geometry that is created by the hot intrusion process. The non-contact nature of the formation of these extruded microreliefs allows a relatively simplified FEM model to be used for this purpose. The model neglects the friction condition during demolding that typically employed when modeling conventional hot embossing.

The results of the FEM study show a strong positive correlation between the extruded width and height as observed in the experiments presented in Chapter 7. This correlation was employed to fabricate several 3D microfeatures such a 3D micronozzle, with the optical grade of surface finishes.

CHAPTER 9

CONCLUSIONS

9.1 Concluding Comments

The objective of this research project has been to develop innovative nonlithographic technologies for the rapid fabrication of high-quality mold masters that enable the cost effective production of disposable polymer microfluidic devices. This thesis was organized into two major parts. The first part of the dissertation described the three novel microfabrication methods (LCWM, LEDM^2, and LHEM) developed in this research and provided detailed experimental demonstrations to illustrate each technique. Each of these methods has its advantages and disadvantages to produce mold masters for replicating polymeric microfluidic devices. The selection of the most appropriate method depends on the intended application and desired dimensional scale of the micromold features. For microstructures with high aspect ratios, the LEDM^2 method is the most suitable because it permits the fabrication of various high strength materials used as the mold master substrates. Unfortunately, the mold masters fabricated by microEDM fabrication process results in non-optical grade surface finishes. For near optical quality surface finishes, the LHEM method is the better option. However, the microstructures produced through hot embossing process have non-rectangular profiles and relatively low aspect ratios. For applications that require microchannels larger than 75μm in width, the LCWM method may be selected.

The second part of this thesis described the detailed characterization and in-depth analysis of the LHEM method, which was determined to be the most promising microfabrication technique proposed in the research project. Specifically, the LHEM method offered several important advantages in the fabrication of micromold masters including the near optical quality of surface finishes, simple setup, and rapid fabrication. Both empirical and FEM modeling of the hot embossing process used by the LHEM technique were conducted to gain additional insight and a fundamental understanding of

how the "contactless" microreliefs were created on these polymer mold masters. Finally, the investigations show that 3D microfeatures with near optical quality surface finish can be fabricated using the LHEM method.

9.2 Thesis Summary

This thesis illustrated several novel techniques for the rapid and inexpensive fabrication of micromold masters that can be used to produce large volumes of polymer microfluidic devices. Microfluidic and LOC devices need to be disposable to avoid sample contamination and, therefore, the device fabrication cost must be low to keep the ever-increasing health care cost within a sustainable level. Using polymer mass-production technologies to produce these LOCs is promising because many polymers are biocompatible and available at low cost. However, the desired micromold masters are typically expensive to design and fabricate.

Chapter 2 discussed several important microfabrication techniques currently used in the fabrication of microfluidic devices. These techniques involve the extensive use of chemicals and, therefore, it is desirable to develop "less-chemical dependent" fabrication techniques. To addresses this need, Chapter 3 presented the first developed method, LCWM, where the metallic micromold masters were created by first laser micromachining the metallic microfluidic network patterns – that is, developing positive imprints of the fluidic flow network and supporting structures. Subsequently, the cut relief pattern is joined by laser microwelding onto the metallic substrate to create the final metallic mold masters. This method is termed LCWM (Laser microCutting, Welding, and Molding). A Y-channel microfluidic mixer was replicated by casting PDMS elastomer onto this master. This micromixer was then successfully tested by mixing two colored waters using pressure driven syringe pumps. However, the smallest fabricated microchannel width was limited to about 75μm.

In light of the dimensional limitation of the LCWM method, Chapter 4 describes the second method developed to fabricate smaller microfeatures. The method also employed laser cutting to create a metallic mask but the negative imprints are used

instead. Subsequently, this mask is employed in micro-spark erosion process, micro-electrodischarge machining, to remove material from a conductive metallic substrate to create a master. The second method is termed as LEDM^2 (Laser cutting, Electro-Discharge-Machining, and Molding). High aspect ratio with around 25μm widths of microchannels on mold masters was demonstrated. However, the surface finish was less than optical quality, around 300nm Ra.

The unique advantage of the two developed methods is the direct fabrication of metal molds but to make near optical surface finishes an additional polishing step is needed. This leads to the investigation of a non-metallic micromold fabrication technique, which the near optical surface finishes can be fabricated without polishing. Chapter 5 discussed the third developed method where polymer substrates were used to "contactlessly" fabricate molds with near optical surface finishes. The LHEM (Laser micromachining, Hot Embossing, and Molding) process uses a laser to cut the mask, similar to the one used in the LEDM^2 method. The micro-spark erosion step is then replaced with a partial hot embossing (hot intrusion) to allow the heated-and-soften polymer intruding into the mask openings to naturally form the near optical quality surface finish microreliefs.

Chapter 6 provided an extensive discussion of each method's unique advantages and disadvantages to fabricate micromold masters. The subsequent comparison drew a conclusion where further investigation efforts should be focused on the technique that had highest potential impact. The evaluation used seven basic criteria such as the shortest fabrication time, excellent surface finishes, and minimum chemicals usage to assess the three methods developed in this study. The LHEM method appears to be the most compatible method with the established micromachining technologies, therefore, was selected for further research work.

An extensive series of experiments intended to characterize the resulting geometry of the LHEM extruded microreliefs under various conditions was presented in Chapter 7. The results were collected and analyzed carefully and show that various heights of extruded microfeatures can be fabricated by selecting a set of suitable hot intrusion process parameters. The empirical model was then derived to make the LHEM

method practically useful to MEMS engineers. This empirical model describes the relationship between the process parameters and the final fabricated geometry.

A *Finite Element Method* (FEM) model was then developed to gain further insights on the hot intrusion process and was described in Chapter 8. The FEM model and the FEM predictions are reasonably accurate to describe the physical formation of these extruded microreliefs when it is slightly above the glass transition temperature. Because of the insights gained from the experimental characterization and the FEM analysis, it had been possible to fabricate a 3D micronozzle feature on a mold master and that demonstrate the 3D microfabrication capability of the LHEM method.

9.3 Recommendations and Future Work

The LEDM^2 method appears to be also a promising fabrication technique for replication of polymer microfluidic devices because high-strength molds with high-aspect microfeatures can be fabricated by this method. Using a higher strength substrate material for mold masters is particular advantageous for high temperature and high pressure molding process. Therefore, further investigation should be conducted to improve the surface finishes of the fabricated LEDM^2 mold masters. One approach could be examining different combinations of materials for the mask and substrate.

The extensive studies on characterizing the cross-sectional profiles of the extruded microfeatures created by hot intrusion were conducted and presented. The methods developed in this thesis appear to be suitable for current designs of microfluidic devices where fluidic network microstructures are planar (2D). The near optical grade of surface finishes produced by the LHEM method provide the most interesting results where the LHEM method would be used to fabricate micro-optical components for MEMS devices where high quality of surface finishes is a must. In addition, the LHEM method presented in this study only demonstrated the smallest microchannel features down to about 25μm. If higher precision hot embossing systems were available, further size reductions may be possible to the submicron level. This would be interesting to see in the future.

Because the experimental findings show that there is a strong positive correlation between the width and height of the extruded microreliefs in 2D case, hot intrusion may be a viable method for creating continuous three-dimensional microrelief profiles. A 3D FEM model for the hot intrusion process may also be of interest.

BIBLIOGRAPHY

Abgrall, P., Gue, A.M. (2007). Lab-on-chip technologies: making a microfluidic network and coupling it into a complete microsystem-a review. *J. Micromech. Microeng.* 17: R15-R49.

Atkinson, G.M., Ounaies, Z. (2006). *The MEMS Handbook.* 2nd ed. CRC Press Taylor & Francis Group.

Banks, D. (2006). *Microengineering, MEMS, and Interfacing: A Practical Guide* CRC Press Taylor & Francis Group.

Becker, B.W., Ehrfeld, W., Hagmann, P., Maner, A., Munchmeyer, D. (1986). Fabrication of microstructures with high aspect ratios and great structural heights by synchrotron radiation lithography, galvano-forming and plastic molding. *Microelectron. Eng.* 4: 35-36.

Becker, H., Heim, U. (2000). Hot embossing as a method for the fabrication of polymer high aspect ratio structures. *Sens. Actuators, A.* 83: 130-135.

Becker, H., Locascio, L. (2002). Review polymer microfluidic devices. *Talanta.* 56: 267-287.

Budynas, R.G. (1999). *Advanced Strength and Applied Stress Analysis*, McGraw-Hill.

Cameron, N.S., Roberge, H., Veres, T., Jakeway, S.C., Crabtreeb, H.J. (2006). High fidelity, high yield production of microfluidic devices by hot embossing lithography: rheology and stiction. *Lab Chip.* 6: 936–941.

Chang, C.Y., Yang, S.Y., Chu, M.H. (2007). Rapid fabrication of ultraviolet-cured polymer microlens arrays by soft roller stamping process. *Microelectron. Eng.* 84: 355-361.

Charschan, S.S. (1993). *Guide to Laser Materials Processing.* Laser Institute of America.

Chen, C., Hirdes, D., Folch, A. (2003). Gray-scale photolithography using microfluidic photomasks. *PNAS* 100(4): 1499–1504.

Chen, L., Ren., J. (2004). High-throughput DNA analysis by microchip electrophoresis. *Comb. Chem. High Throughput Screening.* 7:29-43.

Duffy, D.C., McDonald, J.C., Schueller, O.J.A., Whitesides, G.M. (1998). Rapid prototyping of microfluidic systems in poly(dimethylsiloxane). *Anal. Chem.* 70: 4974-4984.

Elders, J., Jansen, H.V., Elwenspoek, M., Ehrfeld, W. (1995). DEEMO: a new technology for the fabrication of microstructures. *Proc. IEEE MEMS '95.*: 238.

Fleischer, J., Schmidt, J., Haupt, S., (2006). Combination of electric discharge machining and laser ablation in microstructuring of hardened steels. *Microsyst. Technol.* 12: 697-701.

Fredrickson, C.K., Xia, Z., Das, C., Ferguson, R., Tavares, F.T., Fan, Z.H. (2006). Effects of fabrication process parameters on the properties of cyclic olefin copolymer microfluidic devices. *J. Microelectromech. Syst.* 15(5): 1060–1068.

García, C.D., Henry, C.S. (2007). Coupling electrochemical detection with microchip capillary electrophoresis. In: *Bio-MEMS: Technologies and Applications.* CRC Press: Taylor & Francis Group.

Gerlach, A., Keller, W., Schulz, J., Schumacher, K. (2001). Gas permeability of adhesives and their application for hermetic packaging of microcomponents. *Microsyst. Technol.* 7:17 – 22.

Guitrau, E.B. (1997). Basic EDM theory. In: *The EDM Handbook.* Hanser Gardner Publications, Cincinnati, ISBN: 1-56990-242-9:19 – 33.

Gunther, A., Jhunjhunwala, M., Thalmann, M., Schmidt, M.A., Jensen, K.F. (2005). Micromixing of miscible liquids in segmented gas-liquid flow. *Langmuir* 21:1547–1555.

Hanemann, T., Heckele, M., Piotter, V. (2000). Current status of micromolding technology. *Polym. News.*, 25:224-229.

Harrison, D.J., Seiler, K.F.K., Fan, Z., Effenhauser, C.S., Manz, A. (1993). Micromachining a miniaturized capillary electrophoresis-based chemical analysis system on a chip. *Science.* 261(5123): 895 – 897.

Heckele, M., Bacher, W., Muller, K.D. (1998). Hot embossing – the molding technique for plastic microstructures. *Microsyst. Technol.* 4: 122-124.

Heckele, M., Schomburg, W. K. (2004). Topical review – Review on micro molding of thermoplastic polymers. *J. Micormech. Microeng.* 14: R-R14.

Hong, J.W., Quake, S.R. (2003). Integrated nanoliter systems. *Nature Biotechnol.* 21: 1179–1183.

Hupert, M.L., Guy, W.J., Shadpour, S.D.L.H., Nikitopoulos, S.R.D.E., Soper, S.A. (2007). Evaluation of micromilled metal mold masters for the replication of microchip electrophoresis devices. *Microfluid. Nanofluid.* 3: 1–11.

Jacobson, S.C., McKnight, T.E., Ramsey, J.M. (1999). Microfluidic devices for electrokinetically driven parallel and serial mixing. *Anal. Chem.* 71: 4455-4459.

Janz, S., Densmore, A., Xu, D.X., Waldron, P., Delage, A., Cheben, P., Lapointe, J., Schmid, J.H. (2008). Silicon-based microphontonics for biosensing applications, Optical Waveguide Sensing and Imaging. *Springer*, Netherlands. 167-194.

Jo, B.H., Van Lerberghe, L.M., Motsegood, K.M., Beebe, D.J. (2000). Three-dimensional micro-channel fabrication in polydimethylsiloxane (PDMS) elastomer. *J. Microelectromech. Syst.* 9(1): 76-81.

Korvink, J.G., Paul, O. (2006). *MEMS - A Practical Guide to Design, Analysis and Applications.* William Andrew Publishing, Springer-Verlag GmbH.

Larsson, O., Ohman, O., Billman, A., Lundbladh, L., Lindell, C., Palmskog, G. (1997). Silicon based replication technology of 3D-microstuctures by conventional CD-injection molding techniques. *In Proc. of Transducers'97, 9th Int. Conf. on Solid-state Sensors and Actuators* (Chicago, IL, June 16-19): 1415-1418.

Laser, D.J. Santiago, J.G. (2004). A review of micropumps. *J. Micromech. Microeng.* 14: R35–R64.

Lee, G.B., Chen, S.H., Huang, G.R., Lin, Y.H., Sung, W.C., Lin, Y.H., (2001). Microfabricated plastic chips by hot embossing methods and their applications for DNA separation and detection. *Sens. Actuators, B.* 75: 142–148.

Lee, K., Kim, C., Shin, K.S., Lee, J.W., Ju, B.K., Kim, T.S., Lee, S.K, Kang, J.Y. (2007). Fabrication of round channels using the surface tension of PDMS and its application to a 3D serpentine mixer. *J. Micromech. Microeng.* 17: 1533-1541.

Lei, K.F. Li, W.J., Yam, Y. (2005). Effects of contact-stress on hot-embossed PMMA microchannel wall profile. *Microsyst. Technol.* 11: 353–357.

Liao, Y.S., Chen, S.T., Lin, C.S. (2005). Development of a high precision tabletop versatile CNC wire-EDM for making intricate micro parts. *J. Micromech. Microeng.* 15: 245–253.

Luo, Y., Xu, M., Wang, X.D., Liu, C. (2006). Finite element analysis of PMMA microfluidic chip based on hot embossing technique. *J. Phys.: Conf. Ser.* 48: 1102–1106.

Magargle, R., Hoburg, J.F., Mukherjee, T. (2004). An injector component model for complete microfluidic electrokinetic separation systems. *Proc. Nanotechnology Conf. and Trade Show. (NanoTech).* Boston. MA. 77–80.

Magrargle, R., Hoburg, J.F., Mukherjee, T. (2006). Microfluidic injector models based on artificial neural networks. *IEEE Trans Computer-Aided Design Integrated Circuits Systems.* 24(2):378-385.

Manz, A., Graber, N., Widmer, H.M. (1990). Miniaturized total chemical analysis systems: a novel concept for chemical sensing. *Sens. Actuators, B.* 1: 244–248.

Martynova, L., Locascio, L.E., Gaitan, M., Kramer, G.W., Christensen, R.G., MacCrehan, W.A. (1997). Fabrication of plastic microfluid channels by imprinting methods. *Anal. Chem.* 69: 4783-4789.

Masuzawa, T., Kuo, C.L., Fujino, M. (1989). Drilling of deep micro-holes by EDM. *Ann. CIRP* 38: 195-198.

Masuzawa, T., Kuo, C.L., Fujino, M., (1994). A combined electrical machining process for micronozzle fabrication. *Ann. CIRP* 43: 189-192.

McCormick, R.M., Nelson, R.J., Alonso-Amigo, M.G., Benvegnu, D.J., Hooper, H.H. (1997). Microchannel electrophoretic separations of DNA in injection-molded plastic substrates. *Ann. Chem.* 69: 2626–2630.

McDonald, J.C., Duffy, D.C., Anderson, J.R., Chiu, D.T., Wu, H., Schueller, O.J.A., Whitesides, G.M. (2000). Fabrication of microfluidic systems in poly(di-methylsiloxane). *Review Electrophoresis* 21: 27-40.

McDonald, J.C., Whitesides, G. (2002). Poly(dimethylsiloxane) as a material for fabricating microfluidic devices. *Acc. Chem. Res.* 35(7): 491-499.

Neural Networks Toolbox, Mathworks Inc., Natick, MA, USA, www.mathworks.com

Nguyen, N.T., Wu, Z.G. (2005). Micromixers — a review. *J. Micromech. Microeng.* 15: R1–R16.

Nguyen, N.T., Wereley, S.T. (2002). Fabrication techniques for microfluidics. In: *Fundamentals and Applications of Microfluidics*. Artech House.

Nguyen, N.T., Wereley, S.T. (2006). *Fundamentals and Applications of Microfluidics*, 2nd Edition. Artech House.

Niggemann, M., Ehrfeld, W., Weber, L., Günther, R., Sollböhmer, O. (1999). Miniaturized plastic microplates for application in HTS. *Microsyst. Technol.* 6: 48 – 53.

Pan, L.W., Shen, X.J., Lin, L.W. (2004). Microplastic lens array fabricated by a hot intrusion process. *J. Microelectromech.* S13(6): 1063-1071.

Piotter, V., Hanemannl, T., Ruprecht, R., Haußelt, J. (1997). Injection molding and related techniques for fabrication of microstructures. *Microsyst. Technol.* 4: 129-133.

Ready, J.F. (2001). *LIA Handbook of Laser Materials Processing*. Laser Institute of America Magnolia Publishing Inc.

Sato, T., Mizutani, T., Kawata, K. (1985). Electro-discharge machine for micro-hole drilling. *Natl. Techn. Rep.* 31: 725-733.

Shen X. J., Pan, L. W., Lin, L. W. (2002). Microplastic embossing process: experimental and theoretical characterizations. *Sens. Actuators, A.* 97-98: 428-33.

Shiu, P.P., Knopf, G.K., Ostojic, M., Nikumb, S. (2007). Rapid fabrication of micromolds for polymeric microfluidic devices. *Int. IEEE 20th Canadian Conf. Elec. Comp. Eng.* (CCECE) (Vancouver, CA, April 07): 8-11.

Shiu, P.P., Knopf, G.K., Ostojic, M., Nikumb, S. (2008). Rapid fabrication of tooling for microfluidic devices via laser micromachining and hot embossing. *J. Micromech. Microeng.* 18:2:025012.

Shiu, P.P., Ostojic, M., Knopf G.K., Nikumb, S. (2008). Rapid fabrication of polymethylmethacrylate micromold masters using a hot intrusion process. *J. Micro/Nanolith. MEMS MOEMS.* 7(4) 1:(043012).

Shiu, P.P., Knopf, G.K. Ostojic, M., Nukumb, S. (2008). Neural network approach to modeling hot intrusion process for micromold fabrication, Optomechatronic Technologies 2008, Otani et al.(Eds.) *Proc. of SPIE*, vol. 7266, p. V1-V10.

Terry, S.C., Hermann, J.H., Angel, J.B. (1979). A gas chromatographic air analyzer fabricated on a silicon wafer. *IEEE Trans. Electron Devices.* 26: 1880.

Van Ossenbruggen, C. (1969). Micro-spark erosion. *Philips Technisch Tijdschrift.* 20: 200-213.

Vijayendran, R.A., Motsegood, K.M., Beebe, D.J., Leckband, D.E. (2003). Evaluation of a three-dimensional micromixer in a surface-based biosensor. *Langmuir.* 19: 1824–28.

Wang, W., Soper, S.A. (2007). *Bio-MEMS: Technologies and Applications*. CRC Press: Taylor & Francis Group.

Wang, Y., Lin, Q., Mukherjee, T. (2004). Applications of behavioral modeling and simulation on lab-on-a-chip: Micro-mixer and separation system in Behavioral Modeling and Simulation. *Conf. San Jose* CA 1–6.

Wang, Y., Lin, Q., Mukherjee, T. (2004). System-oriented dispersion models of general-shaped electrophoresis microchannels. *Lab Chip.* 4(5): 453–463.

Ward, I.M., Sweeney, J. (2004). *An Introduction to Mechanical Properties of Solid Polymers* (New York: Wiley).

Weibel, D.B., Kruithof, M., Potenta, S., Sia, S.K., Lee, A., Whitesides, G.M. (2005). Torque-actuated valves for microfluidics. *Anal. Chem.* 77: 4726–4733.

Whitesides, G.M. (2006). The origins and the future of microfluidics. *Nature.* 442/27: 368-373.

Whitesides, G.M., Ostuni, E., Takayama, S., Jiang, X., Ingber, D.E. (2001). Soft lithography in biology and biochemistry. *Annu. Rev. Biomed. Eng.* 3: 335-373.

Worgull M., Heckele, M., Hetu, J.F., Kabanemik, K.K. (2006). Modeling and optimization of the hot embossing process for micro- and nanocomponent fabrication. *Microsyst. Technol.* 12: 947–952.

Worgull, M., Heckele, M., Hetu, J.F., Kabanemik, K.K. (2006). Modeling and optimization of the hot embossing process for micro- and nanocomponent fabrication. *J. Micro/Nanolithog. Microfab. Microsys.* 5(1): 1–13.

Youn, S.W., Takahashi, M., Goto, H., Maeda, R. (2007). Fabrication of micro-mold for glass embossing using focused ion beam, femto-second laser, eximer laser and dicing techniques. *J. Mater. Process. Technol.* 187–188: 326–330.

Young, R.J., Lovell, P.A. (1991). *Introduction to Polymers* Routledge, 2nd edition (London: Chapman and Hall).

Ziolkowski, S., Frese, I., Kasprzak, H., Kufner, S. (2003). Contactless embossing of microlenses-a parameter study. *Opt. Eng.* 42(5): 1451-1455.

APPENDIX A

NEURAL NETWORK APPROACH TO MODELING THE HOT INTRUSION PROCESS

In Chapter 7, the characterization of the hot intrusion process used by the LHEM technique was presented. Experiments were conducted with various process parameters and this study led to the development of an empirical model that related these process parameters to the formation of microfeatures. An alternative approach to modeling this relationship is described in this Appendix. The relationship between the microchannel dimensions (height and width) and the hot intrusion process parameters (pressure and temperature) is established using an artificial neural network. Experimental data is used to both train and test the neural network for parameter-selection. Analysis of the preliminary results shows that the trained neural network can predict suitable parameters within 6% error.

A.1 Function Approximation Using a Neural Network

The artificial neural network (ANN) inspired by biological neurons has the ability to approximate non-linear functions (Magrargle et al., 2006). For function approximation applications, the neural network structure can involve either supervised or unsupervised training algorithms. The choice depends upon the data and task being solved by the network. In this work, a supervised back-propagation algorithm is used to train the network parameters. The goal is to accurately map multiple inputs to a single output.

Two neural networks are used to model the LHEM process. The first model, Figure A.1(a), is referred to as a *process model* which relates three independent process parameters (hot intrusion pressure, temperature, and width of the profile base) to the height of the extruded microrelief (ie. output). To quantitatively analyze the fabricated geometric features of these extruded micro-reliefs of the PMMA mold master, a metallic mask of microchannel line features with various widths (25 to 200μm) was designed and

laser cut. The mask was used to fabricate mold masters on 1.5mm thick PMMA substrates under various process conditions. The geometric attributes of the extruded microreliefs were then measured.

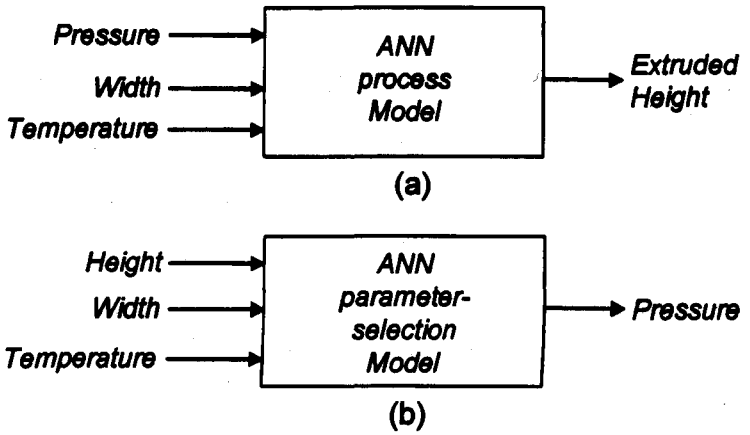

Figure A.1 Neural network models for the LHEM method: (a) ANN taking the process parameters and outputs the height of an extruded microrelief, and (b) taking the desirable profile geometry (W and H) and generates an output corresponding to the suitable process parameter. The pre-defined static parameter is hot intrusion temperature.

The second model is referred to as the *parameter-selection model*, which provides the manufacturing engineers and technicians with the ability to relate the desired microrelief dimensions to a key process variable (pressure). In other words, the parameter-selection model avoids the need for technicians to understand the physical phenomenon underlying the process and yet enable them to complete their tasks effectively. The parameter-selection model accepts inputs as the desired microchannel dimensions (width W, and height H of the extruded profile), and outputs the required process parameters, Figure A.1(b). Although the desired outputs are specific hot intrusion pressures and temperatures, experimental studies have shown that sets of process parameter conditions can result in similar extruded profiles. Therefore, defining one of the process parameters as a static parameter is necessary in order to permit the neural network to generate a single output. In this regard, hot intrusion temperature was selected as the pre-defined static parameter for the parameter-selection model. Furthermore, the

hot intrusion time was not taken into consideration because of the experimental results in Shiu et al. (Shiu, et. al., 2008) showed that the influence of hot intrusion time towards the heights of extruded profiles were limited under the experimental condition (2 to 15 minutes).

Figure A.2 shows a typical structure of a static backward propagated feed-forward network that was employed in modeling the hot intrusion process of the LHEM method (Shiu et al., 2008). This type of networks is selected for modeling the process because of its computational power in approximating non-linear functions. The ANN structures used for the tests below were two-layer ($n \times 1$) networks for both the process model and parameter-selection model. The notation ($n \times 1$) implies n neurons in the hidden layer and 1 output neuron in the second layer. The training was completed when the network reached the preset mean-square error (MSE) goal.

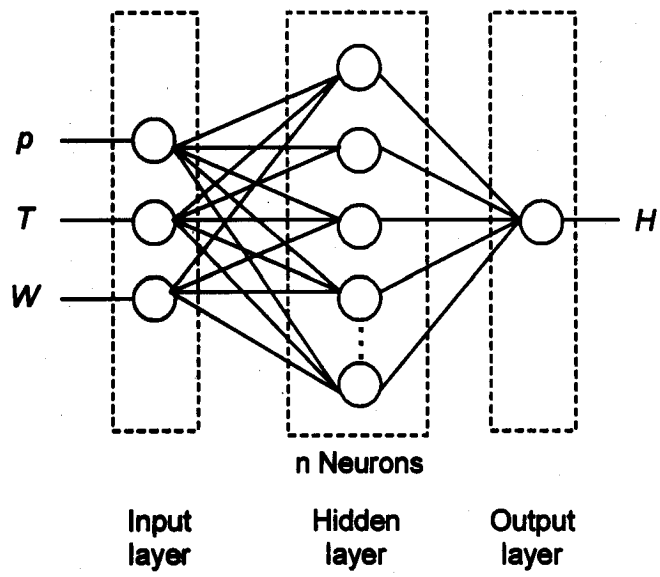

Figure A.2 Two-layer neural network structure for modeling the hot intrusion process (Shiu et al., 2008).

To evaluate the accuracy and identify the appropriate network structure that "best" approximates the experimental data, a number of networks having different n neurons in the hidden layer were tested. The size of the networks was initially large to first obtain a quick convergence solution of the ANN structure. The n number of neurons

was then reduced stepwise, tested, simulated, and evaluated for performance. This procedure is stopped when a network structure (*n*x*1*) having the fewest neurons possible with small average difference, experimental values minus simulated values.

The mean-square errors (MSE) goal was set at one for the process model, implying 1μm MSE. For the parameter-selection model, the MSE goal was also set at one, implying 1Psi MSE. The MSE goal for the process model trained with experimental data was set at one to average out the effects of the possible random errors inherited in the experimental data. The evaluation of ANNs performance was based on the average percentage error between the ANN outputs and the experimental data (all tested networks reached the MSE goal). The number of epochs to reach the goal was set at 10,000. The constructing, training, and testing of the networks were done using the Neural Network ToolBox V. 5.0 from MATLAB, MathWorks, Inc., USA.

Both the process and parameter-selection models were trained and tested using the experimental data reported in Shiu et al. (Shiu, et. al., 2008) and in Chapter 7. The available experimental data pairs were 45 set (90% of these experimental data were used in training and the remaining 10% data, randomly selected, were used as test set data to evaluate the ANN performance). The process and parameter-selection ANN models hold for the experimental conditions found in Chapter 7 and when the pressure ranged from 30 to 60Psi (207 to 414kPa), hot intrusion temperature from 110 to 135°C, hot intrusion time from 2 to 15 minutes, extruded profile width from 25 to 200μm, and the processing material is PMMA.

A.2 Simulated Results

Both the process and parameter-selection ANN models were successfully trained using the backward propagation. The optimal ANN structures for the process and parameter-selection models were found. The optimal size of the process model was (*7x1*) two-layer network structure. The optimal size of parameter-selection model networks was (*20x1*) because smaller sized networks were not able to reduce the output to the target MSE after

a long period of time. The approximation of both ANN models was acceptable because the ANN outputs are less than six percent average error against the test data set.

The results of performance evaluation of the ANN process models are shown in Figures A.3 to A.8. Figure A.3 shows the smallest average percentage difference between the simulated ANN outputs and test set was 3.57% and the smallest average difference was 1.28μm. Figure A.4 and A.5 show a comparison between the ANN simulated outputs and experimental data of the optimal network of (*7x1*). Note that a good approximation of the experimental data by ANN model is clearly shown.

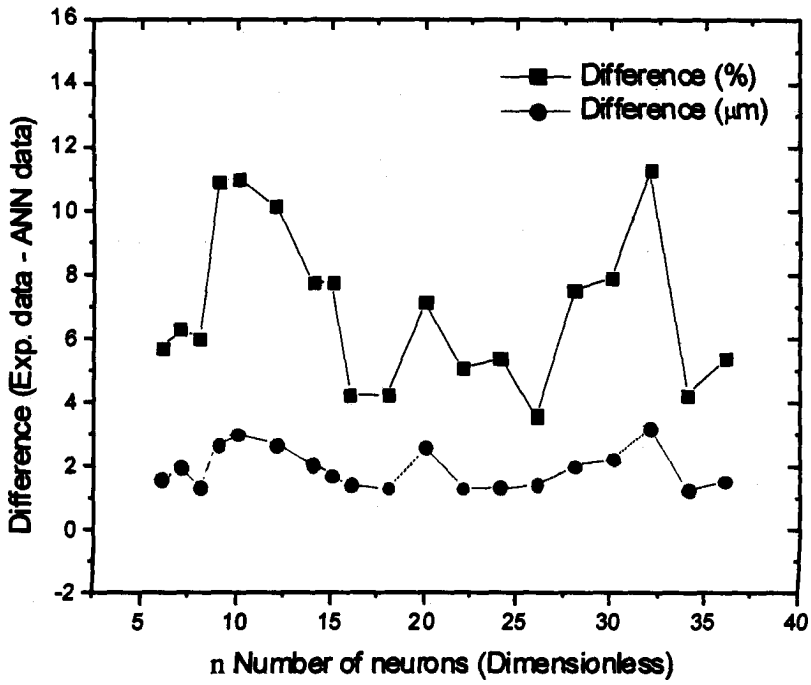

Figure A.3 The differences with *n* neurons in the first layer of the (*n x1*) process model.

Initially, the MSN goals were set as $1x10^{-1}$. After a number of training and testing trials, the resulting ANNs had poor generalization with high degree of undulations. Subsequently, the MSN goal was set as $1x10^{0}$ (MSE 1μm goal instead of 0.1μm). The generalization was greatly improved. The number of neurons in the networks was further reduced and improved generalizations were observed (Figure A.4).

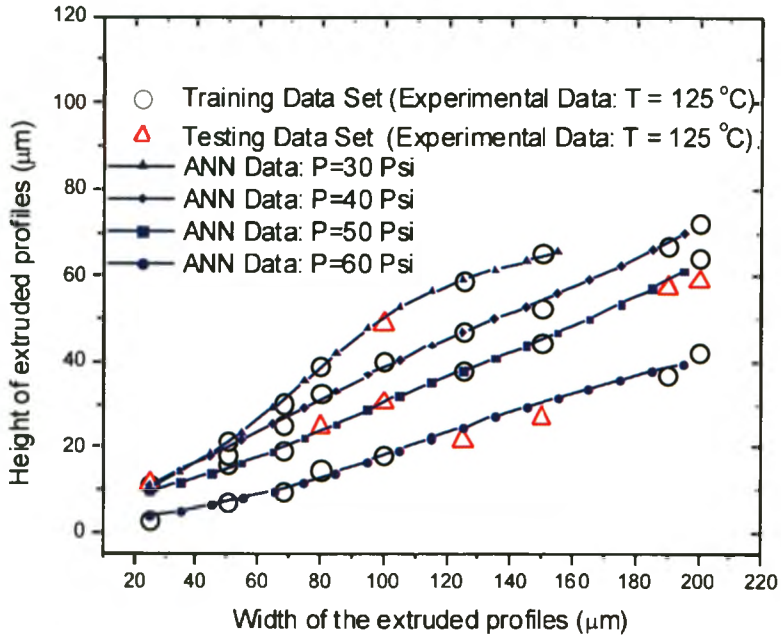

Figure A.4 The outputs of the ANN along with experimental data at hot intrusion conditions of 125°C at 30Psi to 60Psi (207 to 414kPa) of the (*7* x *1*) process model.

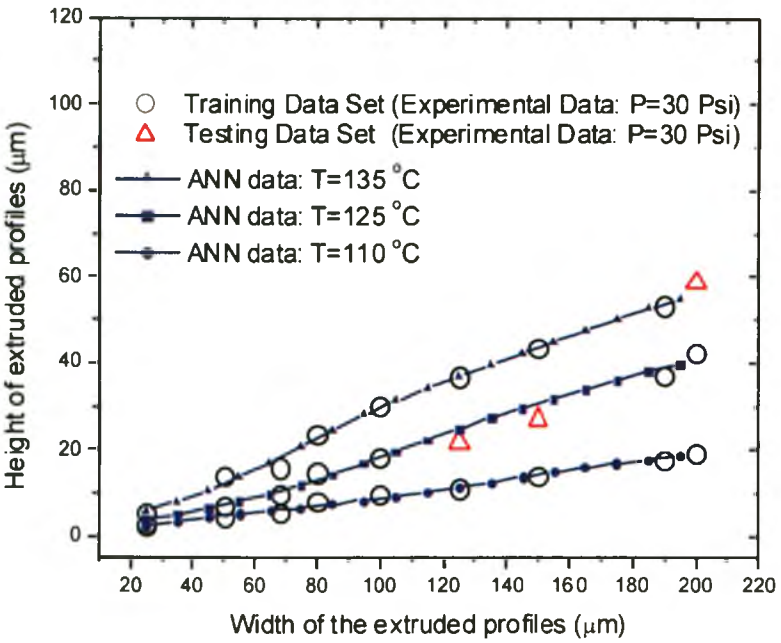

Figure A.5 The outputs of the ANN with experimental data at hot intrusion conditions of 110 to 135°C at 30Psi (207kPa) of the (*7* x *1*) process model.

The results of the parameter-selection model are presented in Figures A.6 to A.8. Figure A.6 describes the results of the percentage error in different *n* numbers of neurons of two-layer structures. The smallest percentage error of ANN structure is 5.15% and 17.24kPa (2.5Psi). Figure A.7 shows that the results of the ANN outputs from the parameter-selection network and demonstrated that the ANN outputs have strong tendency towards 310kPa (45Psi) at smaller widths of the extruded profile, less than 70μm. This tendency can be observed in the difference between the ANN output and the experimental data provided in Figure A.7.

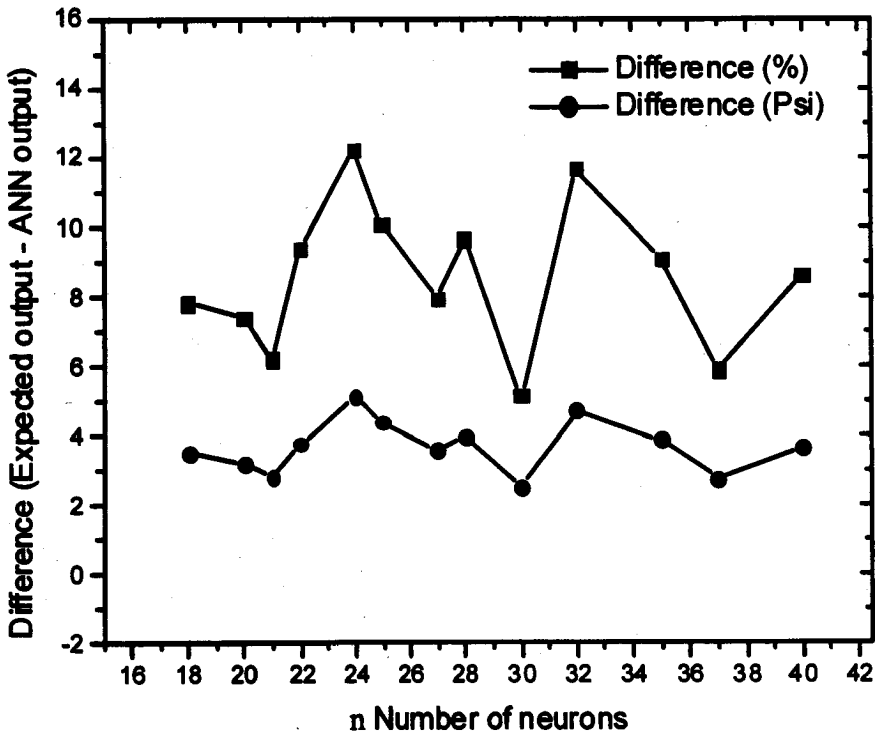

Figure A.6 The differences with *n* neurons in the first layer of the (*n* x *1*) parameter-selection model.

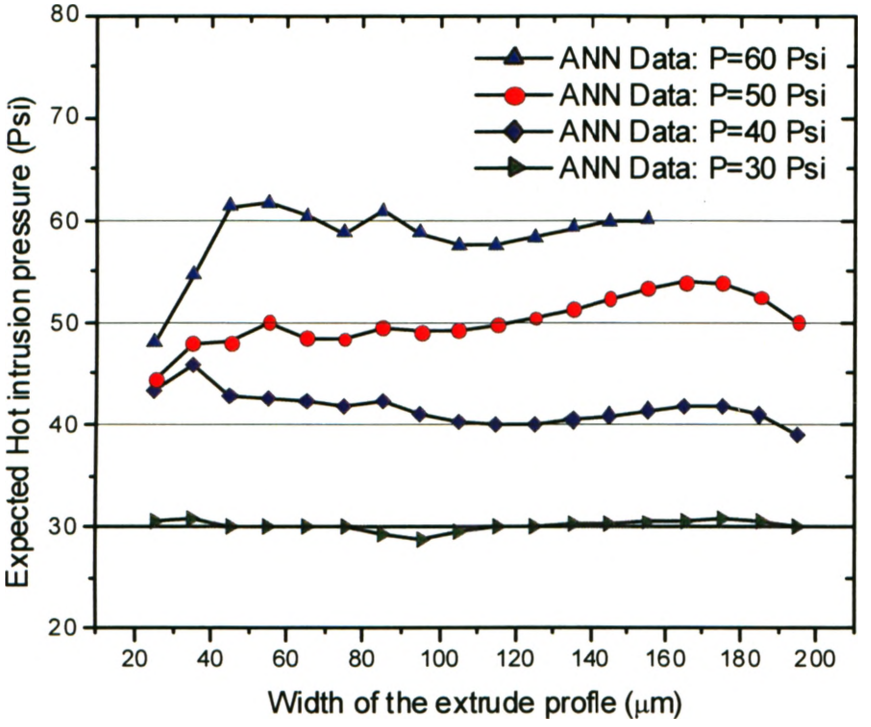

Figure A.7 Comparison of the outputs of ANN and experimental data at hot intrusion conditions of 125°C at 30Psi to 60Psi (207 to 414kPa) of the parameter-selection model (*20* x *1*) ANN structure.

Figure A.8 shows the deviation of the simulated outputs from the expected pressure values. At the smaller widths of the extruded profiles, below 70μm, the deviation of the predicted HI pressure values increased. This implies that when designing smaller microreliefs using the parameter-selection ANN model, the resulting microfeatures may have a larger deviation prediction using the trained ANN model.

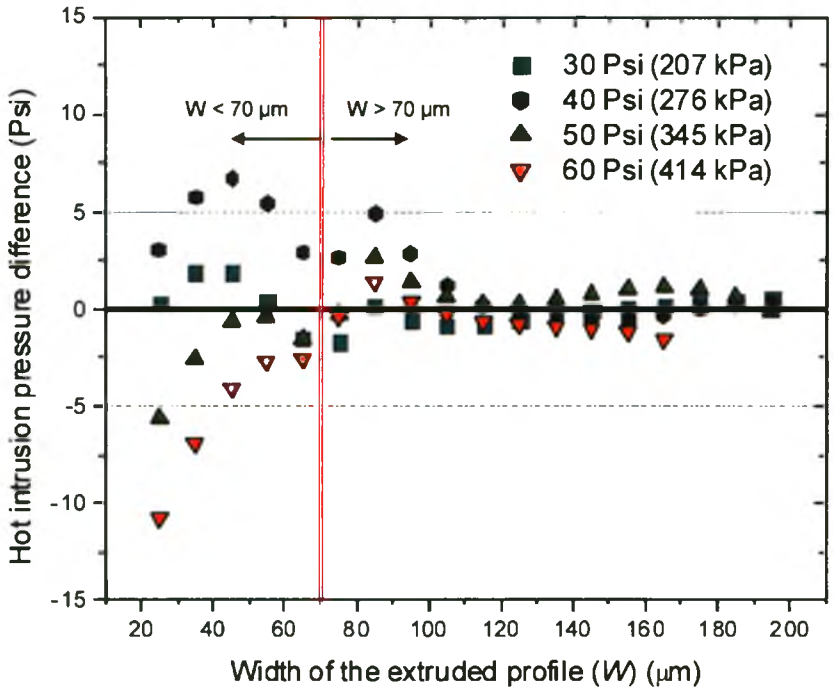

Figure A.8 The deviation of the predicted hot intrusion pressure values vs. width of the extruded profiles, from 30Psi to 60Psi (207 to 414kPa) of the parameter-selection ANN model with a (*20* x *1*) structure.

A.3 Discussion

The number of neurons of the optimal parameter-selection model was about three times larger than the process model, although the same experimental data were used to train both networks. This shows that the arrangement of the data used in training determines the final number of neurons of the network in this study.

All trained networks initially reached the target MSE values. However, high degree of undulation of the simulated ANN outputs was observed, resulting in poor generalizations. Subsequently, the first attempt to minimize the poor generalization was to reduce the number of neurons of the networks because it also reduced the ability of the networks to approximate high order non-linear functions. Poor generalizations of the trained networks were still observed.

The second attempt to minimize the poor generalization of the trained networks was to increase the MSE value. The MSE goal value was set initially to be $1x10^{-1}$ for process model and it implied that a 0.1μm mean-square-error restricted the network to adapt a lower degree order function to represent the data. MSE goal was adjusted to be 1μm. The networks were re-trained. Subsequently, the generalization was largely improved and further improvement was made by reduced the number of neurons of the networks, shown in Figures A.3 and A.6.

The results of the trained parameter-selection model show that some of the simulated ANN outputs (HI pressure values) deviated from the expected values when the input parameter of width of extruded profiles was smaller than 70μm. The contributing factor to this deviation appeared to be that the differences in heights of the extruded profiles are small at smaller widths of extruded profiles, mostly within 5 to 10μm range. The ANN networks may have difficulties to distinguish the difference. However, this problem was not observed in the process model.

If expansion of ANN models is needed for the LHEM method that included different processing material, the modeling approach presented in this paper could be employed. In addition, the trained networks could be incorporated into design/manufacture software (CAD/CAM) to enhance its functionality. For that purpose, portability to different computing devices is necessary; the trained networks could be extracted in a form of analytical equation of simple feed-forward networks of two-layer structure with a single output. The analytical form states as:

$$t_k = y_{out}\left[\sum_{j=0}^{M} g_{kj}\, z_{hid}\left[\sum_{i=0}^{N} w_{ji}\, x_i\right]\right], \qquad \text{(A1)}$$

where t_k is the output of the network, $y_{out}[\varsigma]$ is the activation function of linear output, $z_{hid}[\varsigma]$ is the nonlinear activation function of the hidden layer, g_{kj} and w_{ji} are the weights between each neurons.

A.4 Conclusion

This Appendix presented an artificial neural network (ANN) approach to modeling the hot intrusion process of the LHEM method. The results demonstrated that the ANN model could reasonably predict the expected values of the process parameters related to the desired extruded heights of microreliefs. Therefore, The ANN avoids the complexity of modeling the hot intrusion process using first principle approach that requires an in-depth knowledge of the physical phenomenon.

Further expansion of this model to incorporate for different polymers can be achieved easily via similar approach as presented in this appendix provided a new set of training data for the ANNs. ANNs are highly portable and easy to integrate into different design/manufacture software.